APL Energy

REVIEW ARTICLE | APRIL 24 2023

Monitoring the stability and degradation mechanisms of perovskite solar cells by *in situ* and *operando* characterization

Fanny Baumann ; Sonia R. Raga ; Mónica Lira-Cantú

APL Energy 1, 011501 (2023)
https://doi.org/10.1063/5.0145199

Monitoring the stability and degradation mechanisms of perovskite solar cells by *in situ* and *operando* characterization

Cite as: APL Energy 1, 011501 (2023); doi: 10.1063/5.0145199
Submitted: 3 February 2023 • Accepted: 29 March 2023 •
Published Online: 24 April 2023

Fanny Baumann, Sonia R. Raga,[a] and Mónica Lira-Cantú[a]

AFFILIATIONS

Nanostructured Materials for Photovoltaic Energy Group (NMPE), Catalan Institute of Nanoscience and Nanotechnology (ICN2), Nanostructured Materials for Photovoltaic Energy Group, Autonomous University of Barcelona (UAB), Bellaterra, Barcelona 08193, Spain

[a]**Authors to whom correspondence should be addressed:** sonia.ruizraga@icn2.cat and monica.lira@icn2.cat

ABSTRACT

Solar energy technologies are among the most promising renewable energy sources. The massive growth of global solar generating capacity to multi-terawatt scale is now a requirement to mitigate climate change. Perovskite solar cells (PSCs) are one of the most efficient and cost-effective photovoltaic (PV) technologies with efficiencies reaching the 26% mark. They have attracted substantial interest due to their light-harvesting capacity combined with a low cost of manufacturing. However, unsolved questions of perovskite stability are still a concern, challenging the potential of widespread commercialization. Thus, it is imperative to advance in the understanding of the degradation mechanism of PSCs under *in situ* and *operando* conditions where variable and unpredictable stressors intervene, in parallel or sequentially, on the device stability. This review aims to debate the advantages behind *in situ* and *operando* characterization to complement stability-testing of PV parameters in the strive to achieve competitive stability and reproducibility in PSCs. We consider the impact of applying single and multi-stressors under constant monitoring of alterations observed in PSC components or complete devices. We outline key future research directions to achieve the long-term stability necessary for the successful commercialization of this promising PV technology.

I. INTRODUCTION

Photovoltaic (PV) technologies are important and competitive means to produce electricity from sunlight, offering the potential to transform our society into a low-carbon economy. However, for the technology to become competitive, the leveled cost of electricity (LCOE) must be reduced, and the best strategy is to boost power-conversion efficiency and extend its operational lifetime. However, the efficiency of solar cells is limited by the so-called Shockley–Queisser (SQ) limit.[1] With silicon cells (SiSC) showing current power-conversion efficiency (PCE) values of 26.7% and halide perovskite solar cells (PSCs) at >26%,[2,3] these two powerful PV technologies are almost at the limit of their maximum theoretical SQ value. This indicates that further significant advances in PV efficiency practically require breaking the SQ limit and one possible method to achieve this is by the use of multijunction solar cells where theoretical calculations indicate PCEs around 45% if tandem configurations are employed.[4] Unfortunately, unsolved issues in perovskite stability have important implications for real-world energy yields, challenging the potential of widespread commercialization. Factors that can induce degradation to metal halide perovskite (MOHP) materials and devices, such as humidity, atmosphere, bias voltage, temperature, or light exposure, have been the center of multiple studies and debates for many years. The ISOS stability assessment protocols, elaborated after a consensus among leading international laboratories, have been recently upgraded to incorporate stressors involving the peculiarities of PSCs. Figure 1 depicts a schematic representation of the existing ISOS protocols developed originally for organic solar cells (OPVs) and recently upgraded for PSC (in rectangles).[5,6]

Lifetimes of 10 000 h have been reported for PSCs under dark conditions (ISOS-D protocol),[7] constant light irradiation (ISOS-L protocol),[8] and under various relative humidity (RH) conditions (ISOS-RT),[9] also calculated 30-year lifespan under outdoor operation conditions can be found in the literature (ISOS-O protocol).[10,11]

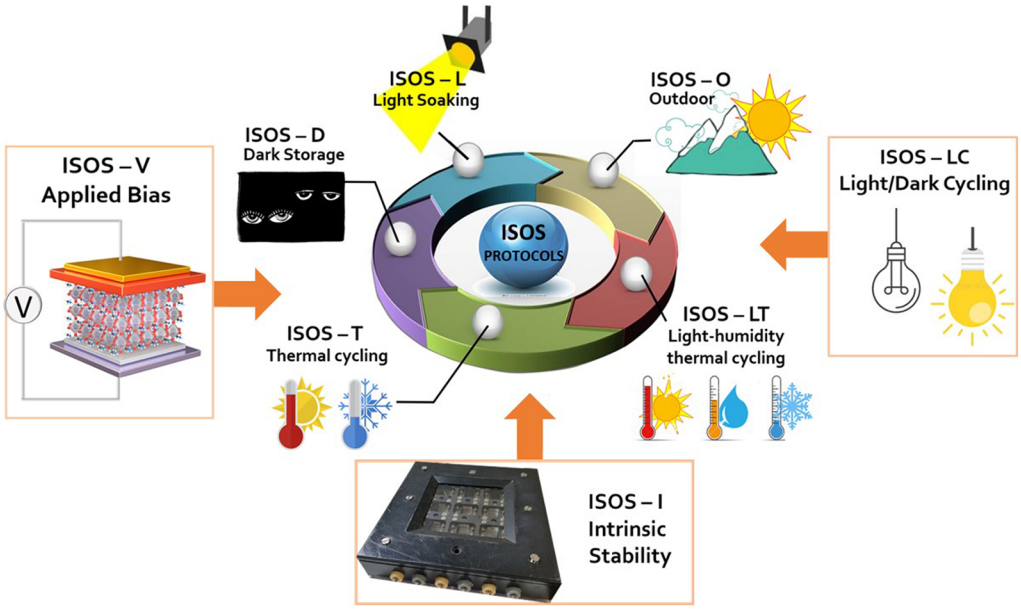

FIG. 1. Schematic representation of the main ISOS protocols employed for OPV and PSC stability assessment: ISOS-L, light irradiation; ISOS-D, dark conditions; ISOS-LT, light/humidity thermal cycling; ISOS-T, thermal cycling; and ISOS-O, outdoor testing. Updated PSC protocols (in rectangles): ISOS-LC, light/dark cycling; ISOS-I, intrinsic stability; and ISOS-V, applied voltage.[5,6]

However, these works are scarce, and they do not always fulfill the requirements of the application of stability stressors under real and *operando* conditions; thus, the stability of PSCs still represents enormous limitations. The understanding of the different degradation mechanisms taking place in materials, solar cells and modules, will only be effective if the applied stressors are as close as possible to an actual functioning device. Outdoor analysis (ISOS-O protocol), where multiple stressors are imposed on the sample with great variability and doses, is one of the most accurate methods to evaluate PSC stability. At the laboratory stage, *in situ* and *operando* characterization techniques are excellent options to evaluate changes observed in the solar cells under single or multiple stressors with time.

In this review, we present a comprehensive and critical summary of the state-of-the-art knowledge regarding *in situ* and *operando* characterization during the process of degradation of PSCs under introduced stressors. We also give insight into the capabilities, the accuracy, and the few limitations of *in situ* characterization techniques. Our aim is to dive deeper into relevant research works to gain insight into the different degradation mechanisms observed in PSCs. We also seek to persuade the reader of the advantages of *in situ* and *operando* characterization under multiple stressors, as these requirements are closer to the real working conditions of PSC. The reader will also notice our incessant association of the reviewed works to ISOS protocols (Fig. 1). The ISOS protocols are internationally recognized experimental conditions that should be followed for the stability assessment of PSCs. These have been identified under a consensus among international experts in the field. The application of ISOS protocols is necessary because most stability studies are conducted under laboratory conditions without following standards or protocols and focusing mostly on one main stress factor.[12,13] However, only by continuously monitoring the degradation of a PSC under stress factors that are well described and known to impact exclusively PSCs (as described in the ISOS protocols), we will be able to compare results among laboratories and understand and construct a long-lasting and enduring PSC technology.

We will also unveil the significance of *in situ* characterization, which is validated by the reversibility of effects and the short timescales of recovery observed in PSCs. This differs from post-mortem and *ex situ* characterization that can draw inaccurate conclusions regarding mechanisms occurring during PSC failure and their long-term prevention. In addition, *in situ* characterization carries out under multi-stressor also permits to monitor synergetic, competitive effects, with the aim of gaining greater understanding of the gaps regarding the elusive stability properties of metal-organic halide perovskite (MOHP) in all varieties of device structures.

This review is organized based on the degree of the different stressors applied to the PSCs (Fig. 2). First, we summarize research works employing single stressors such as humidity and oxygen, light irradiation, thermal stress, bias-loading, and cycling stressors. We finalize the review with the summary of those works where two or more stressors are employed.

II. HUMIDITY AND OXYGEN

External environmental conditions, such as moisture or oxygen, suppose a challenge for the long-term stability of most materials; therefore, the risks of corrosion and oxidation should always be considered. Photovoltaic components of PSC, particularly the MOHPs, are highly sensitive.

As perovskite is exposed to moisture, water molecules penetrate the polycrystalline film crystal lattice, mainly through the gaps and surface defects at the grain boundaries. If or when reaching sufficient concentrations, reactions occur, either in a reversible or

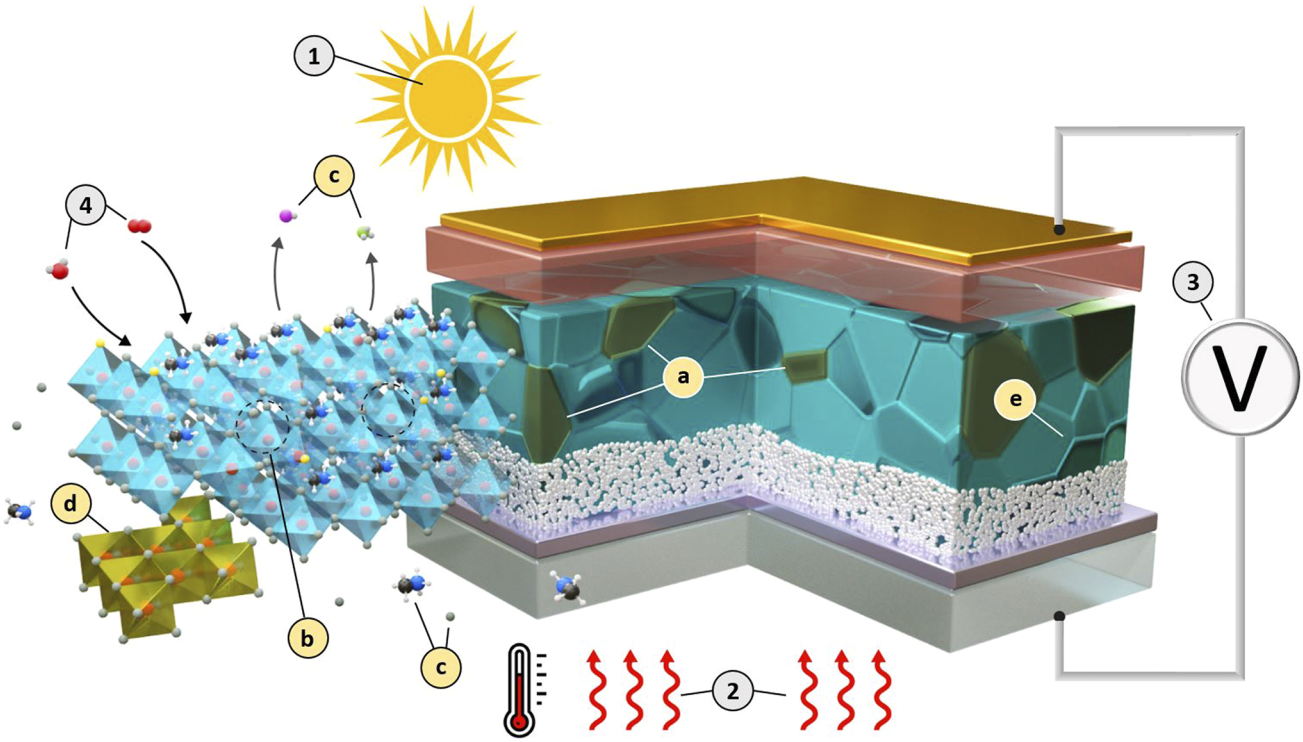

FIG. 2. Degradation in PSCs. (1–4) Schematic representation of a PSC depicting the different stressors affecting an *in operando* PSC: (1) illumination, (2) heat, (3) electrical bias, and (4) atmosphere (moisture and oxygen). (a)–(e) A representation of some of the most characteristic degradation mechanisms observed in halide perovskites: (a) halide/phase segregation, (b) formation of hydrates, crystal decomposition by (c) releasing volatile molecules methylamine (MA), I_2, NH_3, and HI or (d) forming precipitates (Pb^0, I_2, etc.), and (e) morphology changes (e.g., smaller grain size).

irreversible pathway. Water in the lattice form hydrates via hydrogen bonding,[14] i.e., the perovskite crystal structure is separated into smaller units, such as two-dimensional structures. Hydration results in the loss of all or part of the optoelectronic properties of the MOHP layer. Water incorporation is reversible by drying,[15] healing the separated units back to perovskite structure. However, when new grain boundaries are formed or when reaction products evaporate (HI, CH_3NH_2) or precipitate (Pb^0, I_2), changes in morphology or chemical reactions are permanent. Relative humidity exposure, transport at the interface of the crystal, and crystal integrity are determining factors for the outcome; formation of reversible monohydrate, irreversible dehydration, permanent chemical reactions, or drying. In contrast, mixed cation perovskite compositions undergo more complex degradation pathways that can involve phase separation.[16] As we conclude in Sec. III A (light + ambient) and Sec. VII (multistressor), the sole presence of O_2 has no serious effects on perovskite stability unless an external input of energy is added to promote reactions. Oxidation of small molecules and polymers employed as selective contacts in the PSC architecture can however be a source of instability. This modifies charge transport and energy alignment properties (e.g., in the oxidation of spiro-OMeTAD), thus affecting device performance via the conductivity of collecting layers or the carrier mobility at interfaces. For the MOHP layer itself, most essential functions remain intact upon exposure to oxygen in the dark. If MOHP bonds are strengthened to enhance the integrity of the 3D perovskite structure, air stability is improved. This can be done by compositional tuning (cation or halide),[17,18] adding passivating organic molecules(e.g., binding with dangling bonds of surface atoms)[19] or creating a physical barrier that hinders water penetration.[20]

In this article, we will review and put in perspective the recent debate about the pathways in which humidity affects PSC at various conditions, which could be studied in detail, thanks to *in situ* characterization setups. Although largely solved by encapsulation, air-degradation was one of the first issues faced by the PSC research community, we will outline how *in situ* characterization has been used to bring clarity into the mechanisms of physical and chemical degradation under controlled humidity and O_2 stressors.

In the year 2015, two works opened an important discussion about perovskite hydration. Yang *et al.* performed both *in situ* ultraviolet-visible optical absorbance (UV–vis) and *in situ* grazing incidence XRD (GIXRD) measurements on $MAPbI_3$ to study degradation kinetics.[21] They observed a dependence of relative humidity (RH) on the absorbance reduction rate at 410 nm. The degradation "half time" evolved from 4 to 34 h, and from 1000 to 10 000 h upon the reduction of RH from 98% to 80% and from 50% to 20%, respectively, while in dry air no changes on the UV–vis spectra happened for 2 weeks. With *in situ* GIXRD, real-time monitoring of 2D scattering showed that additional diffraction signals appeared at q = 5 and 7 nm^{-1} upon exposure to 80% RH. These new peaks were hypothesized to be an intermediate hydrate phase that could revert to the perovskite structure. Indeed, the absorption

spectra showed partial recovery of the absorption edge at 760 nm after flushing with dry nitrogen. That same year, the formation of perovskite hydrates was revealed by combining time-resolved XRD and *in situ* ellipsometry. Leguy *et al.* explored the crystal changes during hydration (80% RH) and drying (35% RH) of 270 nm thin film $MAPbI_3$ on glass.[15] They concluded that an initial 6% expansion of the crystal lattice occurred by the interpenetration of water molecules into the structure, leading to the creation of monohydrates in the entire perovskite grain [Fig. 3(1b)], while massive expansion to 28% of the initial $MAPbI_3$ volume was attributed to the formation of dihydrate crystals on grain surfaces Fig. 3(1c). Additionally, changes in the refractive index acquired by *in situ* ellipsometry during hydration/dehydration revealed that the macroscopic conversion to monohydrate is isotropic. Similar results were extracted in a more recent work by using GIXRD on full solar cell devices at 60% RH.[22] Results from Yang and Leguy were temporarily considered conflicting regarding the initial hydrate product,[15,21] and detailed studies on the electrical properties and degradation mechanisms of perovskite films followed.

To confirm the results available and further detail the mechanism of degradation under humidity conditions, Li *et al.* conducted detailed studies on $MAPbI_3$ films in p-i configuration (without electron transport layer (ETL) and top electrode) using *in situ* scanning force microscopy (SFM).[23] Their results supported the mechanisms outlined by Leguy *et al.* but found irreversibility in the morphology changes occurring simultaneously with $MAPbI_3$ hydration. The initial smooth crystallites in the film started changing to steps and grooves after 4 h under 80% RH during time-resolved morphology studies with SFM. Complementary *in situ* XRD spectra taken every 15 min (80% RH N_2) revealed the formation of a monohydrate peak ($MAPbI_3 \cdot H_2O$) starting at 5.5 h and increasing intensity over time, coinciding with the observed morphology changes from SFM. After 9 h, dry N_2 gas flow conditions were applied in both experiments to explore the reversibility. While the changes of the XRD spectra were reversed, the morphology changes were not; i.e., the newly formed grain boundaries persisted.[23] With *in situ* grazing incidence neutron scattering (GISANS), Schlipf *et al.* could see that much more water is adsorbed on $MAPbI_3$ crystal surfaces and accumulated in amorphous regions than the amount perceived in the crystal hydrates previously.[24] By using moist air with D_2O molecules, they could determine that, at low RH, D_2O is not incorporated into the crystal structure but rather located in amorphous regions around the crystallite grains. These amorphous regions can be visualized with GISANS, whereas only crystalline degradation products can be visualized using XRD. At ~73% RH, a volume expansion is attributed to the formation of the monohydrate, and, at >93% RH, dihydrate phases are formed inside the $MAPbI_3$ structure. Below 73% RH, the trend of water uptake is found to exhibit a plateau between 30% and 60% RH attributed to the saturation of crystal surfaces with adsorbed water. Smaller crystallites are more affected both regarding D_2O ingress and hydration, making degradation strongly dependent on morphology.

Since many works focused on the perovskite material and surface science to identify the ambient-induced degradation, the real-time effects on the optoelectronic response of the perovskite were less explored. Hu *et al.* used *in situ* electrical resistance measurements of perovskite films with buried interdigitated electrodes and with a controlled atmosphere.[25] No change of resistance was observed under pure N_2 or O_2, but, upon adding moisture, a decrease in resistance over time was observed that could be recovered back by exposing samples to dry N_2, but long-time exposure led to PbI_2 formation. The results fully support chemisorption followed by hydration in the formation of a monohydrate phase. Song *et al.* used laser beam-induced current (LBIC) imaging to create time-dependent maps of the external quantum efficiency (EQE) at a fixed wavelength. While scanning a 532 nm laser beam across the sample every 6 min and measuring the spatially resolved photo-generated current, at N_2 flow with ~50% RH, four stages of degradation [Fig. 3(2a)] were observed:[26] Stage 1: EQE increased until reaching a peak around 10–15 min after condition application. Stage 2 (18–105 min): EQE steadily decreased from ~72% to ~56%. Stage 3 (2 h): a front of sharp EQE decrease swept over the device resulting in merely ~6% EQE. These three stages were reversible, followed by an irreversible fourth stage [Fig. 3(2b)] with loss of the remainder of the EQE signal at ~1300 min. All devices tested showcased the same general behavior [Fig. 3(2c)]. The authors identified doping of spiro-OMeTAD and the perovskite interfaces as the cause for stage 1–2, reversible perovskite-hydration as stage 3, and irreversible hydration as stage 4.[26]

In mixed perovskite compositions, contrary to initial observations on $MAPbI_3$ perovskite, the mechanisms of ambient degradation significantly differ. Hu *et al.* performed *in situ* XRD on four different perovskite films on glass, with various A-site cation combinations (MA, FA, Cs, and Rb) and different halide (I/Br) ratios.[17] They demonstrated that Rb ions in the lattice enhanced moisture instability. When films were exposed to 75% RH air, room T and dark for 60 min using a hydration-chamber made from x-ray-transparent polymers, FAMA and FAMACs (Cs: 5 mol. %)-based films showed minor signs of degradation, only a small PbI_2 peak appeared after 60 min. Rb-containing films, however, showed the onset of a new peak at 11.4° after only 15 min, followed by three additional reflections at 22.9°, 34.7°, and 46.8°. The peak at $2\theta = 11.4°$ was attributed to non-photoactive phases identified as $RbPb_2I_4Br$ and affinity for side-phases containing Rb and Br to thermodynamic favoritism toward lower Goldschmidt tolerance-factor in-between these ions. Two complex and concomitant degradation mechanisms for $Cs_{0.05}(MA_{0.17}FA_{0.83})_{0.95}Pb(Br_{0.17}I_{0.83})_3$ (CsMAFA) mixed perovskite with *in situ* XRD [Fig. 3(3a)] under 85% RH were found by Kazemi *et al.*[18,19] One pathway involved the decomposition of the initial structure through dissolution/recrystallization, leading to PbI_2. A second pathway, in which phase segregation happens, results in the formation of the identified phases (Cs-poor and I-rich)-CsMAFA perovskite and $CsPb_2Br_5$ [Fig. 3(3b)]. Similar to the above, Urwick *et al.* compared different mix MOHP with varying A-site cations (MA, MAFA, CsFA, and CsMAFA) using *in situ* time of flight (ToF) GISANS [Fig. 3(4)] under 90% RH up to 12 h.[27] ToF-GISANS enabled the identification of low atomic weight phases with high depth resolution. They concluded that Cs increased the film stability, preventing the formation of lead halide sub-products. It was observed that the bulk endured a more drastic decay than the film surface, suggesting that degradation initiated in the bulk. Both these reports hinted at crystal integrity and eventually segregation of mixed cation perovskites.

Since air exposure is external and can be isolated via protection, studies have focused on implementing ambient-protection strategies for PSC, and some works employed *in situ* measurements

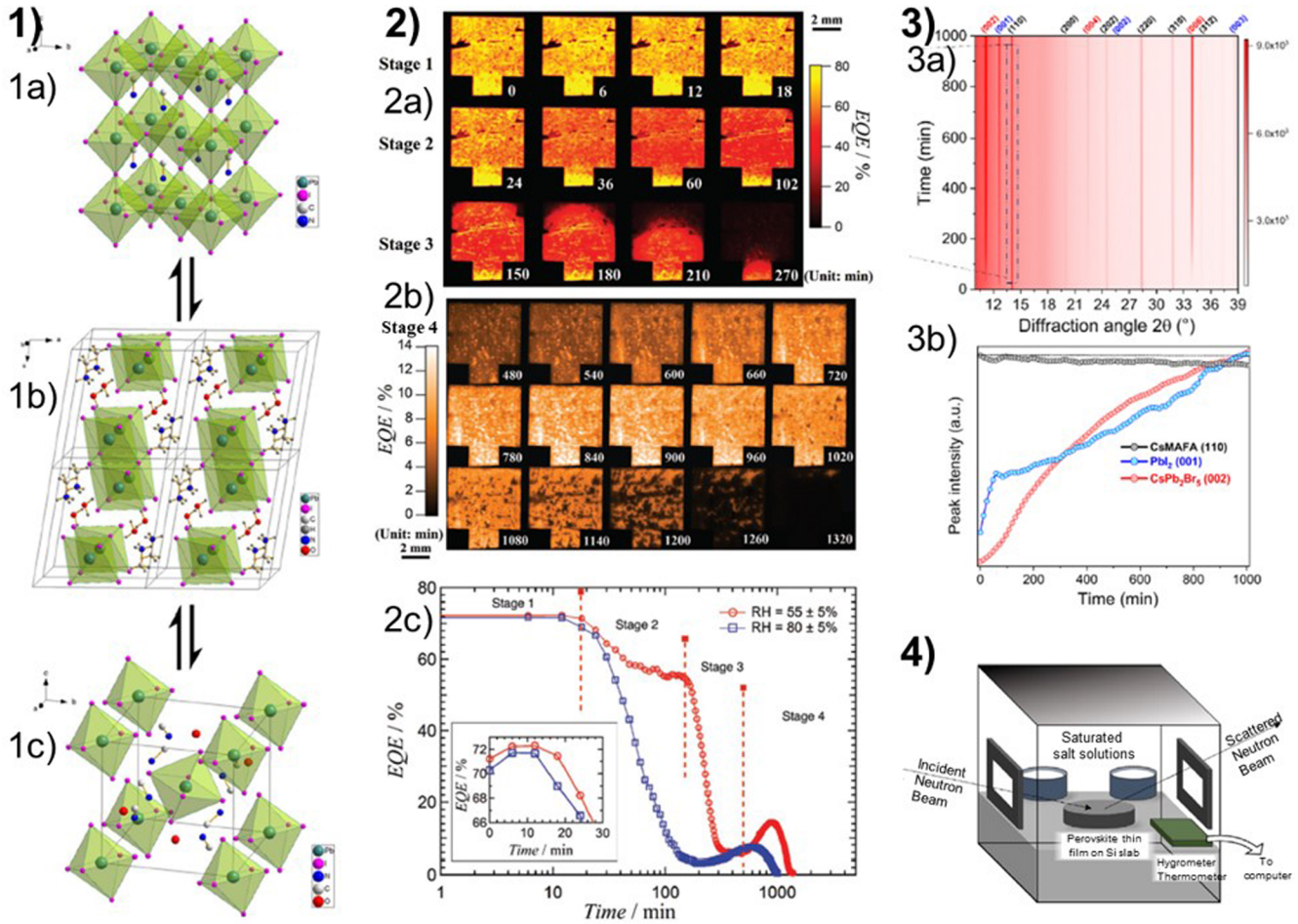

FIG. 3. (1) Structural configurations of (1a) $MAPbI_3$ cubic phase, (1b) monohydrate, $CH_3NH_3PbI_3 \cdot H_2O$, and (1c) dihydrate, $(CH_3NH_3)_4PbI_6 \cdot 2H_2O$. Reprinted with permission from Leguy *et al.*, Chem. Mater. **27**, 3397 (2015). Copyright 2015 American Chemical Society. (2a) LBIC EQE maps (at 532 nm) of a PSC after exposure to 50% ± 5% RH. (2b) high-resolution color scale LBIC images for stage 4 (480–1320 min). (2c) Areal average LBIC EQE (at 532 nm) as a function of time after exposure to humidity. Reprinted with permission from Song *et al.*, Adv. Energy Mater. **6**(19), 1600846 (2016). Copyright 2016 John Wiley & Sons. (3a) *In situ* x-ray diffraction patterns in contour plot of CsMAFA film as a function of aging time under 85% RH. (3b) Evolution of the x-ray diffraction peak intensity as a function of aging time. Reprinted with permission from Kazemi *et al.*, Energy Environ. Mater. **6**, e12335 (2023). Copyright 2023 John Wiley & Sons. (4) GISANS experiment setup for *in situ* moisture degradation. Reprinted with permission from Urwick *et al.*, Energy Rep. **8**, 23–33 (2022). Copyright 2022 Elsevier.

to validate their hypothesis. Yang *et al.* included a study on the protective effects of various HTL, showing that while PTAA and P3HT acted as barriers slowing the rate of decomposition, spiro-OMeTAD accelerated the degradation. Kundu and Kelly performed *in situ* absorbance spectroscopy at saturated humidity (99% RH) flow to prove that a tailor-made hole transport material (HTM) can work well as a protective barrier against humidity.[20] They prepared a poly(methyl metacrylate) (PMMA) film with embedded P3HT nanowires HTL layer to act as a H_2O-barrier protector. *In situ* absorbance spectroscopy at 410 nm revealed that PMMA protection was much greater than P3HT. Decomposition of unprotected $MAPbI_3$ happened in under 6 h, $MAPbI_3$ with P3HT degraded in less than 24 h, and pure PMMA covered $MAPbI_3$ only slightly degraded after 100 h. Decomposition was sequential; when protected samples started to degrade, pinholes formed in the barrier followed by rapid degradation of the perovskite underneath. Kazemi *et al.* demonstrated that modifying the perovskite composition or passivating it with an ammonium additive decreased air-induced degradation substantially.[18] Parallel *in situ* XRD and *in situ* liquid cell TEM on perovskite films exposed to 85% RH air flow demonstrated the known behavior of $MAPbI_3$ hydration described earlier. Emphasizing that the preferential growth of both initial tetragonal $MAPbI_3$ and PbI_2 degradation product was in the [110] direction while intermediate degradation structures grew preferentially in the (001) plane-direction, they supported that hydration originates primarily through crystal planes with more affinity to incorporate water molecules. In contrast, when 9 mol. % excess of PbI_2 was present in the $MAPbI_3$ film, the degradation mechanism skipped the hydrated intermediate. The onset of PbI_2 formation was delayed, but once initiated, degradation proceeded faster, and further, including PbIOH formation. A passivation approach using tetrapropyl ammonium ion (TPA^+),

($TPA_xMA_{(1-x)}PbI_3$), showed drastic improvement of stability, without the formation of hydrates and minimal PbI_2 formation after 400 min. The authors proposed that TPA^+ molecules passivate surface defects, particularly unbounded lead, hindering H_2O penetration into the crystalline structure. Maniyarasu *et al.* incorporated 1-octyl-3-methylimidazolium chloride ionic liquid (IL) into the $FA_{0.9}Cs_{0.1}PbI_3$ perovskite to stabilize it and tracked the humidity-induced degradation with near ambient pressure x-ray photoelectron spectroscopy (NAP-XPS) from 0% RH to 30% RH.[28] It was concluded that cation-mixture improved moisture stability but that the IL additive did not further improve the performance in humid conditions. The pristine IL-perovskite showed signs of water incorporation as an O1s core level signal that increased under humidity conditions, indicating continuous incorporation of water in the IL. Other peaks corresponding to perovskite did not undergo many changes, in contrast to other studies done on $MAPbI_3$. The incorporation of water disrupts the passivation of the ionic liquid, yet as we will mention in Sec. IV, the additive showed usefulness for thermal stability.[28]

With the above examples, ongoing debate about the detrimental effects of humidity on perovskite, more specifically regarding the pathways that result in PbI_2 degradation product, has to some degree been solved. On the basis of complementary works, the moisture ingress in $MAPbI_3$ perovskite causes a reversible intermediate monohydrate that evolves into a permanent perovskite dihydrate.[15] Thanks to the *in situ* studies, the kinetics of the formation of these hydrates are known for different humidity conditions. Large-grain thin films are less receptive to humidity-induced degradation because of the reduced area for moisture ingress, i.e., water molecule permeation is enhanced at surface defects and gaps between crystallites. That vapor-induced degradation occurs via initial deprotonation of the MA^+ by water to form MA (gas) and hydrated HI, apart from the final PbI_2, has consequently been disputed. Such highly volatile products would be flushed out if created, leading to irreversible degradation. When reversibility was seen even in open chambers and during gas-flow,[23,26] it was proof of intermediate steps before decomposition. This provides hope that after-treatments, such as drying, can remedy early degradation before proceeding to chemical decomposition. Isolation of devices from atmosphere gases by encapsulation and passivation are very effective, therefore somewhat rendering humidity discussions extinct. Yet, production and accumulation of degradation products can be self-catalytic; small errors in fabrication where humidity remains can be detrimental to long-term stability. For PSC technology to fulfill its low-cost fabrication promises, stability against oxygen and humidity must be fully understood and controlled.

A lack of consensus in the literature regarding dry and humid air is observed, while in some works 30% RH is referred to as "drying" conditions,[24] other works use UHV or pure O_2 or N_2 gas,[28] while 30% RH is considered "humid." Our proposed general reading among these discrepancies is that, if water molecules are dissociated from the crystal, it is "drying." We would like to clarify that because of single stressing conditions, some authors argued that only the moisture component in ambient conditions plays a role in perovskite degradation, while O_2 itself seldom had any effect. As will be presented later, this is greatly disputed, once other stressors are added O_2 concentration is important.

III. ILLUMINATION

Illumination is an unavoidable part of achieving photovoltaic response in solar cells. Light photoexcite carriers in the perovskite provide the desired electric current, but the free electrons can also trigger unwanted chemical reactions that are detrimental to the stability. Illumination effects also seem to be the strongest when carriers are accumulated inside the structure without being collected (i.e., in films without contacts or devices at an open circuit).

A. Extrinsic material reactions

While perovskite film is rather insensitive to pure oxygen in the dark,[29,30] the photoexcited electrons under illumination react with oxygen molecules creating superoxides (O_2^-) that further catalyze a rapid dissociation of the crystal.[31] Similar reactions can happen with the H_2O molecules in moist air. Whereas almost saturated air with relative humidity (RH) close to 95% can lead to perovskite decomposition in the dark, lower RH does not induce perovskite degradation unless it is triggered by illumination.

The decomposition pathways are diverse, depending on the stress conditions and the perovskite stoichiometry. Below we provide a review of the most relevant *in situ* studies that addressed the synergetic effects of light and ambient stressors.

Senocrate *et al.* studied the $MAPbI_3$ degradation kinetics by *in situ* XRD and UV–vis absorbance of the film under O_2 gas flow with and without illumination.[30] The perovskite gradually depleted in both O_2 and light until only PbI_2 absorption was left, the PbI_2 [0 0 1] peak dominated the XRD spectra, and the decay rate increased proportionally with light intensity. Adding a small partial pressure of I_2 [$P(I_2) = 1.4 \cdot 10^{-5}$ bars] substantially decreased the O_2-induced degradation, reinforcing that I_2 is one of the sub-products of such degradation. Since air contains both oxygen and water, other works employed air with varying humidity conditions to be closer to real conditions.

Tang *et al.* showed unchanged $MAPbI_3$ 2θ peaks for 24 h in dark and 40% RH, which faded almost immediately upon illumination [Figs. 4(1c) and 4(1d)].[32] In a vacuum, the major degradation was attributed to MA loss, which accelerated under illumination vanishing $MAPbI_3$ signal within 6 h [Figs. 4(1a) and 4(1b)], leading to crystalline PbI_2 and Pb^0 [Fig. 4(1b)]. Nakamura *et al.* reported more detailed $MAPbI_3$ degradation products using 2D wide-angle x-ray scattering (2D-WAXS) [Fig. 4(2a)].[33] Under simultaneous light (100 mW/cm^2) and humidity (95% RH) exposure, $MAPbI_3$ degraded into smaller crystallite sizes and crystalline forms of $NH_4PbI_3 \cdot 2H_2O$ and CH_3NH_3I (but no PbI_2). Dark conditions in 95% RH only formed PbI_2 and increased $MAPbI_3$ grain sizes [Figs. 4(2c) and 4(2d)], in contrast with the previous report in which 40% RH in dark did not trigger any XRD changes.[32] Probably there is a threshold on the humidity concentration that is detrimental for the perovskite. Ho *et al.* reported a different degradation mechanism on $FA_{0.85}Cs_{0.15}PbI_3$.[34] Coupled atomic-force microscopy (AFM) with photo-thermal induced resonance (PTIR) enabled (<100 nm) spatial resolution mapping of the FA cation [Fig. 4(3)]. The mixed cation perovskite segregates into δ_o-$CsPbI_3$ needle crystals and large δ-$FAPbI_3$ grains that further degrade to PbI_2. In this work, 10 mW/cm^2 LED illumination and 20%–85% RH were applied *ex situ* in the AFM chamber with the instrument off to avoid laser damage. By using Raman spectroscopy, Pistor *et al.* monitored

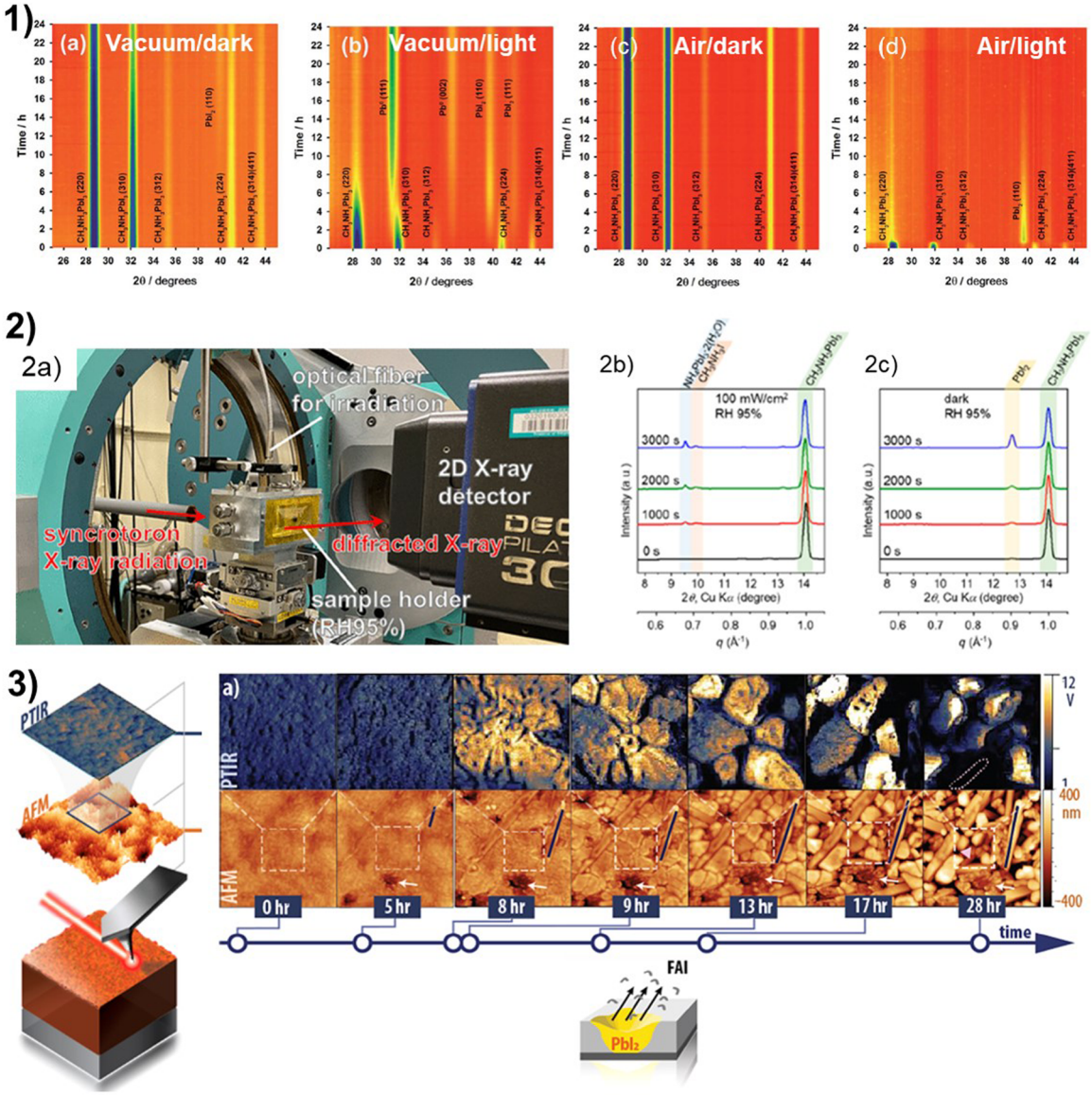

FIG. 4. (1) *In situ* XRD of $CH_3NH_3PbI_3$ films at 350 K under (1a) vacuum/dark, (1b) vacuum/light, and under air without (1c) or with (1d) light illumination. Reproduced with permission from Tang *et al.*, J. Mater. Chem. A **4**, 15896 (2016). Copyright 2016 The Royal Society of Chemistry. (2a) System for *in situ* 2D-WAXS measurement under light radiation and humid conditions. Time evolution of integrated 1D-WAXS patterns of $CH_3NH_3PbI_3$ polycrystalline thin films under (2b) illumination and humid conditions and (2c) humid conditions. Adapted with permission from Nakamura *et al.*, ACS Mater. Lett. **4**, 2409–2414 (2022). Copyright 2022 American Chemical Society. (3) Schematic showing AFM and PTIR images obtained on the same area. AFM morphology (orange) and PTIR (blue) at 1712 cm^{-1} under high humidity and light. Below, the schematic shows formamidinium iodide (FAI) evaporates, and depressions form. Adapted with permission from Ho *et al.*, ACS Energy Lett. **6**(3), 934–940 (2021). Copyright 2021 American Chemical Society.

$MAPbI_3$ film surface in air and found PbI_2 formation after 5 min of laser irradiation (260 W/cm^2).[35]

B. Intrinsic material reactions

Incident photons under illumination excite carriers in the device, providing the desired electrical output, but these charges can also trigger changes in the material. Charge separation creates internal electric potential, which is often larger than the activation energy for the migration of ions, and induces strain in the crystal lattice. Several examples found in the literature refer to this phenomenon with different terms: "halide segregation," "phase separation," "ion migration/distribution," or "ion accumulation at interfaces/grain boundaries." The interested reader can refer to a complete perspective on ion segregation for more details.[36] Often, the changes are reversible in dark, but the light-induced changes can also be irreversible when crystal phase changes or chemical reactions or

are involved, leading to material decomposition. *In situ* characterization of an illuminated sample is an important tool to capture the immediate effects of ion motion on the device and material degradation.

1. Single halide perovskites

One of the first light-soaking effects observed *in situ* was the increase in PL emission intensity (also called *photobrightening*) with longer laser irradiation.[37–40] deQuilettes *et al.* found that the PL photobrightening of $MAPbI_3$ films was correlated with an increase in the time-resolved PL (TRPL) lifetime.[37] The timescale of the photobrightening in an isolated film was similar to the V_{oc} rise of a PSC, suggesting a reduction in the bulk trap state density. ToF-secondary-ion-mass spectrometry (ToF-SIMS) depth profiling measured immediately after the laser excitation [Fig. 5(1)], provided one of the first direct evidence of photo-induced iodide migration. Even though this measurement was done on an isolated $MAPbI_3$ film, its implications for the device's stability were important. A later work by Choi *et al.* spatially resolved the PL evolution in the polycrystalline film and the chemical composition by nanoscale-resolved-ToF-SIMS.[41] They found that higher oxygen content in illuminated samples was correlated with greater PL lifetime and proposed that light promotes O^{2-} diffusion into the grains, passivating lattice defects.

The existence of contradictory reports regarding the PL response upon illumination (increase or decrease) motivated Quitsch *et al.* to study the excitation-wavelength-dependence on PL evolution, in air.[38] Photobrightening occurred with long wavelengths, and a gradual trend to decreased emission toward PL quenching was observed at the 520 nm threshold (PbI_2 bandgap) [Fig. 5(2)]. The authors proposed that the process initiates by photolysis of existing PbI_2 impurities to Pb^0 and I_2,[42] and I_2 further decomposes $MAPbI_3$, quenching its PL.[43] In vacuum and dry air, only photobrightening at 405 nm was observed, suggesting that photo-decomposition requires the presence of moisture. Merdasa *et al.* tracked the film absorption, PL quantum yield (PLQY), and TRPL along 6 h illumination in the humid air.[44] The formation of PbI_2 caused (i) parasitic absorption that reduced the perovskite PLQY below 520 nm and (ii) a gradual increase in TRPL lifetimes. The authors proposed that interfacial PbI_2 is beneficial for defect passivation but bulk PbI_2 provides detrimental non-radiative recombination centers.[44] Besides UV–vis illumination, perovskite is poorly stable under e-beam, posing an uncertainty for the characterizations using accelerated electrons. Yuan *et al.* combined PL and SEM imaging to demonstrate that the 10 keV e-beam quenched the PL signal and reduced the film thickness by releasing volatile compounds.[45] Interestingly, e-beam exposure prevented further film morphology degradation under illumination, indicating a complex relationship between electrical currents and ion migration.

The possibility of fabricating PSC on lightweight substrates makes it appealing for space applications. Outside the protective Earth's atmosphere, *in operando* conditions must include harsh radiation. For that, Paternó *et al.* measured the J–V curve evolution of $MAPb(I_xCl_{1-x})_3$ solar cells under visible light and neutron irradiation in a synchrotron.[46] It was proposed that neutron irradiation forms "benign" traps in the perovskite that decrease the leakage current of the device, concluding that PSC are resilient to neutrons thus could potentially be used in space applications.

The substitution of all or part of the MA with less volatile organic cations, formamidinium (FA^+) and Cs^+, provides an intrinsically higher stable perovskite while retaining an appropriate E_g. Systematic *in situ* XPS analysis comparing various combinations of the three cations confirmed the lower degradation rates for triple cation perovskite upon illumination.[47] However, perovskites with mixed cation still suffer light-induced instabilities that have been less studied in the literature. Lu *et al.* studied compositional changes of α-$FACsPbI_3$ films exposed to LED illumination with different excitation wavelengths (624, 520, 435, and 366 nm) in the XPS chamber.[48] While visible wavelengths resulted in a Cs^+ migration toward the bulk, UV light-induced degradation of the PbI_6^{4-} into Pb^0 and I^-. A similar *in situ* XPS study on iodine-excess $CsFAPbI_3$ revealed that 473 nm light-activated perovskite decomposition, catalyzed by

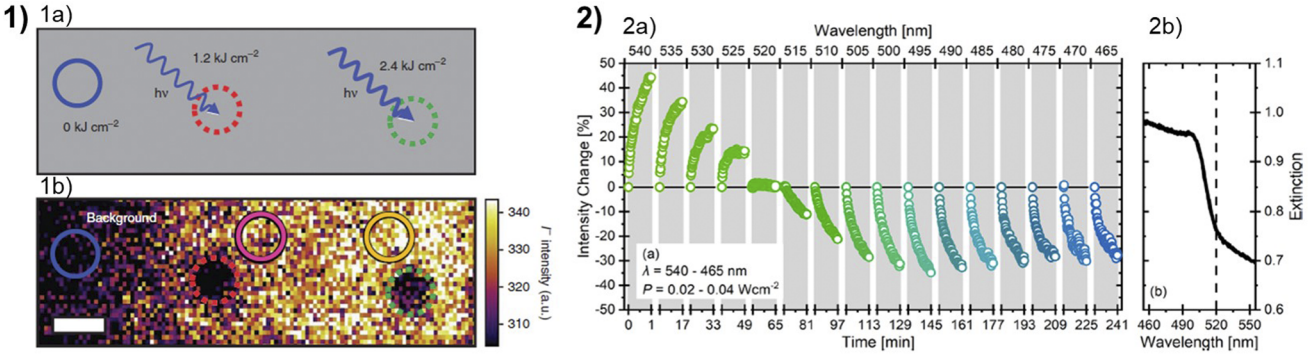

FIG. 5. (1) ToF-SIMS depth profiling. (1a) Schematic of photon dose-dependent experiment indicating the regions exposed to 1.2 kJ cm^{-2} (red dotted circle) and 2.4 kJ cm^{-2} (green dotted circle). (1b) ToF-SIMS image of the iodide (I^-) intensity distribution summed through the film depth after local exposure to the photon doses shown in (1a). Adapted from deQuilettes *et al.*, Nat. Commun. **7**, 11683 (2016). Copyright 2016 Author(s), licensed under a Creative Commons Attribution 4.0 License. (2) Transient PL efficiency change for different excitation wavelengths. (2a) Time traces of the PL intensity of a $MAPbI_3$ film sample for 60 s illumination at each excitation wavelength between 540 and 465 nm and measured in air. (2b) Extinction of a degraded $MAPbI_3$ layer with increased PbI_2 content in the spectral region around the PbI_2 bandgap. Reprinted with permission from Quitsch *et al.*, J. Phys. Chem. Lett. **9**(8), 2062–2069 (2018). Copyright 2018 American Chemical Society.

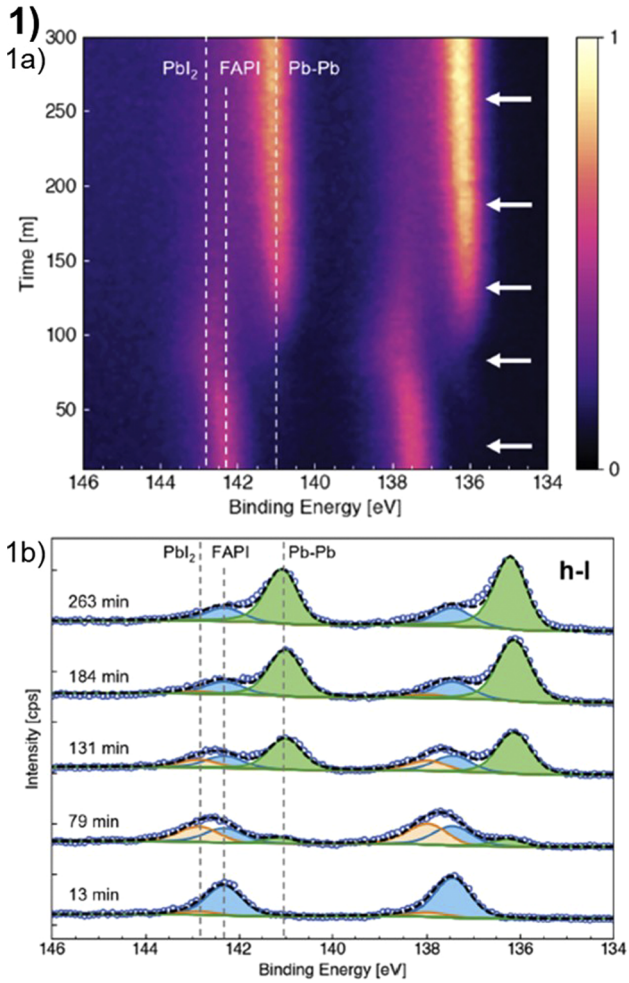

FIG. 6. (1a) Time-resolved *in situ* XPS spectra. Intensity map Pb 4f core-level spectra with time. Dotted lines indicate centroid positions. (1b) XPS fit results for spectra marked with arrows in panel (2a) for blue-laser-exposed perovskite samples with I/Pb = 3.8. Reprinted with permission from Donakowski *et al.*, ACS Energy Lett. **6**(2), 574–580 (2021). Copyright 2021 American Chemical Society.

I^{3-} [Fig. 6(1)]. Donakowski *et al.* suggested that photo- and thermal degradation could be prevented by adjusting the perovskite stoichiometry.[49]

2. Mixed halide perovskites

As the perovskite research field matured, more complex halide perovskite stoichiometries provided greater stabilities than simple $MAPbI_3$, also enabling a broad E_g tuning, but had the issue of the halide segregation. This phenomenon was reported for the first time in 2015 by Hoke *et al.*[50] Several *in situ* PL works revealed the formation of the I-rich phase for various I/Br ratios on $MAPb(Br_xI_{1-x})_3$ perovskite, and some authors refer to it as "the Hoke effect."[51] While the I-rich phase emission increases, the initial mixed-halide emission peak diminishes, such segregation happens for all wavelengths above the perovskite. It was hypothesized that smaller E_g I-rich domains act as carrier sinks for the injected charges from the wider-E_g Br-richer phase. This finding had important implications for the device stability, as it implies a reduction of the maximum achievable V_{oc} of the mixed-halide-based solar cells.

Since then, much work was devoted to understand this phenomenon and all the variables that influence it, such as the A-site cation composition of the perovskite.[51,52] Sutter-Fella *et al.* investigated the reasons for the greater stability of the CsFA compared to MA perovskite for various I:Br ratios.[53] Halide demixing (within 10–20 min) occur for both perovskites with high Br/I ratio, Fig. 7(1), with slight differences. While MA-based perovskite segregation happened in similar pathway to the report of Hoke, CsFA perovskite showed an intensity increase for both emission wavelengths, suggesting a reduction of the non-radiative recombination.[53] *In situ* synchrotron XRD showed significant broadening of the MA-perovskite diffraction peaks and splitting due to formation of I-rich crystals [Figs. 7(1d) and 7(1e)]. In contrast, CsFA-perovskite showed just a small peak broadening [Fig. 7(1f)], i.e., the new I-rich domains are unable to relax the strain to attain a new lattice parameter, constrained by the material around it. The hindered lattice relaxation would therefore be the key for higher stability in mixed cation/halide $CsFAPb(I_xBr_{1-x})_3$ perovskite. A later work on a similar cation composition $[FA_{0.8}Cs_{0.2}Pb(I_{0.7}Br_{0.3})_3]$ demonstrated the suppression of halide segregation by incorporating potassium iodide (2 mol. %) in the lattice, perhaps due to a hindering on the ion migration due to the presence of K^+.[54]

While the scientific community reached a consensus that photo-excited carriers were the main driving force for halide segregation, the exact mechanism remained (and still is) elusive. Knight *et al.* demonstrated that halide segregation is not dependent on the accumulated number of photo-generated carriers, but rather on the number of charges that recombine through trap states.[55] This was based on the observation of a much higher segregation rate (I-rich-peak vs mixed-cation-peak intensity ratio) when illuminating a certain number of photons for long time (low intensity light, long exposure) than when providing the same photons but in a short time (high intensity light, short exposure) [Fig. 7(2)]. At high illumination intensities, the large number of generated carriers were enough to fill the traps, promoting mainly band-to-band recombination, while low photon flux results in substantial trap-mediated recombination that accelerates halide segregation. Therefore, to avoid segregation, the number of carriers recombining via traps should be lower than 0.1%, providing clear guidelines for the optimization of PSCs.[55] *In situ* PL measurements on single-crystal $CsPbBr_{2.1}I_{0.9}$ platelets confirmed that halide segregation routes depend on illumination power and atmosphere conditions, independently on single crystal or polycrystalline film.[56] Low power density resulted in the simultaneous segregation of a pure-I-phase and a I-rich-phase, which later merged to an intermediate I-rich phase after 25 min illumination. The authors proposed that pure I-phase was formed at the crystal surface and eventually reaches a thermodynamic equilibrium with the bulk forming intermediate segregated phase. When the measurements were done in the presence of dry oxygen, the evolution of the segregated phases became more complex, again emphasizing the importance of surfaces in the segregation mechanism.[56] Halide segregation phenomena is not limited to polycrystalline films with abundant defects caused by the solution-based fabrication methods. Mao *et al.* proved that halide segregation was an intrinsic

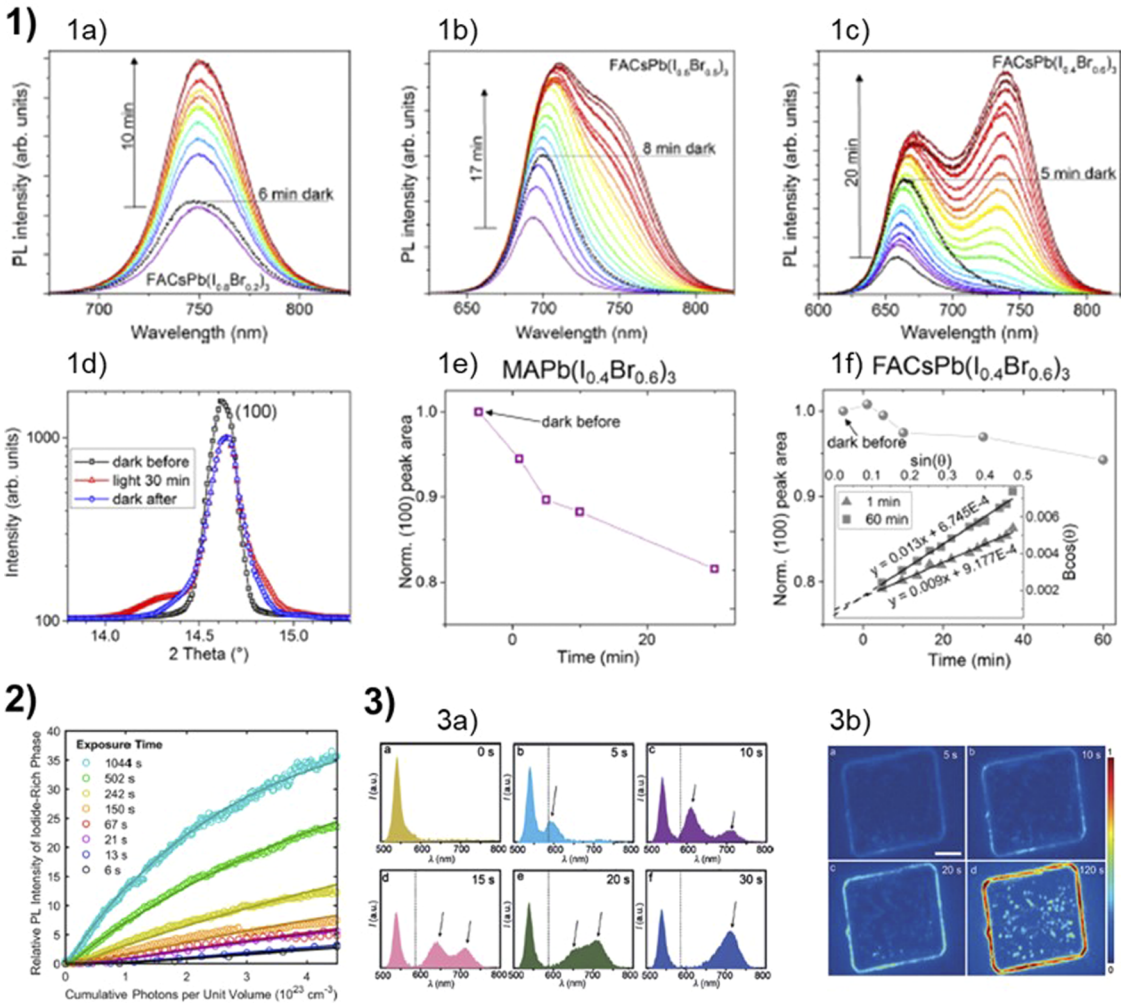

FIG. 7. (1) Time evolution of steady-state PL spectra of $FACsPb(I_{0.8}Br_{0.2})_3$ (1a), $FACsPb(I_{0.5}Br_{0.5})_3$ (1b), and $FACsPb(I_{0.4}Br_{0.6})_3$ (1c) thin films taken at ~50 mW/cm^2 in 1 min increments. Synchrotron x-ray diffraction data and analysis of the [(1d) and (1e)] $MAPb(I_{0.4}Br_{0.6})_3$ and (1f) $FACsPb(I_{0.4}Br_{0.6})_3$ samples. (1d) [100] diffraction peaks before illumination, during, and after relaxation in the dark. (1e) and (1f) Normalized peak area under illumination over time. The inset in (1f) shows the Williamson–Hall plot of the XRD peak FWHM under illumination for 1 and 60 min. Adapted with permission from Sutter-Fella *et al.*, Nano Lett. **18**(6), 3473–3480 (2018). Copyright 2018 American Chemical Society. (2) Evolution of the PL intensity originating from the low-bandgap iodide-rich phase of $MAPb(Br_{0.5}I_{0.5})_3$ plotted against the number of incident photons per unit volume. Adapted from Knight *et al.*, ACS Energy Lett. **4**(1), 75–84 (2019). Copyright 2019 Author(s), licensed under a Creative Commons Attribution 4.0 License. (3a) Time-dependent fluorescence spectra of light-induced phase segregation recorded in the center of a single $MAPb(Br_xI_{1-x})_3$ microplatelet over 30 s, excited by a 400 nm pulsed laser (3.5 W cm^{-2}). (3b) Widefield PL images of a $MAPb(Br_xI_{1-x})_3$ single crystal collected in the I-rich emission region (660–700 nm), excitation source of 400–450 nm, 5 mW cm^{-2} was used. Scale bar: 5 mm. Adapted with permission from Mao *et al.*, Angew. Chem., Int. Ed. **58**(9), 2893–2898 (2019). Copyright 2019 John Wiley & Sons.

phenomena in perfect lattices by studying a single crystal of $MAPb(Br_xI_{1-x})_3$ perovskite with spatially and spectrally resolved *in situ* PL and TRPL.[57] Upon illumination, two segregated PL peaks appeared, similar to the observations on $CsPbBr_{2.1}I_{0.9}$ single crystals,[56] but with the difference that the peak at ~720 nm (I-richest) did not blue shift, while the I-rich intermediate peak gradually redshifted [Figs. 7(3a) and 7(3b)]. Segregation was found to happen at the center of the crystal, proving that it does not happen necessarily at the grain boundaries/crystal surface.

Despite the fruitful information uncovered by PL techniques, they fail to identify the formation of non-emissive Br-rich domains. To overcome this limitation, Halford *et al.* monitored the photo-induced phase segregation using *in situ* grazing incidence wide angle x-ray diffraction (GIWAXS) with ~1 sun illumination for 1 h [Figs. 8(1a) and 8(1b)].[58] Independently on the initial $MAPb(I_{(1-x)}Br_x)_3$ halide ratios, the segregated phases had fixed compositions, i.e., a majority of I-rich (x = 0.20) and (non-emissive) Br-rich (x = 0.93) phases. The reversible remixing in dark [Fig. 8(1c)] was found to be substantially slower. Kim *et al.* employed a combination of AFM, piezoresponse force microscopy (PFM), contact potential difference (CPD), and XRD with *in situ* illumination and biasing to reveal the microscopic structural changes produced in

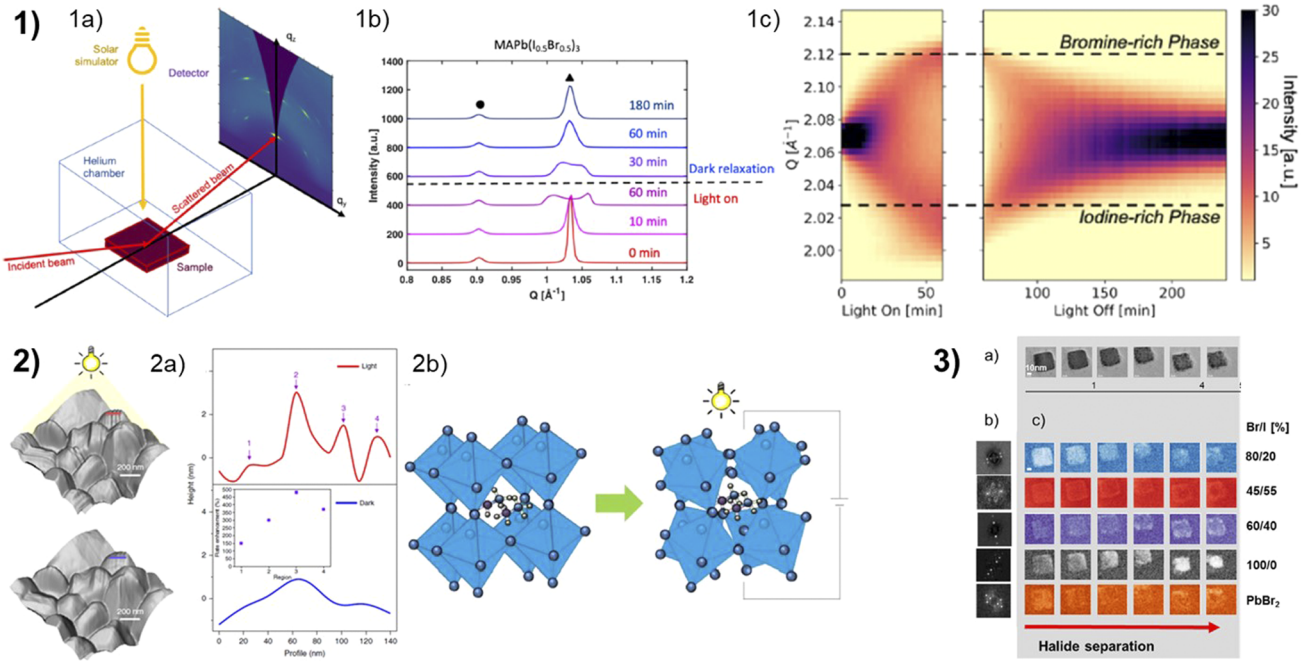

FIG. 8. (1) *In situ* GIWAXS of MOHPs highlighting (1a) the experimental setup used to capture the dynamic structure of MOHPs under ~1 sun illumination and (1b) $MAPb(Br_{0.5}I_{0.5})_3$ structure under 60 min of ~1 sun illumination followed by 180 min in the dark. (1c) Dynamics of structural changes under illumination as shown via changes in diffracted intensity around the (200) perovskite peak for the $MAPb(Br_{0.5}I_{0.5})_3$ perovskite. Adapted with permission from Halford *et al.*, ACS Appl. Mater. Interfaces **14**(3), 4335–4343 (2022). Copyright 2022 American Chemical Society. (2a) 3D topography with (above) and without t (below) and corresponding line profiles (right) for topography under light (red) and dark (blue). The inset represents rate enhancement at the marked regions. (2b) Schematic illustration of the octahedral distortion induced by bias voltage and light illumination. Adapted from Kim *et al.*, Nat. Commun. **10**(1), 444 (2019). Copyright 2019 Author(s), licensed under a Creative Commons Attribution 4.0 License. (3a) HRTEM images acquired during 5 min (3b) characteristic diffraction patterns of the five abundant structures and (3c) corresponding abundance maps identified as $CsPb(Br_xI_{1-x})_3$ for x = 0.8, 0.45, 0.6, 1, as well as $PbBr_2$. Adapted with permission from Funk *et al.*, J. Phys. Chem. Lett. **11**(13), 4945–4950 (2020). Copyright 2020 American Chemical Society.

the $MAPb(Br_xI_{1-x})_3$ film.[59] Illumination caused an increase in the overall piezoresponse signal of the film, larger CPD at the grain boundaries, and the formation of nanoscale ferroelastic domains in some grains of the film, seen also as increased surface corrugation of ±3 nm [Fig. 8(2a)]. A reversible broadening of the FWHM was associated with an increase in the strain disorder [Fig. 8(2b)]. This work found that the illumination induced mostly reversible changes, while bias poling effects were not completely reversible. The irreversible formation of amorphous material upon electrical biasing was a probable causes of device degradation in PSCs.[59]

Funk *et al.* tracked the e-beam-induced phase segregation of CsPb-halide perovskite nanocrystals grown on a TEM grid by using high resolution (HR)-TEM.[60] Multivariate analysis methods enabled the (spatially resolved) deconvolution of diffraction patterns for Br:I ratios 80:20, 45:55, 60:40, 100:0 and $PbBr_2$ [see Fig. 8(3)]. Substantial changes appeared the first 5 min of irradiation, i.e., large parts of the crystal became amorphous, and the original 80:20 uniform composition changed to pure Br-perovskite in the crystal center and predominantly 60/40 (I-richer) around the edges. Note that Br-rich phases could not be detected before by solely using PL methods. The authors hypothesized that the asymmetry in ionic bonding strength of I and Br with Pb caused lattice strain that relaxed under irradiation (e-beam or light) creating separated phases. Cappel *et al.* minimized the x-ray damage on the perovskite by employing the *LowDose* synchrotron beamline for their photoemission spectroscopy (PES) measurements.[61] PES analysis provided two main insights into the surface chemical changes of MAFAPb(I–Br) perovskite illuminated with a 515 nm laser with varying energy. First, a gradual formation of Pb^0 with illumination time, partly reversible in dark, provided that there is I_2 buried in the lattice. Second, an increase in Br^- signal and reduction of I^- and Pb^{2+}, suggesting a phase separation into Br-rich regions at the surface and I-rich regions in the bulk. The authors proposed that Br-rich segregation occur at the grain boundaries, contrasting with the works by Funk *et al.* where single crystal also showed Br-rich segregation in the crystal center.[60] Probably the different perovskite cations (MAFA vs Cs) and stress sources (visible laser vs e-beam) used in the works of Cappel and Funk, respectively, originate diverse mechanisms for halide segregation. Future works would benefit of exploring various perovskite compositions to ultimately obtain a universal model for the phase segregation phenomena.

Among the *in situ* reports found in the literature, we observed that a vast majority of experiments use steady-state PL, TRPL, and photo-induced absorption to track light-induced changes in the optoelectronic properties, taking advantage of the laser excitation of the instrument to perform light soaking.[50,52,62–67] Other reports complemented the knowledge on the material crystallinity and composition with *in situ* XRD techniques and x-ray

photoelectron spectroscopy (XPS), respectively, by adding a light source through the windows of the instrument chambers.[50,68–72] Other less readily available *in situ* techniques, such as ToF-SIMS, TEM, synchrotron beamlines, or custom-made setups, provided valuable insights into complete the overall knowledge on perovskite light-induced degradation.

IV. THERMAL STRESS

Temperature is an unavoidable stressor in photovoltaic applications since sunlight radiation includes infrared heating energy. According to international protocols,[6] heating between 60 and 85 °C should be considered normal during operation, yet margins for higher temperature endurance are important to withstand applications in hot climates or incorporated in technology that might get warm under operation.

There is a consensus in the literature that PbI_2 is the product of thermal degradation of $MAPbI_3$, yet the degradation path depends on stress-level applied and the measurement environment. An intermediate PbI_2-like structure acts as the base for PbI_2 formation, similarly to how this intermediate seems to act as base for MAI intercalation. Therefore, thermal degradation is often called the reverse of perovskite formation. Breakage of the Pb–I–Pb bonds in the [001] direction leads to the formation of an intermediate with channels, allowing for increased migration of species throughout the material. This allows for metallic lead (Pb^0), iodide, I^-, $CH_3NH_3^+$, HI, and CH_3NH_2 to quickly migrate and either diffuse or implant inside the perovskite grains or interfaces. Intermediate structures or even amorphization of the material arises to start recrystallization that stops at the more stable PbI_2. The creation of PbI_2 during heating of $MAPbI_3$ seems to arise from crystal instability caused by the organic cation. Under isolated, low thermal stress (<130 °C), the reaction is a layer-by-layer transformation starting with dangling bonds on the surface of perovskite crystallites. Layer-by-layer decomposition mechanisms can be slowed down by passivation of dangling bonds or increased integrity of the crystal at surfaces and grain boundaries.

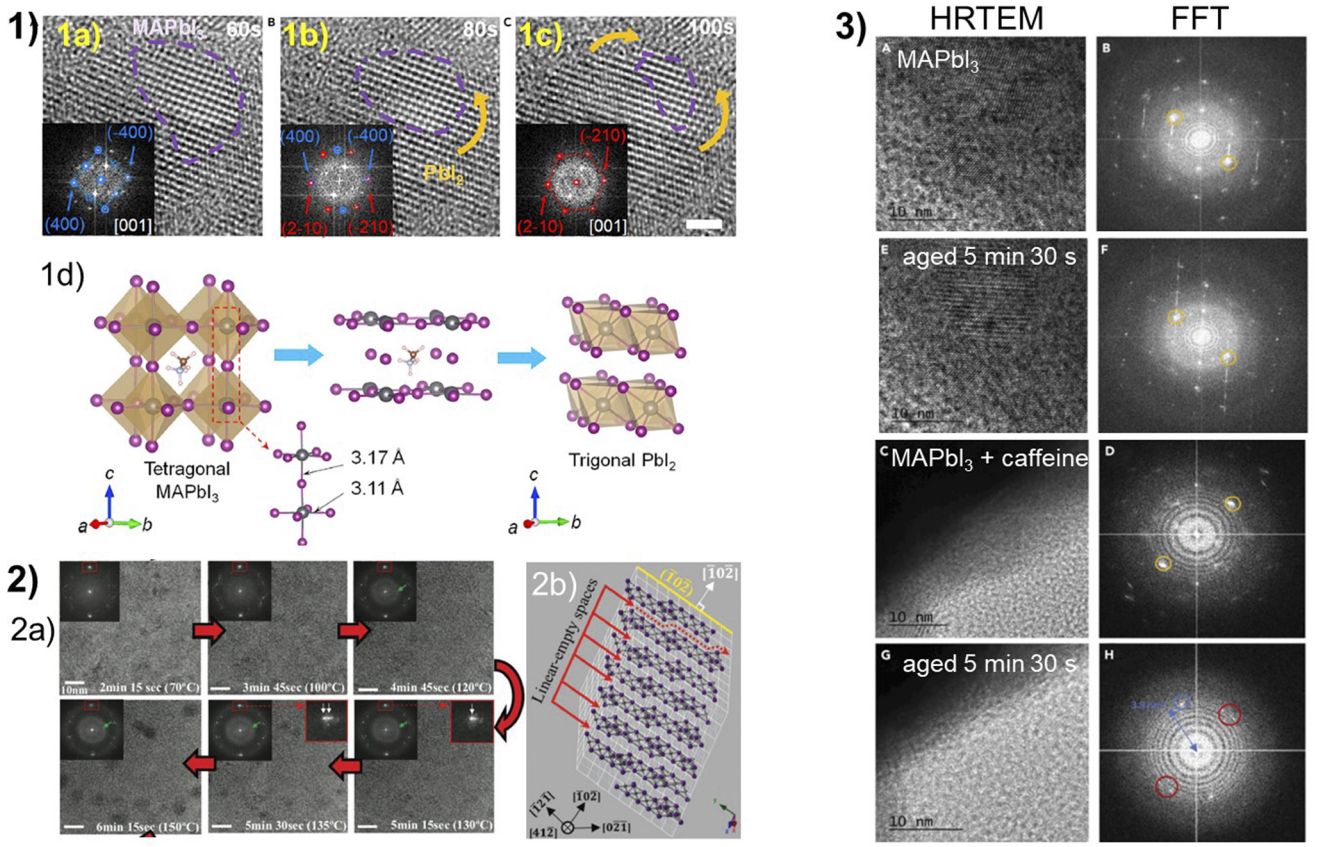

FIG. 9. (1a)–(1c) Degradation process of an individual $MAPbI_3$ grain. The purple dashed lines outline the shrinking perovskite grain as it degrades to PbI_2. Insets: FFT phase diagrams of the corresponding HRTEM images. Scale bar, 2 nm. (1d) Transition from $MAPbI_3$ with a tetragonal configuration to PbI_2 with a trigonal configuration. Reprinted with permission from Fan *et al.*, Joule **1**(3), 548–562 (2017). Copyright 2017 Elsevier. (2a) HRTEM images and FFTs obtained from the *in situ* HRTEM, demonstrating the detailed intermediate process. Critical alterations, emergence of black dots, and splitting of diffraction spots (white arrows in the red rectangles) are observed from ≈130 °C (2b) Simulated cross-sectional thin plate of a perfect trigonal PbI_2 crystalline along [412]. Reprinted with permission from Kim *et al.*, Adv. Funct. Mater. **28**(42), 1804039 (2018). Copyright 2018 John Wiley & Sons. (3) HRTEM of (A) fresh caffeine-containing PVSK, (C) fresh pure PVSK, (E) aged (5 min 30 s) caffeine-containing PVSK, and (G) aged (5 min 30 s) pure PVSK. Corresponding fast Fourier transforms (FFTs) of (B) fresh caffeine containing PVSK, (D) fresh pure PVSK, (F) aged (5 min 30 s) caffeine containing PVSK, and (H) aged (5 min 30 s) pure PVSK. Adapted with permission from Wang *et al.*, Joule **3**(6), 1464–1477 (2019). Copyright 2019 Elsevier.

At higher temperature stress (130–150 °C), the reaction happens fast and seem to pass by a more amorphous soup containing the perovskite components. Degradation of $MAPbI_3$ seems to occur at all elevated temperatures, although the stress seems partly reversible until final formation of PbI_2. For mixed cation perovskite compositions, thermal degradation becomes considerably more complicated. Due to the atomic radius differences, there seems to be an increase in integrity of the crystal lattice. *In situ* electron microscopy has allowed for video-recordings of thermally induced degradation in real-time, and videos can be found in the supporting information of several articles.[73,74] Because of the strong dependence of thermal stability on the crystalline composition, we will first discuss the stability of $MAPbI_3$ followed by mixed cation and mixed halide compositions as seen by *in situ* characterization methods.

Fan *et al.* used *in situ* TEM to monitor the reciprocal selected-area electron diffraction (SAED) signal from the crystalline structure of a $MAPbI_3$ microplate, while it was subjected to 85 °C in a heated environmental gas cell.[75] The initial preferential orientation of the crystal [001] still remained after applying a thermal stress (85 °C), but after 60 s, the hexagonal pattern corresponding to PbI_2 appeared [Figs. 9(1a)–9(1d)]. After only 100 s, 75% of the initial hexagonal $MAPbI_3$ material was estimated to be converted to trigonal PbI_2 phase [Figs. 9(1c) and 9(1d)]. They found that PbI_2 formed similar to the reverse process of formation of $MAPbI_3$ via intercalation of MAI into PbI_2.[76] The conversion showed every indication of being directly sequential and persistence of initial peaks throughout the transition proved that the periodicity of the [400] direction in $MAPbI_3$ coincides with the {210} facets of the PbI_2 structure after transitioning. It is suggested that heating stimulates breakage of the [001] Pb–I–Pb bonds, promoting the release of $CH_3NH_3^+$ and I^- ions in the form of CH_3NH_2 and HI gas. PbI_2 forms immediately but is held in an intermediate lattice structure first (keeping the lattice spacing of the $MAPbI_3$ [400]) before transforming into regular trigonal PbI_2 (at 420 s). The degradation pathway was the same independently of using dry air (2% RH, 700 Torr) or vacuum (0% RH, 1 Torr), and density functional theory (DFT) calculations from the *in situ* SAED data confirmed the reaction and that the degradation was driven from the surface of the crystallite in a layer-by-layer manner.[75] In contrast to the results presented by Kim *et al.*, Fan *et al.* used high resolution TEM (HRTEM) to report an intermediate step in the PbI_2 formation via an amorphized $MAPbI_3$ layer.[74,75] Instead of using a controlled heating stage,[75] the sample was heated with the electron beam from the TEM. The sample was estimated to be heated from 25 to 170 °C, Fig. 9(2a), where a gradual change of $MAPbI_3$ diffraction peaks [by Fast Fourier Transform (FFT)] into amorphous rings started at 70 °C (2 min 15 s). This was followed by the formation of crystalline black dots from 130 °C (3 min 5 s) onwards, seen nucleating on the sample with amorphized surroundings on the TEM image. The intermediate phase shows oriented channels that could enhance ion transport and facilitate the formation of the PbI_2 [Fig. 9(2b)]. Together these two works indicate that, with high irradiation, amorphization may occur due to the faster breaking of Pb–I–Pb bonds, fast segregation of the products led to more condensed crystallites of PbI_2 growing from the amorphous phase. The growth of the PbI_2 grains still showed preference for growth toward the surface.[74] As a last example of *in situ* TEM on $MAPbI_3$, focused ion beam (FIB) cross sections (CS) of full solar cell devices with four different fabrication methods were compared by Divitini *et al.*[73] As they indicate, on cross-sectional samples, particles may migrate on the surface of the sample along the cross-section, i.e., the exposed surface will be an additional migration path that do not exist in an actual device and FIB milling may induce defects seen in the experiment. Still, using a micro-heater *in situ* stage in TEM, they outlined the requisites for obtaining energy dispersive x-ray (EDX) mapping *in situ*. Heating from 50 to 150 °C resulted in iodine and lead migration as a part of the degradation process, but the rate and quantity of such migration occurred differently depending on air exposure during fabrication, and the device fabricated in 50% RH air was more susceptive. For the other samples, the degradation seen in TEM at 200 °C was comparable with degradation seen after storage for a replica device in air for 2 months. Increased susceptibility to heat stress depending on air exposure has also been related to oxygen, as shown by Yang *et al.*[77]

Moving on to mixed composition perovskite, Seo *et al.* reported different thermal-degradation phenomena for devices cross sections, including $MAPbI_3$ and $Cs_{0.175}FA_{0.750}MA_{0.075}Pb(I_{0.880}Br_{0.120})_3$, within device architecture ITO/mp-NiO_x/perovskite/PCBM/mp-ZnO/Ag.[78] It was the first study of *in situ* TEM thermal degradation of triple cation PSC. The perovskite film samples were held for

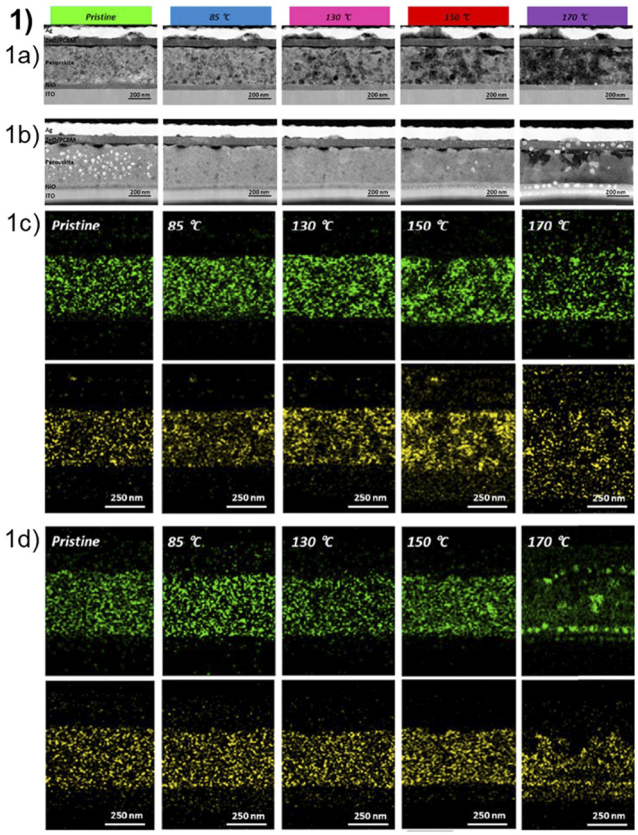

FIG. 10. (1) STEM images of (1a) MA-, and (1b) Cs/FA/MA- based PSC sample and EDS elemental mapping images of lead (green) and iodine (yellow) for (1c) MA-, and (1d) Cs/FA/MA- based PSC sample, after heating from RT to (85, 130, 150, and 170) °C. Reprinted with permission from Seo *et al.*, Nano Energy **77**, 105164 (2020). Copyright 2020 Elsevier.

30 min at 85, 130, 150, and 170 °C, and in-between each step, samples were cooled down and electron dispersive x-ray spectroscopy (EDS) maps were acquired for 10 min. The EDS elemental distribution (Fig. 10) revealed that the MA-based device degraded partly at over 85 °C, with gradual growth of defect phases in the $MAPbI_3$ layer [Fig. 10(1a), 130–170 °C]. The Cs/FA/MA-based device, in contrast, resisted degradation up to 130–150 °C, afterward rapid formation of large metallic lead and PbI_2 particles. There was also some gradual degradation of the Ag electrode for the MA device, not observed for the Cs/FA/MA-based device. As redistribution of iodide and Pb happened at much lower temperatures in $MAPbI_3$ [Fig. 10(1c)] than in Cs/MA/FA [Fig. 10(1d)], the authors concluded that activation energy of ion migration was lower in $MAPbI_3$. Mixed cation perovskite, however, degraded considerably faster with more severe morphology deformation [Fig. 10(1b), 170 °C]. It was hypothesized that the thermally induced Br^- vacancies initiated the fast creation of metallic lead.[78] A similar hypothesis was drawn by Long *et al.* by *in situ* AFM for mixed cation and halide perovskite.[79] Aguiar *et al.* studied $FAPbI_3$ decomposition mechanisms with *in situ* STEM, SAED, and *in situ* XRD. They reported nucleation and growth of precipitates containing high levels of lead (PbI_2, Pb^0) above a 175 °C temperature threshold.[80] In addition, with separate *in situ* XRD and *in situ* XPS measurements, Long *et al.* concluded that the FA^+ and Br^- ions lose their interaction with the perovskite crystal during thermal annealing, resulting in a phase richer in I^- than what was intended during fabrication. A lower angle shift of the (100) perovskite peak of $Cs_{0.17}FA_{0.83}PbI_2Br$ along with increased temperatures. The authors hypothesized that the shift was due to Br-loss, since the Br atom occupies less space in the lattice than iodide, it led to an expansion.[79] Thermal expansion of the lattice could originate a similar XRD observation, according to other works.[81,82] Additionally, confirming their hypothesis, the interaction of Br^+ and FA^+ ion extracted by XPS changed at much lower temperatures (100 °C) than iodine. Borchert *et al.* the Cl-containing $MAPbI_3$ film improved its crystallinity until 200 °C, followed by a rapid decrease and the appearance of PbI_2 and metallic lead, seen with *in situ* XRD.[83] Compared to other authors who performed tests in nitrogen atmosphere,[84] the faster decomposition in vacuum was related to the removal of gaseous products. For the pure $MAPbI_3$ film, the results coincided with future findings, i.e., cubic phase formation at ~50 °C, a later increase in crystallinity followed by various unidentified peak changes starting at 150 °C.[74,85,86] It is likely that the ionic radius of the Cl^- also played a role here. Indeed, the exact perovskite stoichiometry greatly influences the ease in which it degrades under thermal stress. A good example is the different activation energies, ~0.66 and ~0.76 eV reported for the thermal degradation of $Cs_{0.17}FA_{0.83}Pb(I_{0.83}Br_{0.17})_3$ and $Cs_{0.05}(MA_{0.17}FA_{0.83})_{0.95}Pb(I_{0.83}Br_{0.17})_3$ films, respectively. These rough values were found by Tan *et al.*, thanks to *in situ* XRD with temperature controlled stage.[87] It is a clear indication that slightly lower Cs^+ concentration has important stabilizing effects at elevated temperatures (up to 150 °C), despite the presence of volatile MA ions.

Juarez-Perez *et al.* identified that the majority of thermally decomposed gas-products of $MAPbI_3$ crystals were CH_3I and NH_3, contrary to some previous reports that suggested that decomposition products were CH_3NH_2 and HI.[86] Their experiments were done by coupling a quadrupole mass spectrometer (MS) to the exhaust of the heating chamber when monitoring the level of degradation of $MAPbI_3$ with thermal gravimetric and differential thermal analysis (TG-DTA) during heating. They could observe MA loss at 294 °C composed of two sections, first decomposition of $MAPbI_3$ and then decomposition of MAI, but during both steps, the only products detected were CH_3I and NH_3. In a later study, they demonstrated that, at temperatures relevant for PSC operation (<100 °C), FA-based perovskite released degradation products to much lesser scale than MA-based. For FA-based samples, they detected signals from sym-triazine ($C_3N_3H_3$), formamidine [$CH(NH_2)_2^+$], and hydrogen cyanide (HCN) in very different amounts depending on the temperature applied to the sample. Such degradation products originate in irreversible reactions. Noticeably, the heating rate did not have any apparent effect on the chemical reactions that occurred. Kim *et al.* used *in situ* surface analysis techniques to also confirm that thermal degradation of $MAPbI_3$ happens through an intermediate forming end products PbI_2, CH_3I and NH_3.[88] This supported the results obtained by mass spectrometry by Juarez-Perez *et al.*[86,89] It was shown that encapsulated PSC devices were not protected against thermal degradation during operational stability tests at 85 °C. *In situ* surface analysis with 2D GIWAXS, HR-XPS, and near edge x-ray absorption fine structure (NEXAFS) under vacuum to perform heat-stress tests allowed screening the top 125 nm surface a $MAPbI_3$ film as it transformed from tetragonal to cubic phase upon increasing temperature from 25 to 80 °C in 20 min. The process was followed by the creation of the intermediate structure mentioned above at 100 °C for 20 min. Note that this time again the PbI_2 planes were kept with longer inter-planar distance than normal PbI_2. Finally, the crystalline PbI_2 degradation-product appears as the other volatile degradation products are removed. Extended exposure to lower temperatures (80 °C) for over 60 min produced similar changes. Finally, they varied the angle of incidence from 0.1° (5 nm depth) to 0.15° (55 nm depth) to 0.2° (125 nm depth) to confirm that the surface of the film had been more degraded. The authors argue that, in encapsulated devices, the degradation would happen in a different pathway since the volatile degradation products may accumulate at the interface or migrate back into other layers of the PSC.[88] Subsequently, *in situ* HR-XPS on the top 10 nm of a $MAPbI_3$ film heated over 100 °C confirmed MA release from the film. These changes appear at much lower temperatures than those indicated by Juarez-Perez *et al.* (~200 °C),[86] suggesting that $MAPbI_3$ is susceptible to heat stress on the outermost surface much earlier than the bulk. It makes sense that decomposition products are detected later as the surface/volume ratio in a thin film is very small and CH_3I and NH_3 evaporate at trace amounts. It is also proposed that the high vacuum conditions accelerated the thermal degradation. Finally, *in situ* near edge x-ray absorption fine structure (NEXAFS) studies in a similar setup gave insight to the interaction of molecular MA^+ ions with the intermediate structure before PbI_2 formation. The linear polarization of the synchrotron x-rays was used to probe the orientation of the C–N bonds during increasing temperature at UHV conditions. When subjecting the sample to similar conditions as when changes appeared by *in situ* 2D GIWAXD (100 °C for 20 min), they could observe how $CH_3NH_3^+$ ions aligned themselves in an orthogonal fashion with the substrate surface. Over time, during heating, there was also a drop in intensity of the peak corresponding to the C–N

bond. Results indicate that $CH_3NH_3^+$ are more aligned with hydrogens pointing toward the PbI_2 sheets of the intermediate structure before the decomposition into CH_3I and NH_3.[88] To present further support of threshold temperatures for degradation, Wang *et al.* monitored the temperature-dependent degradation of $MAPbI_3$ by *in situ* spectroscopic ellipsometry (SE) to track the PbI_2 content, film thickness and dielectric constant over time.[90] Full degradation was defined as when a dielectric constant no longer changed, happened at different timeframes, inversely proportional to the temperature heating, i.e., 3.8, 14.5, 39.7, and 137.7 min at 220, 200, 180, and 160 °C, respectively, following an Arrhenius equation. Unsurprisingly, the $MAPbI_3$ thickness decreased and PbI_2 content linearly increased over time.

Included above are several good examples on how tuning the stoichiometry can make more robust MOHP against elevated operating temperatures. Other strategies to increase the resistance are the incorporation of additives in the perovskite film. In the work of Maniyarasu *et al.*, 1-octyl-3-methylimidazolium chloride ionic liquid (IL) hindered $FA_{0.9}Cs_{0.1}PbI_3$ perovskite thermal degradation in UHV.[28] The findings were obtained via *in situ* near ambient pressure (NAP)-XPS at room temperature (RT), 100 °C, and 150 °C, comparing a reference and IL-modified sample. While the IL-modified perovskite showed minimal changes at 100 and 150 °C, increased signals of Pb^0 and PbI_2 originated in the reference sample improved crystallinity and reduced the presence of unwanted Pb^0. The authors hypothesized that the IL helped improve the perovskite crystallinity and prevented FA^+ ions from diffusing out of the perovskite crystal lattice. Wang *et al.* increased the thermal stability of $MAPbI_3$ by incorporating the authors own driving force molecule, i.e., caffeine, in the perovskite film.[91] Their observations of *in situ* HRTEM crystal evolution agreed with previous findings by Kim *et al.*,[74] $MAPbI_3$ decomposition happen in the sequence of (i) amorphized material, (ii) intermediate crystalline phase, and (iii) PbI_2. Indeed, improved photovoltaic stability at 85 °C under nitrogen flow was obtained. Caffeine molecule hindered the formation of the intermediate phase (ii), which is the precursor of PbI_2 formation [Fig. 9(3)]. Further exposure to the e-beam (up to ~135 °C) caused the decay of (110) diffraction peak for both samples, but while new diffraction peaks were observed in the control sample, the caffeine-containing sample did not undergo such new peak formation. It was hypothesized that the caffeine acted as a molecular lock via strong interaction with the Pb_2^+ ion, preventing the formation of amorphous phases, thereby preventing the degradation at elevated temperatures. Another strategy was reported by Fan *et al.*, demonstrating improved thermal stability with hexagonal boron nitride (hBN) thin flakes in hBN-perovskite-hBN heterostructures.[75] The B^+ and N^- ions in the flakes passivate the dangling bonds of the $MAPbI_3$ surface, reducing its susceptibility to rearrangement during the thermal stress. This does not completely remove thermal instability but reduces the reactivity of the surface and prolongs the time for layer by layer degradation seven-fold.

A last note is that *in operando* stressors can induce lattice expansion of crystalline materials. Changes in lattice spacing modify the material dielectric constant that, in turn, can be detected by time-resolved and steady-state optical reflectivity (Fig. 11). Li *et al.* employed the technique to study lattice expansion on $MAPbI_3$ single crystal under continuous Xe-lamp illumination and various temperatures.[81] It was observed that illumination by itself did not induce any change in the lattice. Instead, it was found that the heating caused by the illumination source was the main factor causing thermal lattice expansion, similar to heating the sample in the dark. The contrast with the above studies that found substantial ionic redistribution upon illumination relies perhaps in the low irradiation power used in the reflectivity studies.

To conclude this section of *in situ* thermal degradation studies, we extract a general consensus in which the main degradation product is PbI_2, with the release of volatile organic molecules and halide if the device is not encapsulated.[92] For $MAPbI_3$, the decomposition happens through a crystal change that transitions from amorphous to a precursor of the PbI_2 phase. Relative to the protection strategies

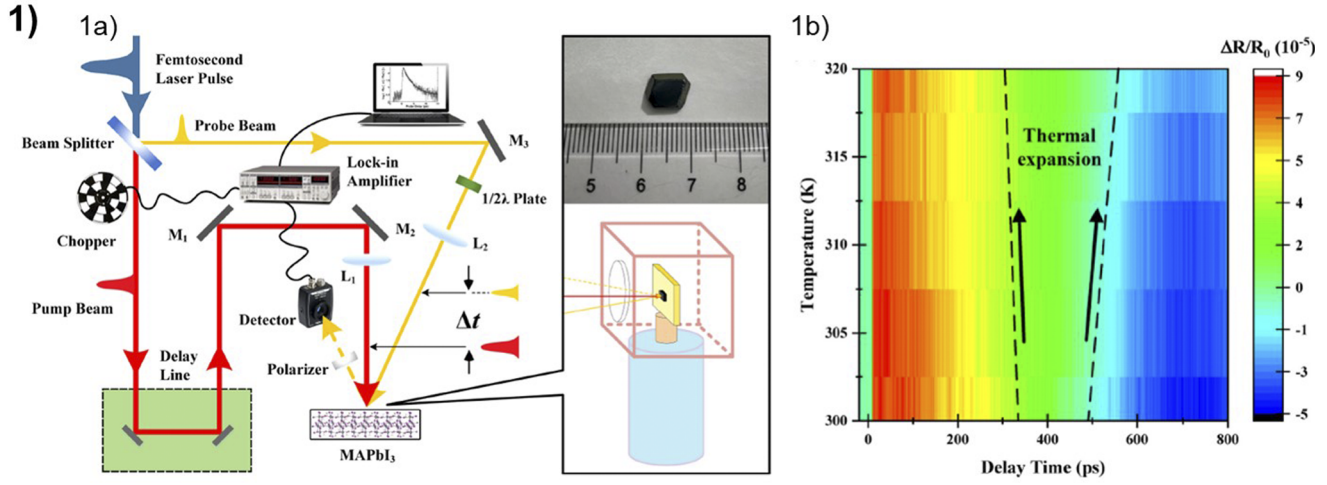

FIG. 11. (1a) Schematic diagram of time-resolved optical reflectivity measurement based on ultrafast pump–probe method. The inset shows the sample photographs of single-crystalline $MAPbI_3$ perovskite and temperature control device with control accuracy from 4.5 to 320 K. (1b) 2D mapping diagram of reflectivity, where the black arrows represent the thermal expansions of lattices. Adapted from Li *et al.*, J. Appl. Phys. **132**(1), 013102 (2022) with the permission of AIP Publishing.

adapted to increase resilience to temperature stress, we can mention the precise tuning of perovskite stoichiometry, the incorporation of additives in the film, or even the addition of surface modifiers to create more robust interfaces.

We would like to point out that several of the reported *in situ* measurements employed illumination or e-beam as the heating energy that indeed cause important temperature increase. High light-induced temperature is an overlooked stressor that may influence the degradation mechanisms in experiments performed under illumination, especially Xe-lamp containing IR fraction of the spectrum, or high-power lasers. Often, sample heating is not considered when providing a hypothesis of the light-induced degradation mechanisms [see Sec. III (illumination stress)].

Measurements on complete solar cell devices are desirable since they incorporate the effects of the adjacent selective contacts; however, some techniques are rather limited in this regard. For example, the creative authors doing FIB cross sections of full PSC for TEM imaging themselves report FIB cutting as a possible factor of degradation.

V. BIAS VOLTAGE-INDUCED DEGRADATION

In commercial solar panels, photovoltaic cells are connected in series to achieve greater output voltages. Generally, panels operate close to the maximum power point (MPP) if all individual cells have similar efficiencies and illumination all will work at similar maximum power point voltages (V_{MPP}). V_{MPP} is a voltage usually close to V_{oc}, which when applied produces the highest product between voltage and current (power), i.e., where the maximum amount of photogenerated energy is extracted through the contacts. Electrical charges that are not extracted and accumulate in the device can trigger instabilities, e.g., in the presence of O_2, free electrons can create reactive superoxide species (O_2^-) that degrade the perovskite.[31] Also, partial or total shading of panel-units may force shaded cells to operate in reverse bias to accommodate passing electrical current. Reverse biases induce high electric fields that can initiate unwanted ion-drift with consequences on the perovskite stability. Eventually, reverse bias leads to breakdown voltages that would destroy the device.

We will also review findings from *in situ* stability studies applying bias voltage stress to complete PSC devices or thin films with symmetric electrodes. First, we will focus on the studies that describe the forward bias or symmetric electrode bias, and second, the reverse bias effect in complete PSC, i.e., diode-like structure.

Li *et al.* presented an important *in situ* PL study to obtain quantitative measurements on the speed of ionic motion. A bias ($\sim 2 \cdot 10^4$ V m^{-1}) was applied between two parallel electrodes separated 150 μm, and this produced a parallel front of darkened PL intensity from the positive to the negative electrode, stretching out over time [see Fig. 12(1a)].[93] By tracking simultaneous current loss along the bias stress [Fig. 12(1b)], the authors determined the ion migration speed as 10 μm/s. The defects induced by the front drastically limited radiative recombination in the film between the lateral contacts.

The development of advanced TEM stages has allowed for visualizing the $MAPbI_3$ degradation under bias. Jeangros *et al.* concluded that the main culprits of bias-induced degradation of $MAPbI_3$ solar cells were the formation of PbI_2 nanoparticles and voids, migration of iodide into the HTL, and the volatilization of iodide and organic molecules under 6 V forward bias by STEM and HAADF.[94] They observed strong preference for degradation at the $MAPbI_3$/HTL interface, believed to be caused by an energy-dissipation process depending on the polarity of the layers at their intersection. In a TEM stage allowing both heating and electrical biasing, Kim *et al.* imaged the amorphization of a 300 nm lamella (prepared by FIB) of a complete PSC, suspended between two Au-electrodes, the first 5 min of 1 V forward biasing [Figs. 12(2a) and 12(2b)].[95] Under +1 V electrical bias, they could observe by HRTEM how perovskite grains lost crystallinity over time, as if the crystalline layer was dissolved [Fig. 12(2c)]. PbI_2 phase present did not lose its crystallinity. No morphological changes were observed, and changes could only be seen when reaching lattice spacing resolution. To discard beam-damage, the results seen in HRTEM were also verified with SAED before and after 5 min at 1 V on a spot of the lamella that was not measured by TEM during the biasing [Fig. 12(2d)]. With SAED they could see clear formation of amorphous rings after the biasing [Fig. 12(2e)]. Interestingly, the device recovered fully by resting in the dark, and also complete recovery was achieved by heating to 50 °C in merely 3 h. The authors proposed a mechanism of amorphization via halide ion migration and defect generation that leads to crystal collapse as the Pb-plane decomposes. Despite sophisticated methods, Kim *et al.* could provide simple and clear conclusions, thanks to the separation of bias, e-beam, and temperature stress.[95] Their results are revolutionizing regarding the increased understanding of perovskite degradation under bias conditions but also the very promising healing of bias stress damage by exposure to mild elevated temperatures.

Functionalized atomic force microscopy (AFM) has been used in several studies to spatially resolve the contact potential difference (CPD), Kelvin probe force microscopy (KPFM), piezoresponse (PFM), and conductivity (c-AFM), simultaneously as the surface topography. These techniques have been used in several works, with both lateral contact samples and cross-sections devices, to apply electrical bias and prove the existence of ionic migration and accumulation at interfaces of the active layer.[59,96–98] The voltage distribution is found to be inhomogeneous and variable across grains under illumination.[59,99,100] With *in situ* AFM methods and the variation upon applying/removing bias, one can obtain insights about the ion distribution over time. Using KPFM, Ahmadi *et al.* investigated the interfaces of a single crystal with lateral Au electrodes under bias to probe the dynamic charge changes.[96] For short times, the authors saw indication of slow changes in charge-distribution produced by higher bias (4 V) conditions. Lower biases (1 V) were not sufficient to activate the motion of slow ionic systems or other charged species. The dynamics in motion were clearly bias-dependent. Given the fact that these phenomena happened at the same time, they proposed that interfacial charge injection and ion migration may be intrinsically linked. The work by Kim *et al.* discussed in Sec. III [Fig. 8(2b)] found that illumination induced mostly reversible changes in a $MAPb(Br_xI_{1-x})_3$ film, while bias poling effects were not completely reversible.[59] From *in situ* XRD, peak broadening during biasing was irreversible, contrary to reversible broadening from illumination. Additionally, they observed that +2 V induced contact potential difference (CPD) variations within grains while no variations were seen under −2 V, suggesting a better charge separation at +2 V than at −2 V.

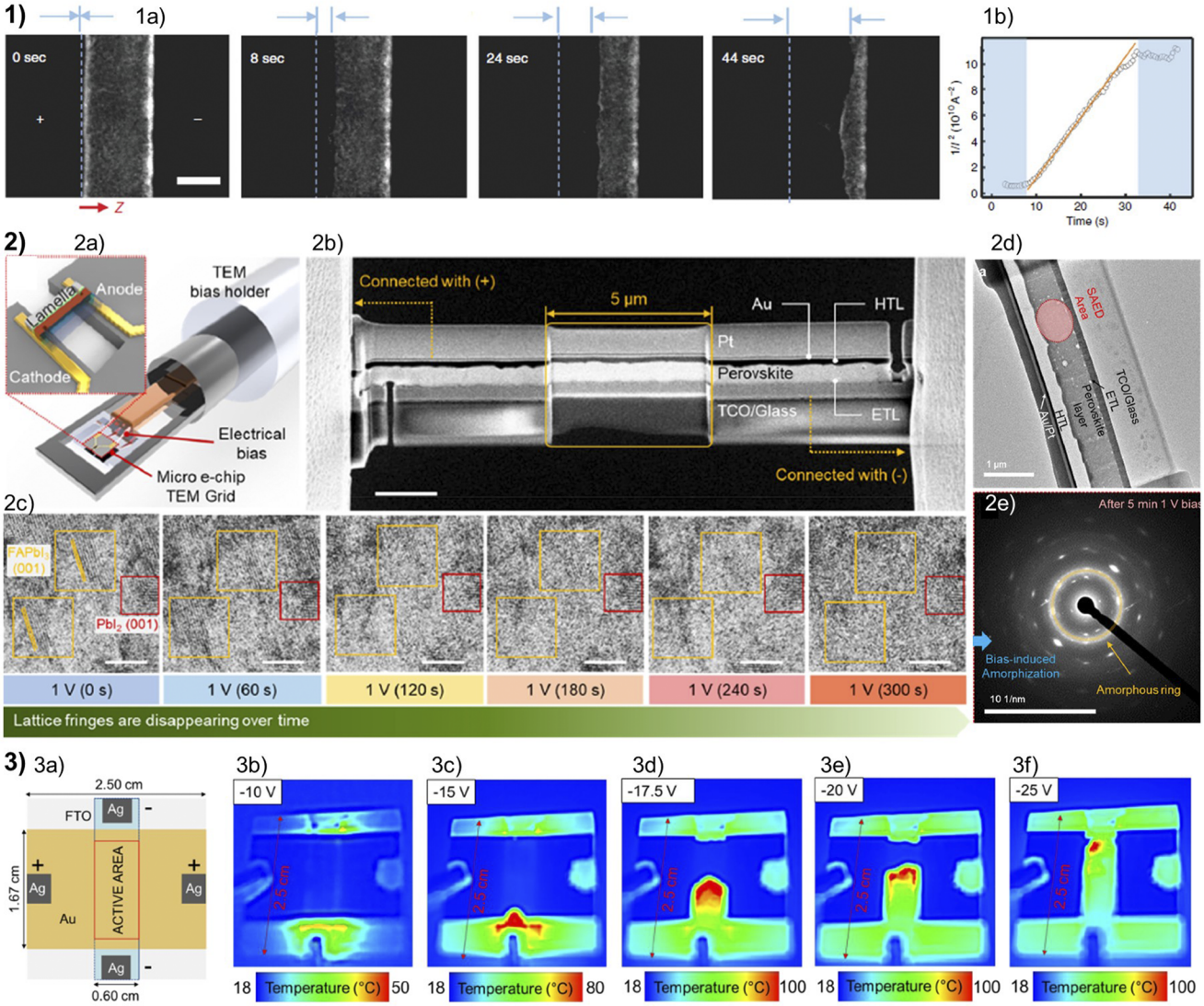

FIG. 12. (1) Observation of a dark front in a light-soaked perovskite. (1a) Time-dependent PL images of a perovskite film $CH_3NH_3PbI_{3-x}Cl_x$ under an external electric field ($\sim 2 \cdot 10^4$ V m^{-1}). The "+ " and "–" signs indicate the polarity of the electrodes. The channel length is ~150 μm. The scale bar represents 100 μm. Blue arrows, $\rightarrow z$, indicate area of PL lost since bias application (1b) Electrical current $1/I^2$ monitored as a function of time during the measurement of experiment (1a). Adapted from Li *et al.*, Nat. Commun. **9**(1), 5113 (2018). Copyright 2018 Author(s), licensed under a Creative Commons Attribution 4.0 License. (2) *In situ* observation of changes in perovskite materials induced by electrical biases. (2a) Schematic of *in situ* TEM sample configuration under electrical bias. (2b) SEM image of the nano-solar cell lamella used for *in situ* observation prepared by FIB. The scale bar is 2 μm. (2c) HRTEM image series of perovskite materials under 1 V electrical bias. (2d) TEM image of nano solar cell indicating the locations of the SAED area. (2e) SAED patterns of perovskite materials at the highlighted region after 5 min of forward bias (1 V) without beam radiation. Reprinted with permission from Kim *et al.*, ACS Energy Lett. **6**(10), 3530–3537 (2021). Copyright 2021 American Chemical Society. (3a) Layout of the electrodes used for the investigated PSCs, designating an active area of 1 cm^2. (3b)–(3f) Temperature maps measured for a PSC with Li-doping of m-TiO_2 at the rear side during operation at increasing reverse biases, from 5 to 25 V. Reprinted from Najafi *et al.*, ACS Appl. Energy Mater. **5**(2), 1378–1384 (2022). Copyright 2022 Author(s), licensed under a Creative Commons Attribution 4.0 License.

Liu *et al.* employed time-resolved (tr)-ToF-SIMS and tr-KPFM to track the *in operando* ion migration and evolution of local charge density in $MAPbI_3$ between parallel Au electrodes [Fig. 13(1)].[101] Direct evidence of $CH_3NH_3^+$ and I^- migration toward opposite directions was found when biasing the electrodes, independently of dark or illumination conditions. The electric field induced further decomposition of $CH_3NH_3^+$ into various sub-products, especially in dark conditions and at the interface with the electrodes. Ni *et al.* employed drive-level capacitance profiling (DLCP) and thermal admittance spectroscopy (TAS) to determine the change on trap

state density and position induced by reverse electrical poling of a PSC, a common scenario in partially shaded PV modules.[102] A progressive density increase of two trap-bands upon continuous biasing at −1 V [Fig. 13(2)] was attributed to iodide interstitials near the C_{60}/perovskite interface.

As stated, reverse biases are relevant to series-connected cells in a module from the well-known effect of partial shading. Therefore, several works attempted to study the influence of reverse bias on device stability. Najafi *et al.* monitored a small area with infrared thermal imaging together with the current density response of a silver-electrode PSC [Fig. 12(2a)].[103] The device architecture was found to be vital for resilience against high reverse bias, something previously inferred by other authors seeing that many irreversible reactions during biasing occur at the device interfaces.[104] As reverse bias was applied gradually from 2.5 to 30 V the temperature of the device increased from 18 to over 160 °C, indicating the formation of shunting pathways that degrade the device [Figs. 12(2b)–12(2f)]. In the study, the authors compared three variations of the FTO/m-TiO_2/perovskite/spiro-OMeTAD/Au architecture, with and without compact TiO_2 (c-TiO_2) and with Li-doped mesoporous TiO_2 (Li-m-TiO_2). The absence of c-TiO_2 layer accelerated the temperature damage induced by reverse bias. Li-doping, however, was found to be an effective method that improves PSC performance while leaving stability against reverse bias unaltered. The authors proposed that the origins of reverse bias degradation on the Au electrodes included local shunts from metal ion migration and local heating from arc faults. It is therefore suggested that using non-metal contacts e.g., carbon-based electrodes can increase resilience against reverse bias.

The contacts are of high importance when performing bias-stress stability tests. Characterization using film-contact methods to apply bias are sensitive, e.g., Ahmadi *et al.* reported that the Au-contact interface with the perovskite is non-ohmic, thus creating interfacial polarization and recombination that could play a role in degradation of the film.[96] Metallic contacts can create filament channels that cause shunts in a device, or metal-halide reactions, such as AgI creation, can occur. Carbon-based electrodes are an alternative to mitigate some bias-induced degradation by substituting the metal.

Overall, most works mention unwanted charged species (e.g., ions) motion and crystal amorphization as a main cause for perovskite degradation under forward bias application. Reversibility of some changes once the electric field is removed is observed, but high bias can induce irreversible decomposition reactions and even inter-diffusion of the metal electrode across the device layers. Despite the fact that reverse bias damage in commercial solar panels can be solved through electrical design adding bypass diodes, it is relevant for other potential applications such as memristors where negative biases can be beneficial. We note that upon applying high biases, changes can occur fast (<2 s) and techniques are limited by the time required to complete a full scan, such as KPFM. To see such fast changes, a higher time-resolution needs to be developed, or results obtained by these methods are analogous to "before and after images" done *in situ* under controlled conditions.

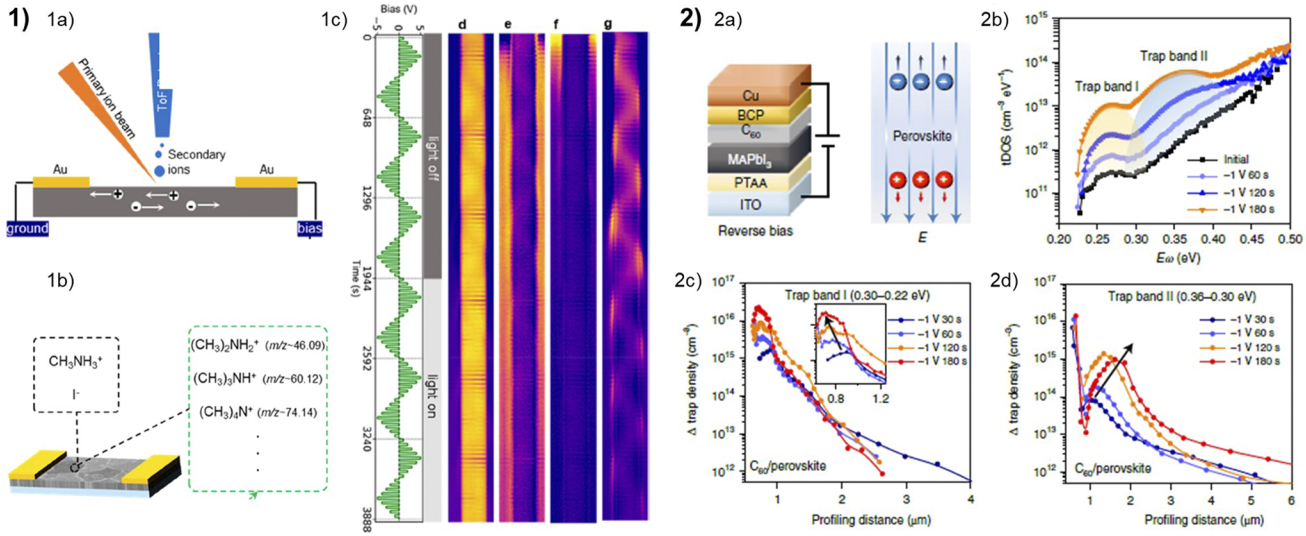

FIG. 13. (1a) Schematic of ToF-SIMS measurement on lateral gold electrodes on a $CH_3NH_3PbI_3$ film. (1b) Schematic shows possible ions existing in $CH_3NH_3PbI_3$, black box shows intrinsic ions including $CH_3NH_3^+$ and I^-, and green box shows $CH_3NH_3^+$ decomposition products. Adapted with permission from Liu *et al.*, ACS Nano **15**(5), 9017–9026 (2021). Copyright 2021 American Chemical Society. (2a) Schematic diagrams of the device structure of a $MAPbI_3$ thin single-crystal solar cell under reverse bias (left) and the movement of charged ions under electric field *E* (right). (2b) Trap density of states (tDOS) spectra before and after applying a reverse bias of −1 V with different durations. Spatial trap density distribution for trap-band (2c) I and (2d) II in the $MAPbI_3$ thin single crystal solar cell after applying the reverse bias measured by DLCP. The inset in (2c) displays the zoomed-in trap density change near the C_{60}/perovskite interface. Adapted with permission from Ni *et al.*, Nat. Energy **7**(1), 65–73 (2022). Copyright 2022 Nature Publishing Group.

VI. CYCLE-APPLIED STRESS

While previous sections II–V reviewed the individual stress factors of humidity, oxygen, illumination, temperature, and bias, we now begin exploring the combination of such conditions to better understand the long-term degradation of PSC in actual operation. Testing reversibility and changing conditions (e.g., day/night) during stability assessment of solar cells is relevant to mimic outdoor operation. Standardized ISOS protocols include various cycling tests (T, LT, LC) to account for the cycles, e.g., day and night, rain and sun, hot and cold, etc., of long term operation in PV installations. Changes in conditions may lead to partial recovery resulting in low overall degradation or lead to destabilization of steady-state conditions and acceleration of performance decay. Most commonly, some irreversible part of PSC degradation accumulates over time during repeated stressing and relaxation.

Some works already mentioned in this review complemented their experiments with cycling. In the original report of the "Hoke effect" in 2014, halide segregation was observed as a shift of PL emission to lower energies [Fig. 14(1a)]. A MAPb($Br_{0.6}I_{0.4}$)$_3$ film during four cycles of 2 min of illumination and 5 min of dark-rest showed a reproducible full recovery after dark of the two emission peaks monitored (1.68 and 1.94 eV) [Fig. 14(1b)].[50] This light-induced, reversible phenomenon was a seminal work for cycling studies. Complete reversibility of light-induced halide segregation in properly protected environments has been argued in further works. In the study by Knight *et al.*, *in situ* PL spectra of MAPb($I_{0.5}Br_{0.5}$)$_3$ films were collected along eight cycles of 15 s illumination followed by 30 min of dark rest, in four different environments: air, vacuum, nitrogen, and encapsulated (PMMA coating done in vacuum before any environmental exposure).[55] Under inert nitrogen or encapsulation [Figs. 14(2c) and 14(2d)], similar PL behavior was obtained under illumination, each time for eight cycles. In vacuum and air [Figs. 14(2a) and 14(2b)], there were changes over time in opposite directions for the conditions. In air, the signal from iodide-rich perovskite reached higher intensities than in other conditions, and the photobrightening was faster each cycle. In vacuum, the iodide-rich photobrightening happened at slower rates with additional cycles and the mixed-phase PL signal decreased exponentially over time independently on the illumination cycles. This suggested that, in both vacuum and air, irreversible processes take place under illumination. The PL increase was attributed to trap passivation due to the

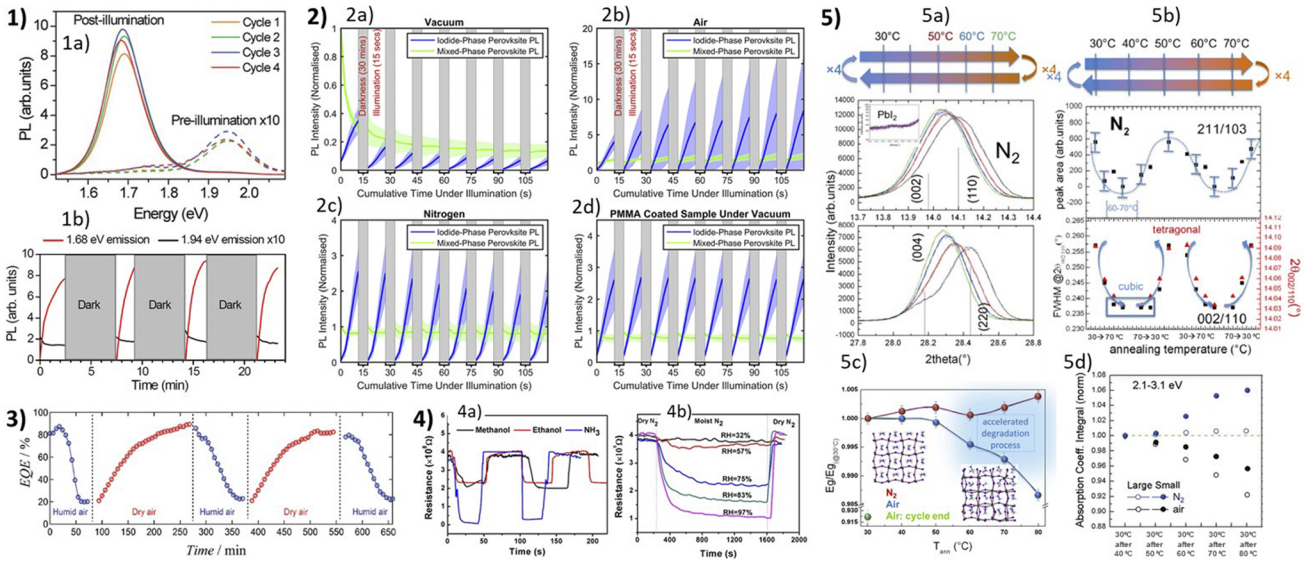

FIG. 14. (1a) PL spectra of a MAPb($Br_{0.6}I_{0.4}$)$_3$ thin film after sequential cycles of illumination for 2 min followed by 5 min in the dark. (1b) PL emission intensity vs time of a MAPb($Br_{0.6}I_{0.4}$)$_3$ thin film at the two emission peaks. Reprinted from Hoke *et al.*, Chem. Sci. **6**(1), 613–617 (2015). Copyright 2015 Author(s), licensed under a Creative Commons Attribution 4.0 License. (2) Evolution of PL emission monitoring the reversibility of halide segregation when MAPb($Br_{0.5}I_{0.5}$)$_3$ films are held under four different atmospheric conditions, (2a) vacuum (~0.2 mbar), (2b) ambient air, (2c) pressurized (2 bars) nitrogen, and (2d) film topped with PMMA and in vacuum. Reprinted from Knight *et al.*, ACS Energy Lett. **4**(1), 75–84 (2019). Copyright 2019 Author(s), licensed under a Creative Commons Attribution 4.0 License. (3) LBIC-extracted average EQE (532 nm) of the device during hydration–dehydration cycles. Reprinted with permission from Song *et al.*, Adv. Energy Mater. **6**(19), 1600846 (2016). Copyright 2016 John Wiley & Sons. (4a) Dynamic resistance curves of the perovskite film upon exposures to methanol, ethanol, and NH_3 at room temperature. (4b) Dynamic resistance curves measured under various moisture levels at room temperature. Reprinted with permission from Hu *et al.*, ACS Appl. Mater. Interfaces **7**(45), 25113–25120 (2015). Copyright 2015 American Chemical Society. (5) XRD data on the thermal cycles in air: (5a) *In situ* thermal cycles in nitrogen environment, two main XRD peak regions. (5b) Reversibility in dry nitrogen. Peak area of the tetragonal 211/103 diagnostic peak (above); peak position and FWHM of the 002/110 peak (below) during *in situ* thermal cycles (upper panel) in nitrogen environment at atmospheric pressure. (5c) Normalized energy gap trend (E_g at 30 °C = 1.62 eV). E_g has a sudden reduction after annealing at 50 °C. The insets represent ideal (left side) vs defective (right side) lattice arrangements. Reprinted with Permission from Alberti *et al.*, Adv. Energy Mater. **9**(12), 1803450 (2019). Copyright 2019 John Wiley & Sons. (5d) Comparison on the absorption capability of large-textured and small-random-grained $MAPbI_3$ layers. Reprinted with Permission from Alberti *et al.*, J. Phys. Chem. C **121**(25), 13577–13585 (2017). Copyright 2017 American Chemical Society.

formation of superoxide species. In contrast, vacuum increases the trap density probably due to loss of volatile species.[55] The authors do note that recovery takes much longer than segregation, something to bear in mind since the outdoor conditions do not present such long relative resting times (see Sec. III).

Descriptions by Song *et al.* (see Sec. II) used LBIC EQE mapping to spatially resolve the loss of EQE during humidity exposure and included two cycles with hydration(80% RH, 90 min) and dehydration (dry air, 4 h).[26] The EQE decayed from 80% to 20% and completely recovered in dark, as recrystallization of the hydrated film happened [Fig. 14(3)]. After repeated cycling with longer hydration, some irreversibility was found. It was hypothesized that, once morphological changes occurred, it resulted in a permanent deterioration of the photogenerated current. Hu *et al.* used *in situ* resistance measurements to monitor a $CH_3NH_3PbI_{3-x}Cl_x$ sample conductivity and the effects produced by different ambient conditions, including different solvents for perovskite fabrication [Fig. 14(4a)].[25] They tested different RH conditions in nitrogen at room temperature (20 °C) during a cycle going from dry N_2 to humid N_2 and back to dry N_2. Figure 14(4b) shows a gradual resistance drop with time (over 1400 s), directly proportional to the amount of RH. The resistance quickly recovered to the initial values once humidity was removed, independently of the level of humidity.

Alberti *et al.* studied $MAPbI_3$ thin films (deposited on TiO_2 compact layers) with *in situ* XRD and *in situ* spectroscopic ellipsometry (SE) during thermal cycles from 30 to 80 °C. Above 50 °C, acceleration of material modification by environmental factors occurred upon transition to cubic lattice, and they proposed increased accessibility and reactivity of humidity species with the lattice at higher temperatures.[105] The authors chose air with 55% RH as a stressor to be below the threshold for hydrate formation reported by other works, and indeed no peaks of hydrated species were observed by XRD, and all signs were of permanent deformations and configurational disorder in the $MAPbI_3$ crystal.[15,21] When comparing cycles in air (55% RH) and dry nitrogen (0.3 bar overpressure) by SE, it was corroborated that the effects seen were environmentally dependent and irreversible. *In situ* ellipsometry on samples with different grain size revealed that similar phenomena for both small and large grains, supporting that the surface stabilization by nitrogen molecules is a universal phenomenon. An exception on small grains was seen in an additional healing effect at higher temperatures in nitrogen, and an increase specifically at the lower bandgap absorption was observed [see Fig. 14(5)].[106] They also saw an increase in PbI_2 formation by *in situ* XRD under humid air environment compared to N_2 environment, in agreement with other *in situ* GIWAXS studies.[92]

Despite full recovery being reported throughout repeated cycling, it is important to note that these studies use long relative resting time, i.e., the stressing time is much shorter than recovery. It would be interesting to see more studies making incomplete recovery to see the physical accumulative effects of more realistic conditions. An outdoor test would be the ultimate cycling experiment, but to our knowledge, there are no outdoor studies done with complementary *in situ* characterization of physical mechanisms. Nitrogen recovery is used in several examples, and it might be important to point out that nitrogen cycling is not found in any outdoor conditions. It is still promising that reversibility possibly can be exploited to find a balance for long-term stability.

VII. MULTI STRESSORS

Most stability studies of perovskite films, crystals, and full solar cells have been carried out in laboratory conditions without following a standard protocol and focusing mostly on one main stress factor. In real outdoor applications, PSC modules will endure simultaneous stressors influencing the device, in varying magnitudes, over the course of one day (day/night) and across the year seasons (weather, sun irradiance, and temperature), or even neutrons in outer space. Stability analyses of PSC under outdoor conditions is the outermost significant assessment because it englobes all the variables (at different intensities and doses) that are difficult to mimic in the laboratory. Outdoor installations are not always feasible for most of the laboratories and definitively not practical to couple it with most of the *in situ* advanced characterization techniques; therefore, efforts need to be put into replicating outdoor conditions in the laboratory. However, mimicking those exact outdoor conditions at laboratory level is a complex task, and real stressors vary in quantity and intensity and are imposed to the PSC in parallel or sequentially to each other. They are also randomly imposed on the solar cell. Examples of the application of multiple stressor factors (multi-stress) to PSCs are scarce in the literature, but they are very important, as the outcome of those analysis can shade light to the working mechanisms taking place under extreme conditions. The multi-stress experiment permits to come closer to the operating conditions that solar cells should endure and can lead to different scenarios on the combined effects:

(1) Competition: Two or more degradation paths compete and act simultaneously [governed by energy/thermodynamics/saturation (mass transfer)].[107–109]
(2) Synergy: One stressor enhances the degrading effect of the other [for example, under heat and light, bias and light, or humidity and light (see Sec. III)].[82,110]
(3) Mitigation: One stressor slows down the effect of the other (for example, e-beam irradiation diminished illumination damage,[45] applying a bias so that charges are extracted decrease the illumination damage, or heating the cell causes "drying" thus reducing the moisture damage).[49,111]
(4) The degradation takes different paths (depending on the magnitude of the irradiation, the atmosphere composition or whether the device is at open or short circuit conditions).[89,107,109,112]
(5) Spatial localization: The degradation effect becomes more heterogeneous/localized (e.g., at the interfaces with the selective layers or grain boundaries).[108,110]

Below, we provide a review on the most relevant publications employing diverse characterization techniques with *in situ* application of various external stressors in various magnitudes and combinations. Table I summarizes different works classified by the stress conditions applied.

In Secs. VII A–VII C, we provide detailed explanation of the works summarized in Table I, classified by the main stressors applied to the PSC.

A. Illumination and bias

In situ PL experiments under continuous illumination, open (OC) and short circuit (SC) conditions, and employing different

TABLE I. Summary of the research works performing *in situ* measurements applying various techniques and combinations of different stressors. T = temperature, RT = room temperature, c- and mp-TiO_2 = compact and mesoporous TiO_2, RH = relative humidity, OC and SC = open and short circuit, P = pressure, and UHV = ultrahigh vacuum.

Conditions	ISOS protocols	PSC structure	*In situ*/*operando* techniques	Finding	References
Light 525/50 nm + OC and SC	ISOS-L	FTO/c-TiO_2/ mp-TiO_2/ $CH_3NH_3PbI_3$/ spiro-OMeTAD Au fingers Au ~10 nm	PL (470 nm) at OC and SC	Pre-accumulated positive ions at the HTL interface are redistributed by light-soaking, faster at OC bias (drift) slower at SC (diffusion). At longer light exposure negative ions accumulate at the HTL interface under OC bias. Ion migration is slower in larger grains at OC	110
Light (422 nm, 0.3 sun) + bias OC and SC	ISOS-L ISOS-V	mp-TiO_2/$Cs_{0.1}$ $FA_{0.9}Pb(I_{0.65}$ $Br_{0.35})_3$ or $Cs_{0.1}$ $FA_{0.9}PbI_3$ spiro-MeOTAD Au	PL (422 nm) + V_{oc} probe (every 3 min)	Non-conductive grains produced from halide segregation due contribute to PL but not to V_{oc} because they are isolated. Non-segregation can be distinguished due to coherence in V_{oc} calculated from PL and V_{oc} measured	108
Light (white LED 100 mW/cm^2) + temperature (20, 44, 53 °C)	ISOS-L-3	500 nm thin film $CH_3NH_3PbI_3$	XRD	Thermal expansion. Excess carriers and heat from illumination are most damaging. Switching light on and off at constant temperature has no effect	82
Light (473 nm), 1 W/cm^2 (~10 suns) T (69 °C)	ISOS-L-3	FTO/NiO_x/ Cs:$FAPbI_x$, I/Pb = 3.8 and 2.8M	XPS	Metallic lead formation via PbI_2. Excess iodide strongly catalytic toward PbI_2 region growth (rates). Nucleation sites neutralized via metallic lead formation in more stoichiometric samples. Wavelength dependant reaction	49
Various (see Table II)	ISOS-D ISOS-L-3	$MAPbI_3$ thin film	Optical transmittance (550 nm)	Dry photooxidation and water assisted photooxidation. H_2O and light synergy for oxidation, strongest at RT. Comparison of rates under different conditions	109
X-ray Irradiation H_2O partial P in UHV	ISOS-L-1I	$MAPbI_3$ films on FTO/glass	(NAP-XPS)	Changes dependent on flux. Degradation path for x-ray exposure. Frenkel defect creation (interstitial MA^+ and I^-)	112
Light (~AM 1.5 G) + vacuum + bias (OC/±1 V)	ISOS-L ISOS-V	$MAPbI_3$ 200 nm mp TiO_2/ spiro/Au	XPS	Production of metallic lead via intermediate state $(CH_3NH_3)_{1-x}PbI_{3-x}$ to PbI_2 to metallic lead and iodide. Photogenerated carriers induce chemical and optoelectronic change if not extracted	111
Light/ Temperature Vacuum or T Vacuum (in cycles)	ISOS-L-2 ISOS-LC	$FAPbI_3$ powder $MAPbI_3$ powder	Vacuum chamber with mass spectrometer (MS)	Competing reactions. CH_3NH_2 and HI from a reversible reaction and CH_3I and NH_3 from an irreversible reaction. PbI_2 degradation into Pb^0 and I_2 (gas). Light and temperature affect balance between reversibility. $FAPbI_3$ is more complex	89 and 107
Light Temperature (70% RH) Bias	ISOS-L-2 ISOS-V	Single crystal $MAPbBr_3$ with contacts	EIS, G-KPFM	Conductivity variations in test device depending on environmental pressure, resistance increase with increase in humidity while the device was under bias in the dark. Triple phase boundary at interfaces	113

perovskite composition revealed distinct conclusions from different laboratories. Ebadi *et al.* used a combination of PL and electroluminescence (EL) to investigate the origins of V_{oc} and J_{sc} loss under light soaking. In their work, a 422 nm homogeneous illumination with a diffused laser (30% sun) was used to ensure that illumination and probing were done on the bulk thickness rather than the interface.[108] They studied two Cs-FA cation perovskite, one with only iodide and a mixed I–Br halide that undergoes the known halide segregation [see Sec. III (illumination)]. The cell was switched from OC to SC while recording "*in operando*" the transients of the J_{sc} and V_{oc} and

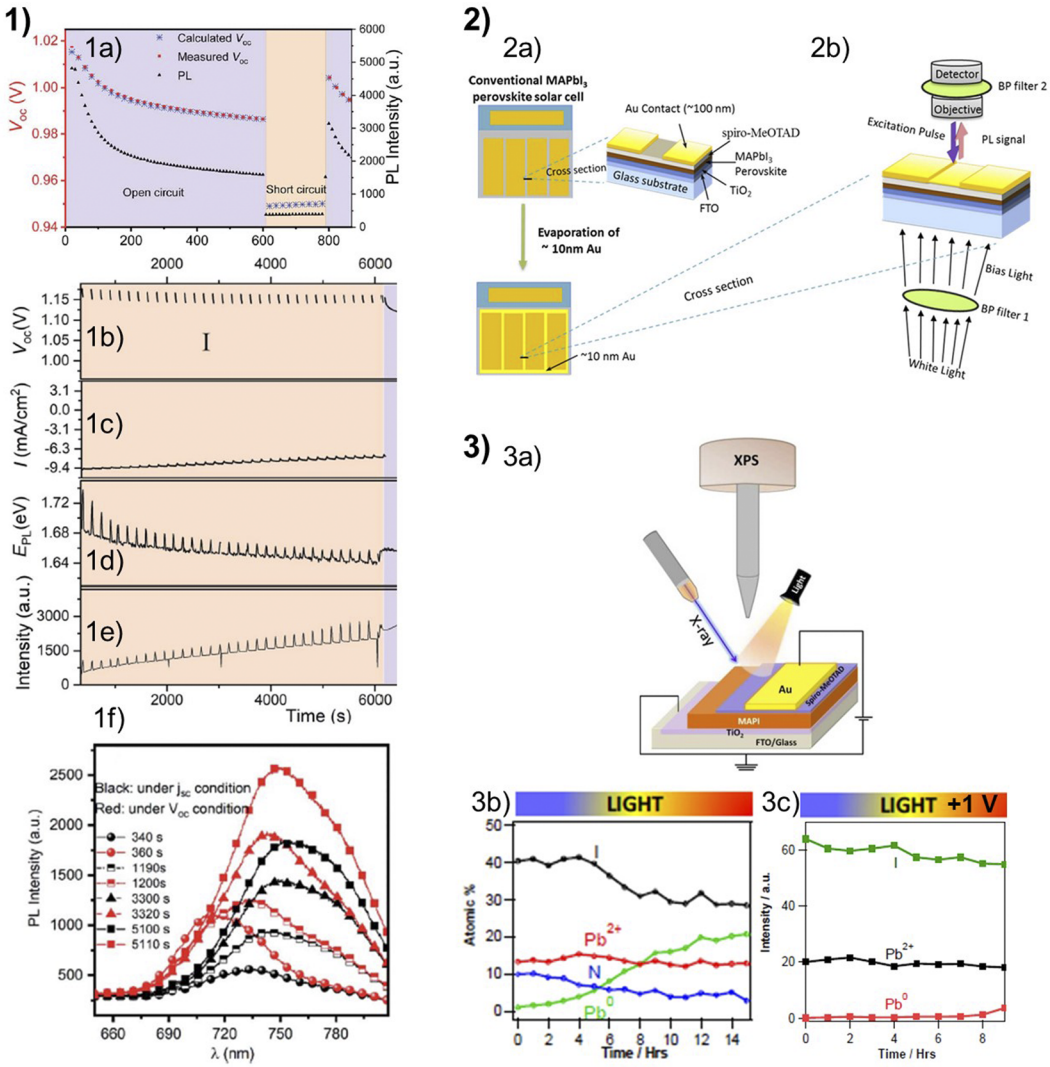

FIG. 15. (1a) Evolution of open-circuit voltage (V_{oc}) and PL intensity during light soaking of a device containing $CsFAPbI_3$. (1b)–(1f) Light-soaking experiment of a device containing $Cs_{0.1}FA_{0.9}Pb(I_{0.65}Br_{0.35})_3$ for 10 000 s. In region I, the device is mainly kept at short circuit and periodically (every 3 min) switched to open circuit. (1b) V_{oc}, (1c) current density, (1d) energy of the PL maximum, and (1e) counts at the PL maximum. (1f) Samples of spectra during region I, under short circuit (black) and the subsequent open circuit conditions (red). Reproduced with permission from Ebadi *et al.*, J. Mater. Chem. A **9**(24), 13967–13978 (2021). Copyright 2021 from The Royal Society of Chemistry. (2a) Schematic diagrams of sample structure and metallization pattern. (2b) Schematic diagram of PL characterization method. Reproduced with permission from Deng *et al.*, Nano Energy **46**, 356–364 (2018). Copyright 2018 Elsevier. (3a) Scheme of the *in situ* XPS setup on a complete solar cell device, probed near the top electrode. (3b) Surface elemental ratio of $MAPbI_3$ under light over the time in vacuum. (3c) The change in elemental ratio of the $MAPbI_3$ surface determined from core level spectra over time. Reprinted with permission from Das *et al.*, Phys. Chem. Chem. Phys. **20**(25), 17180–17187 (2018). Copyright 2018 from The Royal Society of Chemistry.

its corresponding PL intensity and emission wavelength. Both V_{oc} and PL intensity decreased under illumination, and a good correlation between the calculated V_{oc} from the PL yield and the actual V_{oc} was found [Fig. 15(1a)]. The effect shown by this relation was hypothesized to be caused by a build-up of non-radiative recombination at the perovskite interfaces to spiro-OMeTAD and mp-TiO_2, i.e., changes in V_{oc} depend on the non-radiative recombination at the contacts via a barrier or traps, yet the physical origins were not discussed. Interestingly, the PL yield of compositions prone to halide migration was influenced by other effects, such as photobrightening [Fig. 15(1e)]. When investigating $Cs_{0.1}FA_{0.9}Pb(I_{0.9}Br_{0.1})_3$ and $Cs_{0.1}FA_{0.9}PbI_3$, the mixed halide showed halide segregation above certain illumination thresholds, and the behavior of mixed halide perovskite was indeed more complex. Upon light soaking under SC for the mixed halide, with interludes to check V_{oc}, a PL red shift (720–770 nm) was observed [Figs. 15(1d) and 15(1f)], corresponding to a I:Br ratio modification from 0.65:0.35 to 0.8:0.2. In addition, they observed that the reduction of J_{sc} with light soaking

[Fig. 15(1c)] related to the formation of isolated highly emissive perovskite clusters in the film, thus not contributing to the current output of the device. These regions originate from halide segregation to small bandgap iodine-rich clusters. Interestingly, single halide perovskites ($MAPbI_3$ and $MAPbBr_3$) had similar behavior of PL increase, the authors hypothesized that ion migration could create regions that cannot extract photocarriers. The formation of these clusters does not seem to form recombination "traps" or "defects" since the V_{oc} values remain constant along 6000 s of $J_{sc} - V_{oc}$ cycling while the emission had a progressive redshift and intensity increase. Such finding challenges the state-of-the-art knowledge correlating high PL to high V_{oc}, in contrast to the findings described earlier for this same publication. The authors propose that whereas the "high PL = high V_{oc}" assumption [Fig. 15(1a)] is true for flat quasi-Fermi levels (q-E_F), the ion mobility in perovskite can create gradient q-E_F.[108]

Other authors have reached different conclusions regarding how recombination processes vary under illumination at different biases via PL detection. Deng *et al.* studied the effects of continuous light soaking (525/50 nm bandpass filter) on a complete device, targeting the spiro-OMeTAD/$MAPbI_3$ interface region by means of steady state and time-resolved photoluminescence (PL and TRPL).[110] The light (~0.72 sun) shone through the glass side as in regular operation of a solar cell, while a confocal laser microscope focused close to the cathode electrodes, capturing the PL emission (470 nm laser excitation) through semi-transparent 10 nm top Au layer between thicker finger electrodes 2 mm-apart [Figs. 15(2a) and 15(2b)]. This method allowed for probing the HTM interface by PL in a fully operative device (n-i-p).[110] It was found that the PL and TRPL evolved along 10 min illumination both at OC and SC; however, slight differences were found between OC and SC. Changes were attributed to the internal redistribution of ions. Initially, illumination is believed to redistribute pre-accumulated cations at the HTM interface back into the film bulk, a process partly reversible in the dark. An initial PL increase at OC was observed due to reduced nonradiative recombination and PL reduction at SC due to better charge extraction upon annihilation of the ions that pre-accumulated in the dark. The main difference was that, with longer illumination, at OC, the PL intensity and lifetime decreased substantially, while at SC, the PL properties remained constant. PL decrease at OC was hypothesized to be caused by the internal built-in field that produces a drift of negative ions to the HTM interface, creating traps and thus enhancing recombination. At SC, the ion movement is mainly through diffusion, and, without concentration gradient, accumulative ion motion has no driving force. A particularity of this *in situ* study was the very short dwell time (2 ms) used to scan the sample, allowing to capture the instantaneous PL without build-up effect (and interface recombination from the TiO_2-perovskite interface) up to a depth of ~50 nm from the perovskite/spiro-MeOTAD interface. Through the confocal scanning configuration, an increase in dynamics at clusters with smaller grains was observed, contributed to higher boundary/surface to volume ratio in these grains. Both the increased pre-accumulated ion concentration and increased ion diffusivity and concentration at grain boundaries may have sped up migration. With *ex situ* 2D PL mapping, the authors demonstrated a more uniform distribution of PL intensities at SC, while at OC, smaller grains showcased faster rates in changes, indicating increased ionic transport at grain boundaries.[110] It is worth mentioning that this PL characterization was done in air and that bias application was interrupted by periodic j–V measurements to complement with the device performance along the experiment. It is probable that the bias perturbation and moisture may have influenced the actual device evolution. Future works would benefit to include a control sample without perturbations to rule out its effect in the experiment.

The dependence of the applied bias on the device on the degradation upon light soaking was also studied by Das *et al.* via XPS to reveal the differences in chemical composition.[111] $MAPbI_3$-based complete PSC devices were investigated *in situ* by XPS under continuous illumination or dark and near to a biased electrode measured 2 mm-away from an electrode where bias was applied (+1 or 1 V) [Fig. 15(3a)]. XPS under light soaking (spectra close to AM 1.5 G, 100 mW/cm^2) at OC showed a gradual decrease in the N1s signal [Fig. 15(3b)], caused by the removal of volatile organic species driven by the ultra-high vacuum (10^{-9} Torr), and the appearance of Pb^0 core level signals together with new states in valence band (VB) region. In contrast, applying a bias of +1 V, below V_{oc} (thus extracting photogenerated carriers) was found to be beneficial to slow down the decomposition speed [Fig. 15(3c)], while applied bias in the dark did not induce any visible changes in their experiment. With this, they demonstrate that photo-instability is intrinsic of the perovskite rather than induced by ambient O_2 or water. It is worth mentioning that, due to the XPS surface sensitivity limitation, it is not possible to monitor the actual biased perovskite under the contact.[111]

B. Illumination and heating

While *in situ* XPS characterization can infer the causes of perovskite degradation by observing, for example, a reduction of N1s signal or increase in metallic lead, the exact released compounds are elusive to this technique. In this regard, Juarez-Perez *et al.* detected *in situ* the composition of the volatile degradation molecules of PbI_2, $MAPbI_3$, and $MAPbBr_3$ powders under illumination and heating cycles by coupling a mass spectrometer (MS) to a customized vacuum chamber [Figs. 16(1a)–16(1e)].[107] Upon merely exposing the $MAPbI_3$ powders to vacuum, the MS started detecting signals of the decomposition species, including I_2, CH_3NH_2, HI, CH_3I, and NH_3, and occluded dimethylformamide (DMF) solvent molecules, indicating the low stability of such material. Illumination and temperature cycles of 5 min resulted on an overall increase of all these signals [Figs. 16(1a) and 16(1b)]. Interestingly, they found that, once illuminated with 0.5 suns, $MAPbI_3$ continues to decompose in the dark, even after several minutes. Similarly, photolysis of PbI_2 by releasing I_2 was also found, in all cases leaving Pb^0 in the remaining powders, in accordance to previous findings.[42,111] Photodecomposition of PbI_2 to I_2 was found to have a lower activation energy (E_a) than that of illuminated $MAPbI_3$; thus, any impurities existing in the film may initiate further decomposition reactions.[38,43] In addition, heating PbI_2 in the dark did not trigger I_2 release, but it did for heating $MAPbI_3$, indicating that $MAPbI_3$ is an unstable perovskite in general. $MAPbBr_3$ was found to be more stable than its iodine counterpart because it released only CH_3NH_2 and HBr under illumination and/or mild heating (40–80 °C). CH_3NH_2 and HX (X = halide) are reversible decomposition

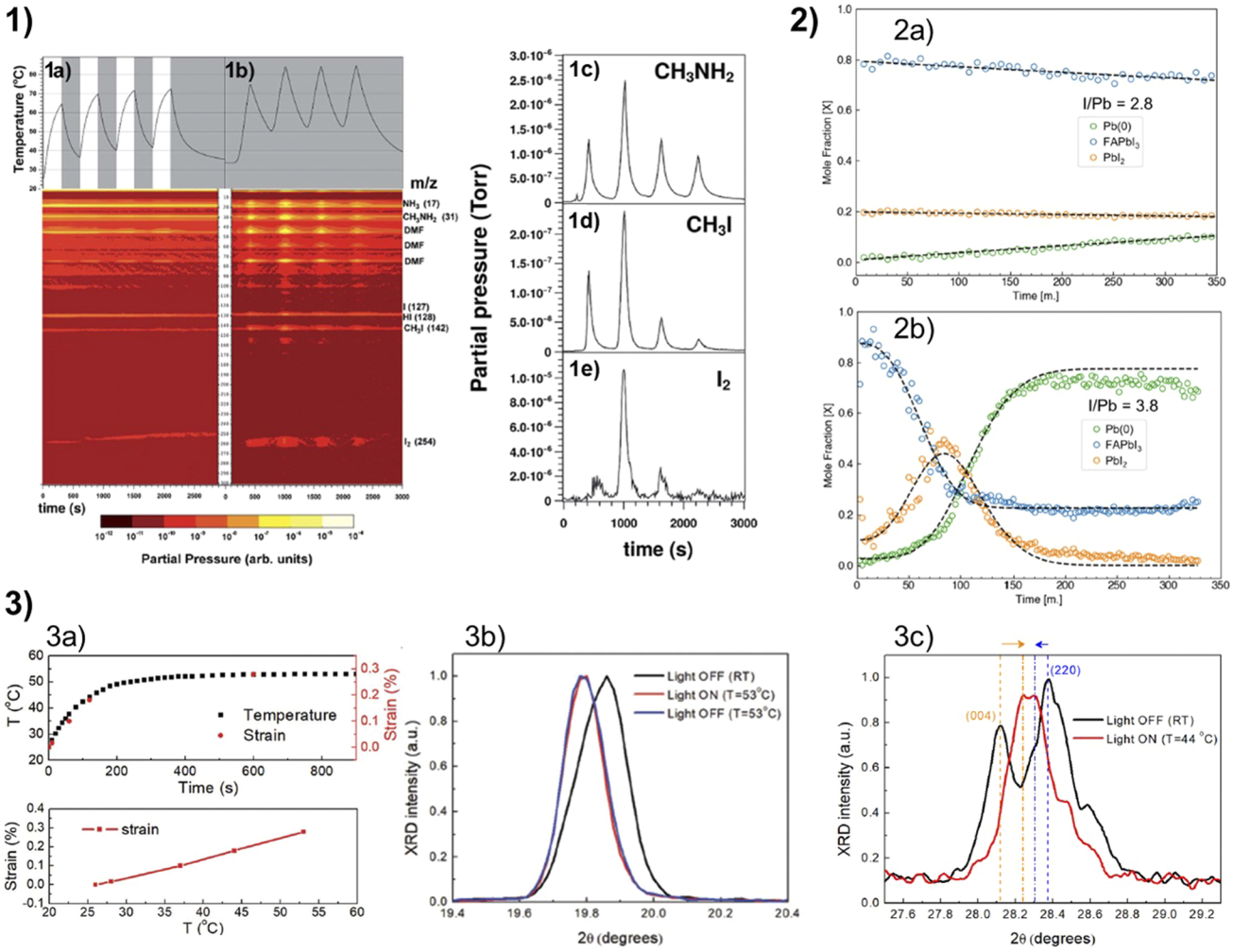

FIG. 16. (1) Mass spectrometry profiles of $MAPbI_3$ decomposition products during illumination and heating-in-the-dark pulse experiments. (1a) Light/dark intervals (5 min each) on $MAPbI_3$ perovskite using a Xe-lamp delivering 55 mW/cm^2 of light power. (1b) Heating on/off intervals (5 min each) on the $MAPbI_3$ sample under dark conditions. Species of interest detected in MS are labeled on the right side. The right panel shows calibrated mass traces for (1c) CH_3NH_2, (1d) CH_3I, and (1e) I_2 during the heating intervals under dark conditions. Reprinted from Juarez-Perez *et al.*, J. Mater. Chem. A **6**(20), 9604–9612 (2018). Copyright 2018 Author(s), licensed under a Creative Commons Attribution 4.0 License. (2) Time-resolved *in situ* XPS Pb 4f areal fit results from Pb/I = 3.2 (2a) and Pb/I = 2.8 (2b) perovskite samples. Molar fraction of Pb is normalized by the total Pb 4f signal. Reprinted with permission from Donakowski *et al.*, ACS Energy Lett. **6**(2), 574–580 (2021). Copyright 2021 American Chemical Society. (3a) Change of temperature and strain with illumination duration time and relation of light-induced strain and sample temperature for in $CH_3NH_3PbI_3$ single crystal under illumination of 100 mW/cm^2 white LED. (3b) XRD patterns of $CH_3NH_3PbI_3$ single crystal under light off at room temperature (RT), light (100 mW/cm^2, white LED) on at 53 °C, and light off at 53 °C. (3c) XRD patterns of $CH_3NH_3PbI_3$ single crystal powders under light off at RT and under light on at 44 °C. Reprinted with permission from Chen *et al.*, Adv. Mater. **31**(35), 1902413 (2019). Copyright 2019 John Wiley & Sons.

products that convert back to perovskite spontaneously, in contrast of the irreversibility of CH_3X and NH_3. Similar conclusions were obtained in a later publication for FA-based perovskites.[89] Upon inserting $FAPbBr_3$ perovskite into vacuum, MS detected signals of the degasification products FA, HCN, and NH_3, which did not increase with mild illumination (0.55 suns, <60 °C). Heating over 75 °C in the dark produced a significant increase in the above-mentioned signals, and the appearance of HBr, Br isotopes and, above 95 °C, the HCN dimer fragment, HCN–(H)CN attributed to the presence of sym-triazine.[89] There is an agreement in these *in situ* works that the illumination is an important cause of instability for the $MAPbI_3$, releasing MA and halide. Changing the halide to Br increases its stability, and substituting MA with the longer alkyl cation FA increases its light and temperature resistance.[89] Regarding the relationship between compositional ratio and stability, Donakowski *et al.* demonstrated the utter importance of the

halide excess/deficiency of (Cs,FA)PbI_3 in the kinetics and mechanism during thermal and photo-decomposition via *in situ* XPS.[49] By fitting the different peaks of the Pb $4f_{5/2}$ core-level spectra, the authors deconvoluted the signals of Pb^0, PbI_2, and $FAPbI_3$. When conditioning Cs:$FAPbI_3$ thin films (FTO/nickel oxide/perovskite) at 69 °C and 473 nm light irradiation (1000 mW/cm^2, over a circular area of 800 μm diameter), excess I^- is shown to catalyze the production of metallic lead via PbI_2 impurities. While near-stoichiometric samples (Pb/I = 2.8) showcased only a small increase of Pb^0 signals [Fig. 16(2a)], excess iodide samples (Pb/I = 3.8) showed a rapid loss of $FAPbI_3$ simultaneous to PbI_2 formation, followed by a gradual formation of Pb^0, suggesting a two-step reaction [Fig. 16(2b)].[49]

It is very common to find discrepancies in the literature regarding the beneficial or detrimental effects of illumination on perovskites. Motti *et al.* demonstrated that such conflicting reports can originate from the competing processes happening simultaneously in the perovskite film, which, depending on the sample conditions, one can dominate over other processes.[114] To demonstrate that, they employed *in situ* PL measurements with combined light and thermal stress. Illumination was tuned to various wavelengths and laser pulse repetition rates (varying incident power) and the sample was heated in inert atmosphere. It was concluded that the long living trapped carriers mediate the ionic movement under illumination. This induces different photochemical reactions that cause either PL increase or decrease. Moreover, their work demonstrates that passivating the coordinated I_2 by organic additives (or other passivation strategies) is key for a substantial enhancement of the device stability.

C. Illumination, bias, and temperature

Elevated light-induced heat and excess of photogenerated carriers were also found to be the main culprits in rapid photoinduced perovskite degradation. Chen *et al.* studied the effects of various light-induced stresses (heat, lattice strain, electric field, and charge carriers) in the stability of $MAPbI_3$.[82] The light-induced lattice strain was tracked with *in situ* XRD while the temperature of the sample was recorded [Fig. 16(3a)]. Upon illumination with 100 mW/cm^2, a shift to lower 2θ was observed uniformly across the reported XRD peaks, indicating an increase in the lattice strain. With further measurements with heating in the dark [Fig. 16(3b)], it was found that the strain was mostly induced by the light-induced heat. By measuring powder XRD, it was found that the light induced strain (T = 40 °C) was orientation-dependent [Fig. 16(3c)], in contrast with previous reports. With interferometry measurements, sub-millisecond changes in the film thickness could be detected, confirming that neither illumination alone nor piezoelectricity contributed to the lattice strain. However, the rapid initial degradation of PSC was not due to such lattice strain but originated by the coupled effect of heating and excess carriers that catalyze the process of defect formation.[82]

Another important implication of approaching operational conditions during *in situ* characterization is considering the environmental factors of PSC, independently on whether cells are encapsulated or not. It has been shown that the environmental conditions and variation of gas-pressure show an impact on the conductivity of a contacted single crystal perovskite.[113] Interaction of the perovskite with the environment can be avoided by encapsulation or passivation but, instead, interaction with its own degradation products should be considered.[109] Albeit the environment alone seldom produce drastic changes on perovskites (unless in extreme conditions), Siegler *et al.* prove that the atmosphere gases can have drastic impact under operational conditions. Optical transmittance of 550 nm light was used to quantify degradation rates under various combinations of stressors (see Table II) and illumination intensities. By adapting the probe and detection wavelengths to exclude the absorption/emission of the solid degradation products, they could monitor exactly the disappearance of $MAPbI_3$ in a thin film over time *in situ*. Two degradation pathways could be distinguished: (i) a dry photo-oxidation induced by the interaction of photoexcited electrons with the O_2 and (ii) a humidity accelerated photo-oxidation.

The increase in degradation rate with water and oxygen could not be explained by additive effects but only by synergy between water and oxygen in an accelerated mechanism. It was proposed that H_2O lowered the kinetic barrier for photo-oxidation as well as providing additional pathways to form reactive oxygen species, the superoxides are considered the rate-determining step for photo-oxidation. We note that, in this work, dark conditions could not be considered *in situ* since the probe changes the conditions by illumination, something supported by the rate in dark being affected by the sampling frequency when oxygen was present. In inert atmosphere, accelerated degradation was negligible either by probe laser or keeping the light on or off. Mass transport limited and kinetically limited processes are discussed with regard to the presence of water during degradation. These experiments were performed in high vacuum under gas flow to ensure kinetically limited conditions not slowed by mass transport. In real operational systems, mass transport may become dominant, especially at longer timescales. Water and oxygen may need to compete for adsorption sites on the surface, and

TABLE II. Observed degradation rates for all possible combinations of environmental stresses.

Observed rate of $MAPbI_3$ disappearance (mol m^{-2} s^{-1})		
Environmental condition	25 °C	85 °C
H_2O, O_2, light[a]	1×10^{-7}	2×10^{-7}
O_2, light	2×10^{-9}	1×10^{-7}
H_2O, light	5×10^{-10}	2×10^{-9}
H_2O, O_2, dark	$<1 \times 10^{-11}$	2×10^{-9}[b]
H_2O, dark	$<1 \times 10^{-11}$	5×10^{-11}
O_2, dark	2×10^{-10}[b]	1×10^{-9}[b]
Light, inert	$<1 \times 10^{-11}$	2×10^{-10}
Dark, inert	$<1 \times 10^{-11}$	3×10^{-10}

[a]H_2O: 50% RH; O_2: air (21% oxygen); light: 1 sun equivalent photon flux; inert: pure N_2 (<0.01% O_2).

[b]Samples in dark oxygen-containing environments degrade through photo-oxidation while the probe beam is active, making it unclear whether a distinct oxidation pathway operates under fully dark conditions (extended discussion can be found in the supplementary material of Ref. 109). Reprinted with permission from Siegler *et al.*, J. Am. Chem. Soc. **144**(12), 5552–5561 (2022). Copyright 2022 American Chemical Society.

passivation layers may occur on the surface from degradation products. If any water is created during any degradation in encapsulated samples, it could have detrimental effects on stability.[109] The experiments done by Siegler *et al.* demonstrated that, depending on the environmental conditions, perovskite degradation can take different pathways.[109] Related to this, changes in the degradation mechanisms can also be induced in more extreme conditions, such as high energy photon flux. To prove that, Kot *et al.* employed *in situ* near-ambient-pressure x-ray photo-electron spectroscopy (NAP-XPS) at almost dark conditions with very low intensity x-ray exposure ($6.1 \cdot 10^9$ photons/s) and different H_2O vapor pressure (10^{-3}, 10^{-2}, 10^{-1}, and 1 mbar).[112] No significant changes of the XPS spectra over time were obtained in dark, independently of the water vapor pressure. However, high x-ray photon fluxes ($7.4–9.9 \cdot 10^{11}$ photons/s, 520 eV) in humid conditions induced a pronounced degradation with changes in all the core level element binding energies. The authors propose that irreversible chemical reactions between the perovskite and water are catalyzed by the x-rays, in agreement with Das *et al.*[111] The irreversible decomposition from the break of the C–N bond generated a new N1s peak, attributed to NH_3, an irreversible decomposition product also proposed by Juarez-Perez *et al.*[107] The changes were attributed to the creation of Frenkel defects (such as interstitial MA^+ and I^- interstitials). It was proposed that this mechanism was mainly due to the weakening of the structure due to humidity, together with the intense radiation, yet oxygen presence could not be entirely excluded because of OH^- bonds created during sample transportation and as the method is highly surface sensitive.[112]

VIII. TOWARD THE PREDICTION OF OPERATIONAL STABILITY OF PSC UNDER OUTDOOR CONDITIONS

Before the publication in 2020 of the ISOS protocols for the stability assessment and reporting of PSCs,[6] and even in later publications, the reports of PSC stabilities were difficult to compare and unify in a table or chart.[6] A few review articles have attempted to tabulate the record stabilities reported including the most relevant details on the stress conditions and measurement protocols, which largely varies among publications. Noticeable is the lack of information in the description of measurement conditions in many publications reporting stability, where we find missing temperature or humidity values, incomplete characterization protocol description, or normalized stability without the value of the PCEs reported.[115–119] In this section, we will provide a brief overview of the state-of-the-art of outdoor studies, as an effort to correlate outdoor and indoor measurements and machine learning approaches to predict stability.

Zhang *et al.* have provided the first study employing a statistical comparison of a large stability data obtained from the reported literature and gathered in the Perovskite Database.[12,13,120] Over 7000 stability reports were categorized into the closest ISOS protocols [see Fig. 17(2)], and the authors proposed a unified indicator to enable the comparison between different stress conditions that led to several generalized conclusions. The authors emphasize that more detailed data are needed to feed the algorithms and extract more solid conclusions in the future. Their study is a great example of why data need to be standardized and why it is important to discuss practice of measurement, including more accurate models for describing device stability under the compounded stress of temperature, light, bias, humidity, and environmental stress cycles.

Velilla *et al.* reported in 2021 that while 19 407 documents were found when searching for "perovskite and solar cell" on SCOPUS (cite) database, only 100 articles could be found when adding the word "outdoor."[121,122] Köbler and Khenkin *et al.* have tabulated 14 outdoor stability studies (ISOS-O) on single junction perovskite from 2015 to 2021. They noted that in all the studies (except one) the device is set at open circuit while periodic j–V curves are measured in the solar simulator (ISOS-O-1) or under real sunlight (ISOS-O-2), not specified in the table. One of the works employed ISOS-O-3,[123] where the MPP is monitored *in situ*, which is the closest condition to *in operando* conditions and the recommended approach to perform the measurement. Previous studies have shown that periodic OC/J–V measurements provide different stability results than MPP tracking, as the ionic migration at different internal bias of the cell largely influences the degradation mechanisms.[124]

Reports on the prediction of PSC lifetime from stability studies have shown to be distinct depending on the type of analysis: indoor or outdoor. Currently, several important projects are being established where indoor and outdoor stability analyses are combined with machine learning tools. Thus, a surge of interesting new results is expected soon. However, some interesting relationships have been initially observed and, in a few cases, similar results were reported, as will be described below. There are some aspects of outdoor characterization that are difficult to incorporate into predictions of PSC stability performance from indoor testing. Indoor stability setups have the advantage of applying well-controlled dosage-specific combination of stressors with advanced *in situ* material characterization, while outdoor conditions impose multiple stressors in a variable and unpredictable way.

Song and Aernouts argued the importance of meteorological and diurnal variation during outdoor testing and indicated that variable conditions are essential if indoor testing must reflect real stability.[125] A PSC that reaches a steady state under accelerated testing conditions or during a constant stress test does not necessarily show a stable behavior outdoors. The large variation on diversity and intensity of outdoor stressors, such as temperature and light, occurs in diurnal and seasonal cycles. Therefore, it is important to emphasize that, although accelerated testing can prove the resistance of a device against certain conditions, resistance against variation of multiple stressors in a rather unpredicted manner would be the end goal for a solar cell with high lifespan.[125]

There are some reports successfully reproducing indoor studies in outdoor testing. Emery *et al.* compared PSC fabricated with two different encapsulation methods and could, by the ISOS-D3 (IEC 61215, 1000 h at 85 °C and 85% RH) protocol, see how results in the indoor controlled environment corresponded to the outdoor results [see Fig. 17(3)].[126] Devices that retained over 95% PCE at ISOS-D3 also passed an outdoor stability test according to ISOS-O3 procedures for over 10 months. The authors attempted to diagnose failure mechanisms in devices that did not pass the test, but unfortunately, *ex situ* EL and JV measurements were not sufficient to reveal what microstructural, compositional, and interfacial changes occurred in devices when changes in performance were seen.[126]

Köbler *et al.* showed that, for two different device structures, indoor constant illumination tests failed to predict the outdoor behavior of the PSCs, but cycling test ISOS-LC1-I could predict

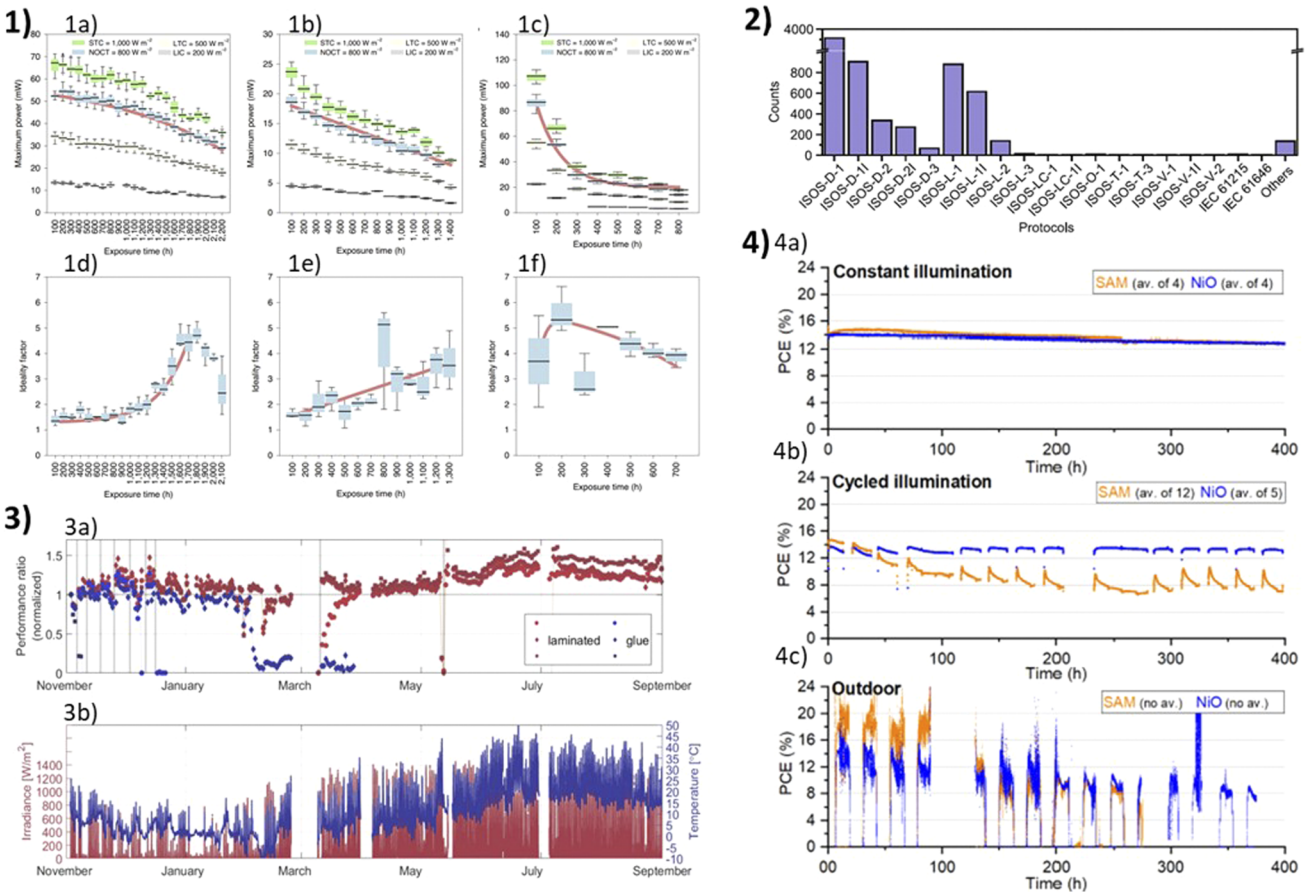

FIG. 17. (1) Patterns of degradation in the maximum power and the ideality factor. (1a)–(1c) Maximum power under different power rating conditions suggested by IEC 61863 for the convex (1a), linear (1b), and concave (1c) degradation behavior patterns. (1d)–(1f) Ideality factor (nID) analysis of the same samples: (1d) exhibits a concave pattern for samples exhibiting a convex Pmax pattern, (1e) nID exhibits a linear pattern for samples exhibiting a linear Pmax pattern, and (1f) nID exhibits a convex pattern for samples exhibiting a concave Pmax pattern. The thick black line on each box represents the average performance in the corresponding time window. Adapted with permission from Velilla *et al.*, Nat. Energy **6**(1), 54–62 (2021). Copyright 2021 Nature Publishing Group. (2) The distribution of stability protocols used for stability data in the Perovskite Database. The most widely used protocol is ISOS-D-1, where devices are stored in ambient air in the dark at open circuit. Adapted from Zhang *et al.*, Nat. Commun. **13**(1), 7639 (2022). Copyright 2022 Author(s), licensed under a Creative Commons Attribution 4.0 License. (3a) Evolution of PSC performance ratio of glued ("LAB") and laminated ("COM") cells during the outdoor exposure. Days of indoor control measurements are shown in gray. (3b) Irradiance in the plane of cells and cell temperature during the outdoor experiment. Adapted from Emery *et al.*, ACS Appl. Mater. Interfaces **14**(4), 5159–5167 (2022). Copyright 2022 Author(s), licensed under a Creative Commons Attribution 4.0 License. (4) Comparison of indoor and outdoor stability for two solar cells using a different HTL. (4a) Indoor experiment with constant illumination. (4b) Indoor experiment with cycled illumination. Both indoor experiments are conducted at 25 °C and in nitrogen. (4c) Outdoor experiment, conducted in Berlin, July–August 2020. Values not averaged for better display; averaged performance ratio over five and six cells. All experiments (a)–(c) were performed under continuous MPP-tracking. Adapted from Köbler *et al.*, "The challenge of designing accelerated indoor tests to predict the outdoor lifetime of perovskite solar cells" (2021). Copyright 2021 Author(s), licensed under a Creative Commons Attribution 4.0 License.

outdoor performance for one of the devices.[127] When aging tests were performed following ISOS-L1I [constant illumination, 25 °C, indoor, Fig. 17(4a)], ISOS-LC-1I [cycled illumination, 25 °C, indoor, Fig. 17(4b)], and ISOS-O2 [outdoor, Fig. 17(4c)], the different kinetics of the slow transients between samples delivered different results when comparing ISOS-L1I, ISOS-LC-1I, and ISOS-O2. The authors point out the importance of exercising caution when correlating stress changes to photovoltaic parameters during outdoor measurements, as levels of stress factors often change together during the day. Higher performance from irradiance soaking and higher temperature both peak at midday, resulting in an apparent positive effect of the temperature on device efficiency, something contested by controlled studies under indoor conditions. These common trends propose a problem in outdoor data analysis, making *in situ* outdoor measurements a necessary tool for PSC commercialization. Still, this also argues the importance of having performed indoor studies to achieve the separate picture of stressor effects before trying to see the effects of a multitude of stressors varying simultaneously.

In tandem devices, the comparisons of silicon SCs and PSCs have led to observations in what outdoors variations set off a difference PSC stability compared to its silicon counterpart. Babics *et al.* identified that light intensity and temperature variations in combination with dust accumulation (soiling) differentiate outdoor from indoor laboratory conditions when monitoring all the photovoltaic parameters and matching current between the Si and perovskite part of tandem device.[128]

Tress *et al.* performed long-term indoor operational tests on efficient PSC devices under a simulation of temperature and illumination outdoor conditions, flushed with dry nitrogen, to find reversible degradation as the main responsible factor for efficiency fluctuation. They observed that the intrinsic response-differences of the PSC in these conditions were dependent of the time of day and season. Changing conditions, as outlined in Secs. VI and VII, can produce synergetic, competitive, escalating effects.[129]

By monitoring the temporal evolution of the MPP and JV curves of PSC minimodules tested at an outdoor testing site, Velilla *et al.* observed three different trends in MPP loss vs time (degradation-shape): concave, linear, and convex evolution [Fig. 17(1)].[121,122] The mean solar cell junction temperature as a function of solar irradiation, ambient temperature and thermal properties of the photovoltaic material, and IV curves from tested devices obtained every minute helped the authors gain suspicion of the physical mechanisms that could be responsible for the different slopes in the power decrease. By monitoring the ideality factor evolution, the authors added another measure of the quantitative cell degradation, one that combined readout from cells that can be more related to the device physical and chemical properties, although physical phenomena were not immediately observed.

Zhao *et al.* observed that the degradation of PSC followed an Arrhenius dependence on temperatures between 35 and 100 °C in their experiments at constant illumination. This observation was used to predict the 5-year lifetimes for a certain cell stack. Yet they assumed continuous temperature of 35 °C for this prediction, which is far from the actual outdoor operating conditions, and recent studies have debated the validity of constant condition tests to portrait real operational stability with outdoor unpredictable conditions under variation.[10]

While accelerated testing may provide a shortcut to seeing the processes that occur over time, quantification of the performance lifetime of a device by prediction from accelerated tests has not yet been demonstrated. Reproducing exact outdoor conditions along operation lifetimes of years in indoor setups is extremely challenging and unpractical, limiting the accuracy of the conclusions extracted. To establish a correlation between indoor and outdoor stability measurements together with material changes, the scientific community must work in parallel toward (i) increasing the reports on outdoor stability tests for various device structures and perovskite compositions, together with additional *in situ* characterization besides j–V or MPP tracking and (iii) increasing the parameter combination of the simulated stressors that are applied in indoor setups imitating the ambient variations. It is worth mentioning that correlating indoor and outdoor tests and reaching a consensus on its relationship and the development of accelerated tests seems only feasible through the implementation of automated analysis and machine learning that can cope with the vast parameter space, statistics, and weather variability. It is also important to consider the conclusions obtained by authors working on big data analysis, indicating that research efforts may be inconsistent due to differences in sample quality and history, common practices, laboratory facilities, among others. Despite the current challenge to categorize the reports into a certain ISOS protocol, it is encouraging that recent publications provide more complete description of the methods, indicating a general trend on reaching standardized stability measurements. This is particularly interesting to facilitate machine learning studies to make predictions and design and validate the accelerated indoor tests.

IX. GOOD PRACTICES AND CONCLUSIONS

In situ and *operando* characterization of PSCs under different stressors has provided significant insights into physical, chemical, mechanical, and electrochemical transformation in these materials and systems. Given the "soft material" nature of halide perovskites, where reversible effects and special features are observed at short timescales (e.g., recovery in the dark, ion migration), *in situ* and *operando* characterization appears as the holy grail on providing new degradation insights from continuous monitoring. We have observed that most characterization techniques investigate singular physics/chemistry of the material system; however, there is strong interdependent interplay of degradation mechanisms in PSCs, which can only be identified under *in situ* and *operando* conditions.

These methods can accurately monitor the relationship between different stressors imposed sequentially or at one single time, resembling the real testing conditions of a PSC. The application of *in situ* multi-modal characterization under several stressors has not been reported yet but is foreseen as the optimal step in characterization complexity.

It is apparent from the publications mentioned in this article that many *in situ* studies have multi-stressor components, although multi-stressor comparison might not have been the main target of the studies. The source of stressor, especially for the light/thermal stressors section, describes an ambiguity as one stressor may be the source of the other, unless conditions are carefully controlled. A similar response is observed for environmental conditions where the removal of gases has indeed been studied as a separate environment. Different environments should be considered in cases where the atmosphere is in continuous flow mode (such as in a holder with N_2 flux) or the device is sealed, and the initial volume is the same throughout experiments. This is especially important since encapsulation is crucial for the commercialization of PSCs, and thus, analyses under gas flux is probably not the most accurate condition to understand PSCs degradation.

Many are the working mechanisms behind PSC degradation that are still unresolved, for example, localized heating and hotspot phenomena, and the effect of irradiation under vacuum or extreme temperature (e.g., freezing) cycling. Similarly, the nature of reverse bias voltage imposed to PSC (related to shading under real operation conditions) and its effect on irreversible degradation and hysteresis are still open questions that need to be resolved.

We expect that *in situ* and *operando* characterization will be extrapolated to the scale up and fabrication of PSCs in a production line (from synthesis, processing, and integration of the components at industrial level). Although consensus protocols for stability assessment of PSC have already been reported, these are still missing for

the characterization of PSC technology. In this regard, we must also consider that the current technological benchmark for PSCs comprises modeling approaches and relies on AI tools, such as machine learning. Therefore, it is crucial for the practical implementation of PSC technology to move the attention onto technological aspects related to *in situ* and *operando* characterization under *real-world* functioning of the entire PV systems.

ACKNOWLEDGMENTS

We thank the Project ProperPotoMile, which is supported under the umbrella of SOLAR-ERA.NET Cofund 2 by the Spanish Ministry of Science and Education and the AEI under the Project No. PCI2020-112185 and CDTI Project No. IDI-20210171. The ICN2 was supported by the Severo Ochoa Centers of Excellence program (AEI) (SEV-2017) and is currently supported by the Severo Ochoa Centers of Excellence program (Grant No. CEX2021-001214-S), both funded by MCIN/AEI/10.13039.501100011033, and also funded by the CERCA Program/Generalitat de Catalunya. Thanks to the Agència de Gestiód'Ajuts Universitaris i de Recerca (AGAUR) for the support to the consolidated Catalonia research group 2021 (Grant No. SGR 01617) and the Xarxa d' R + D + I Energy for Society (XRE4S). S.R.R. acknowledges the support from "la Caixa" Foundation (ID 100010434) with fellowship code LCF/BQ/PI20/11760024 and Grant No. PID2021-122349OA-I00 funded by MCIN/AEI/10.13039/501100011033 and "ERDF A way of making Europe." The authors acknowledge the Spanish Ministry of Science and Innovation for the predoctoral contract to F.B. with Reference No. PRE2020-092669 of the Project No. SEV-2017-0706-20-3. The authors thank Dámaso Torres for his valuable help with 3D image design and rendering.

AUTHOR DECLARATIONS

Conflict of Interest

The authors have no conflicts to disclose.

Author Contributions

F.B. and S.R.R. contributed equally to this work.

Fanny Baumann: Conceptualization (equal); Data curation (equal); Investigation (equal); Writing – original draft (equal); Writing – review & editing (equal). **Sonia R. Raga**: Conceptualization (equal); Data curation (equal); Funding acquisition (equal); Project administration (equal); Supervision (equal); Validation (equal); Writing – original draft (equal); Writing – review & editing (equal). **Monica Lira-Cantú**: Conceptualization (equal); Funding acquisition (equal); Project administration (equal); Resources (equal); Supervision (equal); Writing – original draft (equal); Writing – review & editing (equal).

DATA AVAILABILITY

Data sharing is not applicable to this article as no new data were created or analyzed in this study.

REFERENCES

[1]W. Shockley and H. J. Queisser, "Detailed balance limit of efficiency of *p-n* junction solar cells," J. Appl. Phys. **32**(3), 510–519 (1961).
[2]J. Park, J. Kim, H.-S. Yun, M. J. Paik, E. Noh, H. J. Mun, M. G. Kim, T. J. Shin, and S. I. Seok, "Controlled growth of perovskite layers with volatile alkyl ammonium chlorides," Nature (published online).
[3]National Renewable Energy Laboratory, Best Research-Cell Efficiency Chart, 2023, https://www.nrel.gov/pv/assets/pdfs/best-research-cell-efficiencies.pdf.
[4]M. H. Futscher and B. Ehrler, "Modeling the performance limitations and prospects of perovskite/Si tandem solar cells under realistic operating conditions," ACS Energy Lett. **2**(9), 2089–2095 (2017).
[5]M. O. Reese, S. A. Gevorgyan, M. Jørgensen, E. Bundgaard, S. R. Kurtz, D. S. Ginley, D. C. Olson, M. T. Lloyd, P. Morvillo, E. A. Katz *et al.*, "Consensus stability testing protocols for organic photovoltaic materials and devices," Sol. Energy Mater. Sol. Cells **95**(5), 1253–1267 (2011).
[6]M. V. Khenkin, E. A. Katz, A. Abate, G. Bardizza, J. J. Berry, C. Brabec, F. Brunetti, V. Bulović, Q. Burlingame, A. Di Carlo *et al.*, "Consensus statement for stability assessment and reporting for perovskite photovoltaics based on ISOS procedures," Nat. Energy **5**(1), 35–49 (2020).
[7]Y. Li, B. Shi, Q. Xu, L. Yan, N. Ren, Y. Chen, W. Han, Q. Huang, Y. Zhao, and X. Zhang, "Wide bandgap interface layer induced stabilized perovskite/silicon tandem solar cells with stability over ten thousand hours," Adv. Energy Mater. **11**(48), 2102046 (2021).
[8]G. Grancini, C. Roldán-Carmona, I. Zimmermann, E. Mosconi, X. Lee, D. Martineau, S. Narbey, F. Oswald, F. De Angelis, M. Graetzel, and M. K. Nazeeruddin, "One-year stable perovskite solar cells by 2D/3D interface engineering," Nat. Commun. **8**, 15684 (2017).
[9]P. Guo, H. Zhu, W. Zhao, C. Liu, L. Zhu, Q. Ye, N. Jia, H. Wang, X. Zhang, W. Huang *et al.*, "Interfacial embedding of laser-manufactured fluorinated gold clusters enabling stable perovskite solar cells with efficiency over 24%," Adv. Mater. **33**(36), 2101590 (2021).
[10]X. Zhao, T. Liu, Q. C. Burlingame, T. Liu, R. Holley, G. Cheng, N. Yao, F. Gao, and Y.-L. Loo, "Accelerated aging of all-inorganic, interface-stabilized perovskite solar cells," Science **377**(6603), 307–310 (2022).
[11]S. Sun, A. Tiihonen, F. Oviedo, Z. Liu, J. Thapa, Y. Zhao, N. T. P. Hartono, A. Goyal, T. Heumueller, C. Batali *et al.*, "A data fusion approach to optimize compositional stability of halide perovskites," Matter **4**(4), 1305–1322 (2021).
[12]Z. Zhang, H. Wang, T. J. Jacobsson, and J. Luo, "Big data driven perovskite solar cell stability analysis," Nat. Commun. **13**(1), 7639 (2022).
[13]T. J. Jacobsson, A. Hultqvist, A. García-Fernández, A. Anand, A. Al-Ashouri, A. Hagfeldt, A. Crovetto, A. Abate, A. G. Ricciardulli, A. Vijayan *et al.*, "An open-access database and analysis tool for perovskite solar cells based on the FAIR data principles," Nat. Energy **7**(1), 107–115 (2022).
[14]J. A. Christians, P. A. Miranda Herrera, and P. V. Kamat, "Transformation of the excited state and photovoltaic efficiency of $CH_3NH_3PbI_3$ perovskite upon controlled exposure to humidified air," J. Am. Chem. Soc. **137**, 1530 (2015).
[15]A. M. A. Leguy, Y. Hu, M. Campoy-Quiles, M. I. Alonso, O. J. Weber, P. Azarhoosh, M. van Schilfgaarde, M. T. Weller, T. Bein, J. Nelson, P. Docampo, and P. R. F. Barnes, "Reversible hydration of $CH_3NH_3PbI_3$ in films, single crystals, and solar cells," Chem. Mater. **27**, 3397 (2015).
[16]W. Chi and S. K. Banerjee, "Achieving resistance against moisture and oxygen for perovskite solar cells with high efficiency and stability," Chem. Mater. **33**(12), 4269–4303 (2021).
[17]Y. Hu, M. F. Aygüler, M. L. Petrus, T. Bein, and P. Docampo, "Impact of rubidium and cesium cations on the moisture stability of multiple-cation mixed-halide perovskites," ACS Energy Lett. **2**, 2212 (2017).
[18]M. A. A. Kazemi, N. Folastre, P. Raval, M. Sliwa, J. M. V. Nsanzimana, S. Golonu, A. Demortiere, J. Rousset, O. Lafon, L. Delevoye *et al.*, "Moisture-induced non-equilibrium phase segregation in triple cation mixed halide perovskite monitored by *in situ* characterization techniques and solid-state NMR," Energy Environ. Mater. **6**, e12335 (2021).
[19]M. A. Akhavan Kazemi, P. Raval, K. Cherednichekno, J. N. Chotard, A. Krishna, A. Demortiere, G. N. M. Reddy, and F. Sauvage, "Molecular-level insight into

correlation between surface defects and stability of methylammonium lead halide perovskite under controlled humidity," Small Methods **5**(2), 2000834 (2021).
[20]S. Kundu and T. L. Kelly, "Improving the moisture stability of perovskite solar cells by using PMMA/P3HT based hole-transport layers," Mater. Chem. Front. **2**(1), 81–89 (2018).
[21]J. Yang, B. D. Siempelkamp, D. Liu, and T. L. Kelly, "Investigation of $CH_3NH_3PbI_3$ degradation rates and mechanisms in controlled humidity environments using *in situ* techniques," ACS Nano **9**(2), 1955–1963 (2015).
[22]Y. Ying-Guo, Y. Guang-Zhi, F. Shang-Lei, L. Meng, J. Geng-Wu, S. Fei, W. Wen, and G. Xing-Yu, "An in-situ real time study of the perovskite film micro-structural evolution in a humid environment by using synchrotron based characterization technique," Acta Phys. Sin. **66**(1), 018401 (2017).
[23]D. Li, S. A. Bretschneider, V. W. Bergmann, I. M. Hermes, J. Mars, A. Klasen, H. Lu, W. Tremel, M. Mezger, H.-J. Butt *et al.*, "Humidity-induced grain boundaries in $MAPbI_3$ perovskite films," J. Phys. Chem. C **120**(12), 6363–6368 (2016).
[24]J. Schlipf, L. Bießmann, L. Oesinghaus, E. Berger, E. Metwalli, J. A. Lercher, L. Porcar, and P. Müller-Buschbaum, "In situ monitoring the uptake of moisture into hybrid perovskite thin films," J. Phys. Chem. Lett. **9**(8), 2015–2021 (2018).
[25]L. Hu, G. Shao, T. Jiang, D. Li, X. Lv, H. Wang, X. Liu, H. Song, J. Tang, and H. Liu, "Investigation of the interaction between perovskite films with moisture via in situ electrical resistance measurement," ACS Appl. Mater. Interfaces **7**(45), 25113–25120 (2015).
[26]Z. Song, A. Abate, S. C. Watthage, G. K. Liyanage, A. B. Phillips, U. Steiner, M. Graetzel, and M. J. Heben, "Perovskite solar cell stability in humid air: Partially reversible phase transitions in the PbI_2-CH_3NH_3I-H_2O system," Adv. Energy Mater. **6**(19), 1600846 (2016).
[27]A. N. Urwick, F. Bastianini, G. E. Pérez, and A. Dunbar, "Deciphering perovskite decomposition in a humid atmosphere with TOF-GISANS," Energy Rep. **8**, 23–33 (2022).
[28]S. Maniyarasu, B. F. Spencer, H. Mo, A. S. Walton, A. G. Thomas, and W. R. Flavell, "Surface stability of ionic-liquid-passivated mixed-cation perovskite probed with *in situ* photoelectron spectroscopy," J. Mater. Chem. A **10**(35), 18206–18217 (2022).
[29]Y. Li, X. Xu, C. Wang, B. Ecker, J. Yang, J. Huang, and Y. Gao, "Light-induced degradation of $CH_3NH_3PbI_3$ hybrid perovskite thin film," J. Phys. Chem. C **121**, 3904 (2017).
[30]A. Senocrate, T. Acartürk, G. Y. Kim, R. Merkle, U. Starke, M. Grätzel, and J. Maier, "Interaction of oxygen with halide perovskites," J. Mater. Chem. A **6**(23), 10847–10855 (2018).
[31]N. Aristidou, I. Sanchez-Molina, T. Chotchuangchutchaval, M. Brown, L. Martinez, T. Rath, and S. A. Haque, "The role of oxygen in the degradation of methylammonium lead trihalide perovskite photoactive layers," Angew. Chem., Int. Ed. **54**, 8208 (2015).
[32]X. Tang, M. Brandl, B. May, I. Levchuk, Y. Hou, M. Richter, H. Chen, S. Chen, S. Kahmann, A. Osvet, F. Maier, H.-P. Steinrück, R. Hock, G. J. Matt, and C. J. Brabec, "Photoinduced degradation of methylammonium lead triiodide perovskite semiconductors," J. Mater. Chem. A **4**, 15896 (2016).
[33]Y. Nakamura, N. Shibayama, K. Fujiwara, T. Koganezawa, and T. Miyasaka, "Degradation mechanism of halide perovskite crystals under concurrent light and humidity exposure," ACS Mater. Lett. **4**, 2409–2414 (2022).
[34]K. Ho, M. Wei, E. H. Sargent, and G. C. Walker, "Grain transformation and degradation mechanism of formamidinium and cesium lead iodide perovskite under humidity and light," ACS Energy Lett. **6**(3), 934–940 (2021).
[35]P. Pistor, A. Ruiz, A. Cabot, and V. Izquierdo-Roca, "Advanced Raman spectroscopy of methylammonium lead iodide: Development of a non-destructive characterisation methodology," Sci. Rep. **6**(1), 35973 (2016).
[36]M. C. Brennan, S. Draguta, P. V. Kamat, and M. Kuno, "Light-induced anion phase segregation in mixed halide perovskites," ACS Energy Lett. **3**(1), 204–213 (2018).
[37]D. W. deQuilettes, W. Zhang, V. M. Burlakov, D. J. Graham, T. Leijtens, A. Osherov, V. Bulović, H. J. Snaith, D. S. Ginger, and S. D. Stranks, "Photo-induced halide redistribution in organic–inorganic perovskite films," Nat. Commun. **7**, 11683 (2016).
[38]W.-A. Quitsch, D. W. deQuilettes, O. Pfingsten, A. Schmitz, S. Ognjanovic, S. Jariwala, S. Koch, M. Winterer, D. S. Ginger, and G. Bacher, "The role of excitation energy in photobrightening and photodegradation of halide perovskite thin films," J. Phys. Chem. Lett. **9**(8), 2062–2069 (2018).
[39]S. D. Stranks, V. M. Burlakov, T. Leijtens, J. M. Ball, A. Goriely, and H. J. Snaith, "Recombination kinetics in organic-inorganic perovskites: Excitons, free charge, and subgap states," Phys. Rev. Appl. **2**(3), 034007 (2014).
[40]Y. Tian, M. Peter, E. Unger, M. Abdellah, K. Zheng, T. Pullerits, A. Yartsev, V. Sundström, and I. G. Scheblykin, "Mechanistic insights into perovskite photoluminescence enhancement: Light curing with oxygen can boost yield thousandfold," Phys. Chem. Chem. Phys. **17**(38), 24978–24987 (2015).
[41]H. Choi, J. C.-R. Ke, S. Skalsky, C. A. Castle, K. Li, K. L. Moore, W. R. Flavell, and P. Parkinson, "Visualizing the role of photoinduced ion migration on photoluminescence in halide perovskite grains," J. Mater. Chem. C **8**(22), 7509–7518 (2020).
[42]M. G. Albrecht and M. Green, "The kinetics of the photolysis of thin films of lead iodide," J. Phys. Chem. Solids **38**, 297 (1977).
[43]S. Wang, Y. Jiang, E. J. Juarez-Perez, L. K. Ono, and Y. Qi, "Accelerated degradation of methylammonium lead iodide perovskites induced by exposure to iodine vapour," Nat. Energy **2**(1), 16195 (2016).
[44]A. Merdasa, A. Kiligaridis, C. Rehermann, M. Abdi-Jalebi, J. Stöber, B. Louis, M. Gerhard, S. D. Stranks, E. L. Unger, and I. G. Scheblykin, "Impact of excess lead iodide on the recombination kinetics in metal halide perovskites," ACS Energy Lett. **4**(6), 1370–1378 (2019).
[45]H. Yuan, E. Debroye, K. Janssen, H. Naiki, C. Steuwe, G. Lu, M. Moris, E. Orgiu, H. Uji-i, F. De Schryver *et al.*, "Degradation of methylammonium lead iodide perovskite structures through light and electron beam driven ion migration," J. Phys. Chem. Lett. **7**(3), 561–566 (2016).
[46]G. M. Paternò, V. Robbiano, L. Santarelli, A. Zampetti, C. Cazzaniga, V. Garcia Sakai, and F. Cacialli, "Perovskite solar cell resilience to fast neutrons," Sustainable Energy Fuels **3**(10), 2561–2566 (2019).
[47]J. Yang, Q. Hong, Z. Yuan, R. Xu, X. Guo, S. Xiong, X. Liu, S. Braun, Y. Li, J. Tang *et al.*, "Unraveling photostability of mixed cation perovskite films in extreme environment," Adv. Opt. Mater. **6**(20), 1800262 (2018).
[48]L. Lu, K.-C. Shen, J. Wang, Z. Su, Y. Li, L. Chen, Y. Luo, F. Song, X. Gao, and J.-X. Tang, "Interaction of the cation and vacancy in hybrid perovskites induced by light illumination," ACS Appl. Mater. Interfaces **12**(37), 42369–42377 (2020).
[49]A. Donakowski, D. W. Miller, N. C. Anderson, A. Ruth, E. M. Sanehira, J. J. Berry, M. D. Irwin, A. Rockett, and K. X. Steirer, "Improving photostability of cesium-doped formamidinium lead triiodide perovskite," ACS Energy Lett. **6**(2), 574–580 (2021).
[50]E. T. Hoke, D. J. Slotcavage, E. R. Dohner, A. R. Bowring, H. I. Karunadasa, and M. D. McGehee, "Reversible photo-induced trap formation in mixed-halide hybrid perovskites for photovoltaics," Chem. Sci. **6**(1), 613–617 (2015).
[51]A. J. Barker, A. Sadhanala, F. Deschler, M. Gandini, S. P. Senanayak, P. M. Pearce, E. Mosconi, A. J. Pearson, Y. Wu, A. R. Srimath Kandada, T. Leijtens, F. De Angelis, S. E. Dutton, A. Petrozza, and R. H. Friend, "Defect-assisted photoinduced halide segregation in mixed-halide perovskite thin films," ACS Energy Lett. **2**, 1416 (2017).
[52]D. P. McMeekin, G. Sadoughi, W. Rehman, G. E. Eperon, M. Saliba, M. T. Hörantner, A. Haghighirad, N. Sakai, L. Korte, B. Rech, M. B. Johnston, L. M. Herz, and H. J. Snaith, "A mixed-cation lead mixed-halide perovskite absorber for tandem solar cells," Science **351**, 151 (2016).
[53]C. M. Sutter-Fella, Q. P. Ngo, N. Cefarin, K. L. Gardner, N. Tamura, C. V. Stan, W. S. Drisdell, A. Javey, F. M. Toma, and I. D. Sharp, "Cation-dependent light-induced halide demixing in hybrid organic–inorganic perovskites," Nano Lett. **18**(6), 3473–3480 (2018).
[54]J. Liang, C. Chen, X. Hu, Z. Chen, X. Zheng, J. Li, H. Wang, F. Ye, M. Xiao, Z. Lu *et al.*, "Suppressing the phase segregation with potassium for highly efficient and photostable inverted wide-band gap halide perovskite solar cells," ACS Appl. Mater. Interfaces **12**(43), 48458–48466 (2020).
[55]A. J. Knight, A. D. Wright, J. B. Patel, D. P. McMeekin, H. J. Snaith, M. B. Johnston, and L. M. Herz, "Electronic traps and phase segregation in lead mixed-halide perovskite," ACS Energy Lett. **4**(1), 75–84 (2019).
[56]N. Aihemaiti, Y. Jiang, Y. Zhu, and S. Peng, "Light-induced phase segregation evolution of all-inorganic mixed halide perovskites," J. Phys. Chem. Lett. **14**(1), 267–272 (2023).

[57]W. Mao, C. R. Hall, A. S. R. Chesman, C. Forsyth, Y. B. Cheng, N. W. Duffy, T. A. Smith, and U. Bach, "Visualizing phase segregation in mixed-halide perovskite single crystals," Angew. Chem., Int. Ed. **58**(9), 2893–2898 (2019).
[58]G. C. Halford, Q. Deng, A. Gomez, T. Green, J. M. Mankoff, and R. A. Belisle, "Structural dynamics of metal halide perovskites during photoinduced halide segregation," ACS Appl. Mater. Interfaces **14**(3), 4335–4343 (2022).
[59]D. Kim, J. S. Yun, P. Sharma, D. S. Lee, J. Kim, A. M. Soufiani, S. Huang, M. A. Green, A. W. Y. Ho-Baillie, and J. Seidel, "Light- and bias-induced structural variations in metal halide perovskites," Nat. Commun. **10**(1), 444 (2019).
[60]H. Funk, O. Shargaieva, A. Eljarrat, E. L. Unger, C. T. Koch, and D. Abou-Ras, "In situ TEM monitoring of phase-segregation in inorganic mixed halide perovskite," J. Phys. Chem. Lett. **11**(13), 4945–4950 (2020).
[61]U. B. Cappel, S. Svanström, V. Lanzilotto, F. O. L. Johansson, K. Aitola, B. Philippe, E. Giangrisostomi, R. Ovsyannikov, T. Leitner, A. Föhlisch, S. Svensson, N. Mårtensson, G. Boschloo, A. Lindblad, and H. Rensmo, "Partially reversible photoinduced chemical changes in a mixed-ion perovskite material for solar cells," ACS Appl. Mater. Interfaces **9**, 34970 (2017).
[62]S. J. Yoon, M. Kuno, and P. V. Kamat, "Shift happens. How halide ion defects influence photoinduced segregation in mixed halide perovskites," ACS Energy Lett. **2**, 1507 (2017).
[63]S. J. Yoon, S. Draguta, J. S. Manser, O. Sharia, W. F. Schneider, M. Kuno, and P. V. Kamat, "Tracking iodide and bromide ion segregation in mixed halide lead perovskites during photoirradiation," ACS Energy Lett. **1**(1), 290–296 (2016).
[64]R. E. Beal, D. J. Slotcavage, T. Leijtens, A. R. Bowring, R. A. Belisle, W. H. Nguyen, G. F. Burkhard, E. T. Hoke, and M. D. McGehee, "Cesium lead halide perovskites with improved stability for tandem solar cells," J. Phys. Chem. Lett. **7**, 746 (2016).
[65]W. Rehman, R. L. Milot, G. E. Eperon, C. Wehrenfennig, J. L. Boland, H. J. Snaith, M. B. Johnston, and L. M. Herz, "Charge-carrier dynamics and mobilities in formamidinium lead mixed-halide perovskites," Adv. Mater. **27**(48), 7938–7944 (2015).
[66]S. Chen, Y. Hou, H. Chen, M. Richter, F. Guo, S. Kahmann, X. Tang, T. Stubhan, H. Zhang, N. Li *et al.*, "Exploring the limiting open-circuit voltage and the voltage loss mechanism in planar $CH_3NH_3PbBr_3$ perovskite solar cells," Adv. Energy Mater. **6**(18), 1600132 (2016).
[67]D. Guo, Z. Andaji Garmaroudi, M. Abdi-Jalebi, S. D. Stranks, and T. J. Savenije, "Reversible removal of intermixed shallow states by light soaking in multication mixed halide perovskite films," ACS Energy Lett. **4**(10), 2360–2367 (2019).
[68]A. Ruth, M. C. Brennan, S. Draguta, Y. V. Morozov, M. Zhukovskyi, B. Janko, P. Zapol, and M. Kuno, "Vacancy-mediated anion photosegregation kinetics in mixed halide hybrid perovskites: Coupled kinetic Monte Carlo and optical measurements," ACS Energy Lett. **3**(10), 2321–2328 (2018).
[69]T. Duong, H. K. Mulmudi, Y. Wu, X. Fu, H. Shen, J. Peng, N. Wu, H. T. Nguyen, D. Macdonald, M. Lockrey *et al.*, "Light and electrically induced phase segregation and its impact on the stability of quadruple cation high bandgap perovskite solar cells," ACS Appl. Mater. Interfaces **9**(32), 26859–26866 (2017).
[70]Z. Yang, A. Rajagopal, S. B. Jo, C.-C. Chueh, S. Williams, C.-C. Huang, J. K. Katahara, H. W. Hillhouse, and A. K.-Y. Jen, "Stabilized wide bandgap perovskite solar cells by tin substitution," Nano Lett. **16**(12), 7739–7747 (2016).
[71]F. Lehmann, A. Franz, D. M. Többens, S. Levcenco, T. Unold, A. Taubert, and S. Schorr, "The phase diagram of a mixed halide (Br, I) hybrid perovskite obtained by synchrotron X-ray diffraction," RSC Adv. **9**(20), 11151–11159 (2019).
[72]K. Suchan, J. Just, P. Becker, C. Rehermann, A. Merdasa, R. Mainz, I. G. Scheblykin, and E. L. Unger, "Broad distribution of local I/Br ratio in illuminated mixed halide perovskite films revealed by correlative X-ray diffraction and photoluminescence," arXiv:2101.00645 (2021).
[73]G. Divitini, S. Cacovich, F. Matteocci, L. Cinà, A. Di Carlo, and C. Ducati, "*In situ* observation of heat-induced degradation of perovskite solar cells," Nat. Energy **1**, 15012 (2016).
[74]T. W. Kim, N. Shibayama, L. Cojocaru, S. Uchida, T. Kondo, and H. Segawa, "Real-time in situ observation of microstructural change in organometal halide perovskite induced by thermal degradation," Adv. Funct. Mater. **28**(42), 1804039 (2018).
[75]Z. Fan, H. Xiao, Y. Wang, Z. Zhao, Z. Lin, H.-C. Cheng, S.-J. Lee, G. Wang, Z. Feng, W. A. Goddard *et al.*, "Layer-by-layer degradation of methylammonium lead tri-iodide perovskite microplates," Joule **1**(3), 548–562 (2017).
[76]S. R. Raga, L. K. Ono, and Y. Qi, "Rapid perovskite formation by CH_3NH_2 gas-induced intercalation and reaction of PbI_2," J. Mater. Chem. A **4**(7), 2494–2500 (2016).
[77]B. Yang, O. Dyck, W. Ming, M.-H. Du, S. Das, C. M. Rouleau, G. Duscher, D. B. Geohegan, and K. Xiao, "Observation of nanoscale morphological and structural degradation in perovskite solar cells by in situ TEM," ACS Appl. Mater. Interfaces **8**(47), 32333–32340 (2016).
[78]Y.-H. Seo, J. H. Kim, D.-H. Kim, H.-S. Chung, and S.-I. Na, "*In situ* TEM observation of the heat-induced degradation of single- and triple-cation planar perovskite solar cells," Nano Energy **77**, 105164 (2020).
[79]M. Long, T. Zhang, M. Liu, Z. Chen, C. Wang, W. Xie, F. Xie, J. Chen, G. Li, and J. Xu, "Abnormal synergetic effect of organic and halide ions on the stability and optoelectronic properties of a mixed perovskite via in situ characterizations," Adv. Mater. **30**(28), 1801562 (2018).
[80]J. A. Aguiar, S. Wozny, T. G. Holesinger, T. Aoki, M. K. Patel, M. Yang, J. J. Berry, M. Al-Jassim, W. Zhou, and K. Zhu, "*In situ* investigation of the formation and metastability of formamidinium lead tri-iodide perovskite solar cells," Energy Environ. Sci. **9**(7), 2372–2382 (2016).
[81]Y.-C. Li, C. Ge, H.-Y. Song, P. Wang, X.-R. Ma, and S.-B. Liu, "Analysis of ultrafast carrier dynamics and steady-state reflectivity on lattice expansion in metal halide perovskite during continuous illumination," J. Appl. Phys. **132**(1), 013102 (2022).
[82]B. Chen, J. Song, X. Dai, Y. Liu, P. N. Rudd, X. Hong, and J. Huang, "Synergistic effect of elevated device temperature and excess charge carriers on the rapid light-induced degradation of perovskite solar cells," Adv. Mater. **31**(35), 1902413 (2019).
[83]J. Borchert, H. Boht, W. Fränzel, R. Csuk, R. Scheer, and P. Pistor, "Structural investigation of co-evaporated methyl ammonium lead halide perovskite films during growth and thermal decomposition using different PbX_2 (X = I, Cl) precursors," J. Mater. Chem. A **3**(39), 19842–19849 (2015).
[84]A. Dualeh, P. Gao, S. I. Seok, M. K. Nazeeruddin, and M. Grätzel, "Thermal behavior of methylammonium lead-trihalide perovskite photovoltaic light harvesters," Chem. Mater. **26**, 6160 (2014).
[85]J.-Y. Ma, J. Ding, H.-J. Yan, D. Wang, and J.-S. Hu, "Temperature-dependent local electrical properties of organic–inorganic halide perovskites: In situ KPFM and c-AFM investigation," ACS Appl. Mater. Interfaces **11**(24), 21627–21633 (2019).
[86]E. J. Juarez-Perez, Z. Hawash, S. R. Raga, L. K. Ono, and Y. Qi, "Thermal degradation of $CH_3NH_3PbI_3$ perovskite into NH_3 and CH_3I gases observed by coupled thermogravimetry–mass spectrometry analysis," Energy Environ. Sci. **9**(11), 3406–3410 (2016).
[87]W. Tan, A. R. Bowring, A. C. Meng, M. D. McGehee, and P. C. McIntyre, "Thermal stability of mixed cation metal halide perovskites in air," ACS Appl. Mater. Interfaces **10**(6), 5485–5491 (2018).
[88]N.-K. Kim, Y. H. Min, S. Noh, E. Cho, G. Jeong, M. Joo, S.-W. Ahn, J. S. Lee, S. Kim, K. Ihm *et al.*, "Investigation of thermally induced degradation in $CH_3NH_3PbI_3$ perovskite solar cells using *in-situ* synchrotron radiation analysis," Sci. Rep. **7**(1), 4645 (2017).
[89]E. J. Juarez-Perez, L. K. Ono, and Y. Qi, "Thermal degradation of formamidinium based lead halide perovskites into *sym*-triazine and hydrogen cyanide observed by coupled thermogravimetry-mass spectrometry analysis," J. Mater. Chem. A **7**(28), 16912–16919 (2019).
[90]X. Wang, J. Gong, X. Shan, M. Zhang, Z. Xu, R. Dai, Z. Wang, S. Wang, X. Fang, and Z. Zhang, "In situ monitoring of thermal degradation of $CH_3NH_3PbI_3$ films by spectroscopic ellipsometry," J. Phys. Chem. C **123**(2), 1362–1369 (2019).
[91]R. Wang, J. Xue, L. Meng, J.-W. Lee, Z. Zhao, P. Sun, L. Cai, T. Huang, Z. Wang, Z.-K. Wang *et al.*, "Caffeine improves the performance and thermal stability of perovskite solar cells," Joule **3**(6), 1464–1477 (2019).
[92]K. W. Tan, D. T. Moore, M. Saliba, H. Sai, L. A. Estroff, T. Hanrath, H. J. Snaith, and U. Wiesner, "Thermally induced structural evolution and performance of mesoporous block copolymer-directed alumina perovskite solar cells," ACS Nano **8**(5), 4730–4739 (2014).
[93]C. Li, A. Guerrero, S. Huettner, and J. Bisquert, "Unravelling the role of vacancies in lead halide perovskite through electrical switching of photoluminescence," Nat. Commun. **9**(1), 5113 (2018).

[94]Q. Jeangros, M. Duchamp, J. Werner, M. Kruth, R. E. Dunin-Borkowski, B. Niesen, C. Ballif, and A. Hessler-Wyser, "In situ TEM analysis of organic–inorganic metal-halide perovskite solar cells under electrical bias," Nano Lett. **16**(11), 7013–7018 (2016).
[95]M.-c. Kim, N. Ahn, D. Cheng, M. Xu, S.-Y. Ham, X. Pan, S. J. Kim, Y. Luo, D. P. Fenning, D. H. S. Tan *et al.*, "Imaging real-time amorphization of hybrid perovskite solar cells under electrical biasing," ACS Energy Lett. **6**(10), 3530–3537 (2021).
[96]M. Ahmadi, L. Collins, K. Higgins, D. Kim, E. Lukosi, and S. V. Kalinin, "Spatially resolved carrier dynamics at $MAPbBr_3$ single crystal–electrode interface," ACS Appl. Mater. Interfaces **11**(44), 41551–41560 (2019).
[97]Y. Yuan, T. Li, Q. Wang, J. Xing, A. Gruverman, and J. Huang, "Anomalous photovoltaic effect in organic-inorganic hybrid perovskite solar cells," Sci. Adv. **3**(3), e1602164 (2017).
[98]I. E. Gould, C. Xiao, J. B. Patel, and M. D. McGehee, "In-operando characterization of P-I-N perovskite solar cell under reverse bias," in *2021 IEEE 48th Photovoltaic Specialists Conference (PVSC), 20–25 June 2021, USA* (IEEE, 2021).
[99]J. L. Garrett, E. M. Tennyson, M. Hu, J. Huang, J. N. Munday, and M. S. Leite, "Real-time nanoscale open-circuit voltage dynamics of perovskite solar cells," Nano Lett. **17**(4), 2554–2560 (2017).
[100]E. M. Tennyson, J. M. Howard, B. Roose, J. L. Garrett, J. N. Munday, A. Abate, and M. S. Leite, "The effects of incident photon energy on the time-dependent voltage response of lead halide perovskites," Chem. Mater. **31**(21), 8969–8976 (2019).
[101]Y. Liu, N. Borodinov, L. Collins, M. Ahmadi, S. V. Kalinin, O. S. Ovchinnikova, and A. V. Ievlev, "Role of decomposition product ions in hysteretic behavior of metal halide perovskite," ACS Nano **15**(5), 9017–9026 (2021).
[102]Z. Ni, H. Jiao, C. Fei, H. Gu, S. Xu, Z. Yu, G. Yang, Y. Deng, Q. Jiang, Y. Liu *et al.*, "Evolution of defects during the degradation of metal halide perovskite solar cells under reverse bias and illumination," Nat. Energy **7**(1), 65–73 (2022).
[103]L. Najafi, S. Bellani, L. Gabatel, M. I. Zappia, A. Di Carlo, and F. Bonaccorso, "Reverse-bias and temperature behaviors of perovskite solar cells at extended voltage range," ACS Appl. Energy Mater. **5**(2), 1378–1384 (2022).
[104]A. R. Bowring, L. Bertoluzzi, B. C. O'Regan, and M. D. McGehee, "Reverse bias behavior of halide perovskite solar cells," Adv. Energy Mater. **8**(8), 1702365 (2018).
[105]A. Alberti, I. Deretzis, G. Mannino, E. Smecca, S. Sanzaro, Y. Numata, T. Miyasaka, and A. La Magna, "Revealing a discontinuity in the degradation behavior of $CH_3NH_3PbI_3$ during thermal operation," J. Phys. Chem. C **121**(25), 13577–13585 (2017).
[106]A. Alberti, I. Deretzis, G. Mannino, E. Smecca, F. Giannazzo, A. Listorti, S. Colella, S. Masi, and A. La Magna, "Nitrogen soaking promotes lattice recovery in polycrystalline hybrid perovskites," Adv. Energy Mater. **9**(12), 1803450 (2019).
[107]E. J. Juarez-Perez, L. K. Ono, M. Maeda, Y. Jiang, Z. Hawash, and Y. Qi, "Photodecomposition and thermal decomposition in methylammonium halide lead perovskites and inferred design principles to increase photovoltaic device stability," J. Mater. Chem. A **6**(20), 9604–9612 (2018).
[108]F. Ebadi, B. Yang, Y. Kim, R. Mohammadpour, N. Taghavinia, A. Hagfeldt, and W. Tress, "When photoluminescence, electroluminescence, and open-circuit voltage diverge – light soaking and halide segregation in perovskite solar cells," J. Mater. Chem. A **9**(24), 13967–13978 (2021).
[109]T. D. Siegler, W. A. Dunlap-Shohl, Y. Meng, Y. Yang, W. F. Kau, P. P. Sunkari, C. E. Tsai, Z. J. Armstrong, Y.-C. Chen, D. A. C. Beck *et al.*, "Water-accelerated photooxidation of $CH_3NH_3PbI_3$ perovskite," J. Am. Chem. Soc. **144**(12), 5552–5561 (2022).
[110]X. Deng, X. Wen, J. Zheng, T. Young, C. F. J. Lau, J. Kim, M. Green, S. Huang, and A. Ho-Baillie, "Dynamic study of the light soaking effect on perovskite solar cells by in-situ photoluminescence microscopy," Nano Energy **46**, 356–364 (2018).
[111]C. Das, M. Wussler, T. Hellmann, T. Mayer, and W. Jaegermann, "*In situ* XPS study of the surface chemistry of MAPI solar cells under operating conditions in vacuum," Phys. Chem. Chem. Phys. **20**(25), 17180–17187 (2018).
[112]M. Kot, L. Kegelmann, H. Köbler, M. Vorokhta, C. Escudero, P. Kúš, B. Šmíd, M. Tallarida, S. Albrecht, A. Abate *et al.*, "In situ near-ambient pressure X-ray photoelectron spectroscopy reveals the influence of photon flux and water on the stability of halide perovskite," ChemSusChem **13**(21), 5722–5730 (2020).
[113]M. Ahmadi, E. S. Muckley, I. N. Ivanov, M. Lorenz, X. Li, O. Ovchinnikova, E. D. Lukosi, J. T. Tisdale, E. Blount, I. I. Kravchenko *et al.*, "Environmental gating and galvanic effects in single crystals of organic–inorganic halide perovskites," ACS Appl. Mater. Interfaces **11**(16), 14722–14733 (2019).
[114]S. G. Motti, D. Meggiolaro, A. J. Barker, E. Mosconi, C. A. R. Perini, J. M. Ball, M. Gandini, M. Kim, F. De Angelis, and A. Petrozza, "Controlling competing photochemical reactions stabilizes perovskite solar cells," Nat. Photonics **13**(8), 532–539 (2019).
[115]S. S. Dipta and A. Uddin, "Stability issues of perovskite solar cells: A critical review," Energy Technol. **9**(11), 2100560 (2021).
[116]T. A. Chowdhury, M. A. Bin Zafar, M. Sajjad-Ul Islam, M. Shahinuzzaman, M. A. Islam, and M. U. Khandaker, "Stability of perovskite solar cells: Issues and prospects," RSC Adv. **13**(3), 1787–1810 (2023).
[117]R. Wang, M. Mujahid, Y. Duan, Z. K. Wang, J. Xue, and Y. Yang, "A review of perovskites solar cell stability," Adv. Funct. Mater. **29**(47), 1808843 (2019).
[118]S. Mazumdar, Y. Zhao, and X. Zhang, "Stability of perovskite solar cells: Degradation mechanisms and remedies," Front. Electron. **2**, 712785 (2021).
[119]M. Hadadian, J.-H. Smått, and J.-P. Correa-Baena, "The role of carbon-based materials in enhancing the stability of perovskite solar cells," Energy Environ. Sci. **13**(5), 1377–1407 (2020).
[120]E. Unger and T. J. Jacobsson, "The perovskite database project: A perspective on collective data sharing," ACS Energy Lett. **7**(3), 1240–1245 (2022).
[121]E. Velilla Hernández, J. B. Cano Quintero, J. F. Montoya, I. Mora-Seró, and F. Jaramillo Isaza, "Outdoor performance of perovskite photovoltaic technology," in *Thin Films Photovoltaics*, edited by Z. Beddiaf and S. Chander (IntechOpen, 2021), Chap. 5.
[122]E. Velilla, F. Jaramillo, and I. Mora-Seró, "High-throughput analysis of the ideality factor to evaluate the outdoor performance of perovskite solar minimodules," Nat. Energy **6**(1), 54–62 (2021).
[123]M. Jošt, B. Lipovšek, B. Glažar, A. Al-Ashouri, K. Brecl, G. Matič, A. Magomedov, V. Getautis, M. Topič, and S. Albrecht, "Perovskite solar cells go outdoors: Field testing and temperature effects on energy yield," Adv. Energy Mater. **10**(25), 2000454 (2020).
[124]M. Saliba, M. Stolterfoht, C. M. Wolff, D. Neher, and A. Abate, "Measuring aging stability of perovskite solar cells," Joule **2**, 1019 (2018).
[125]W. Song and T. Aernouts, "Novel test scenarios needed to validate outdoor stability of perovskite solar cells," J. Phys.: Energy **2**(2), 021003 (2020).
[126]Q. Emery, M. Remec, G. Paramasivam, S. Janke, J. Dagar, C. Ulbrich, R. Schlatmann, B. Stannowski, E. Unger, and M. Khenkin, "Encapsulation and outdoor testing of perovskite solar cells: Comparing industrially relevant process with a simplified lab procedure," ACS Appl. Mater. Interfaces **14**(4), 5159–5167 (2022).
[127]H. Köbler, M. V. Khenkin, R. Roy, N. Phung, Q. Emery, M. Remec, R. Schlatmann, C. Ulbrich, and A. Abate, "The challenge of designing accelerated indoor tests to predict the outdoor lifetime of perovskite solar cells," PREPRINT (Version 1) available at Research Square, 17 August (2021).
[128]M. Babics, M. De Bastiani, E. Ugur, L. Xu, H. Bristow, F. Toniolo, W. Raja, A. S. Subbiah, J. Liu, L. V. Torres Merino *et al.*, "One-year outdoor operation of monolithic perovskite/silicon tandem solar cells," Cell Rep. Phys. Sci. **4**(2), 101280 (2023).
[129]W. Tress, K. Domanski, B. Carlsen, A. Agarwalla, E. A. Alharbi, M. Graetzel, and A. Hagfeldt, "Performance of perovskite solar cells under simulated temperature-illumination real-world operating conditions," Nat. Energy **4**(7), 568–574 (2019).